Christian Stickler, BSc

Dolomitization of Upper Jurassic Limestone at Oker (Langenberg, Germany)

MASTER'S THESIS

to achieve the university degree of

Master of Science

Master's degree programme: Earth Sciences

submitted to

Graz University of Technology

Supervisor

Univ.-Prof. Dipl.-Min. Dr.rer.nat., Martin Dietzel

Institut für Angewandte Geowissenschaften

Andre Baldermann, M.S.c.

Graz, March 2015

AFFIDAVIT

I declare that I have authored this thesis independently, that I have not used other than the declared sources/resources, and that I have explicitly indicated all material which has been quoted either literally or by content from the sources used.
The text document uploaded to TUGRAZonline is identical to the present master's thesis dissertation.

_____   _____
             Date   Signature

Contents

Abstract

Precipitation of dolomite at low temperatures in modern aquatic environments is limited mainly due to the inhibitory effect of complexed Mg^{2+} aquo-complexes. The hindering effect of dolomite precipitation by Mg seems to be less effective in marine-anaerobic, organic-rich sediments, where bacterial sulfate reduction occurs.

In order to shed light on the process of ancient dolomite formation in (Mg,S)-rich environments, partly dolomitized limestone and pure dolostone beds of Upper Jurassic age (~153 Ma), that were formed in a shallow-marine, sabkha environment at Oker (Langenberg, Germany) were investigated in the present study. X-ray diffraction (XRD), electron microprobe (EMP) analysis, X-ray fluorescence (XRF), cathodoluminescence and $\delta^{18}O$ and $\delta^{13}C$ isotope measurements were completed to decipher the geochemical and (micro)structural relationships between dolomite, low-Mg calcite (LMC) and high-Mg calcite (HMC) at the bulk and micron-scale. The investigated lithological profile starts with layers of massive limestone that gradually transforms into fine-grained dolostone, followed by a thick limestone horizon at the upper part of the section.

The lower limestone section consists of micritic calcite of marine origin and is characterized by an isotopic composition of -1.7 to -2.9‰ of $\delta^{18}O$, VPDB, and 1.3 to -0.7‰ of $\delta^{13}C$, VPDB. The chemical composition is $(Ca_{0.93-0.996}Mg_{0.003-0.03}Mn_{0-0.054}Sr_{0-0.001}Na_{0-0.001}Fe_{0-0.001})_{0.99-1.0}[(C_{0.94-1}S_{0-0.004})O_3]_2$. The upper limestone unit has an isotopic composition of -1.8 to -3.4‰ of $\delta^{18}O$, VPDB, and -1.6 to -4.0‰ of $\delta^{13}C$, VPDB, respectively, indicative of deposition under marine to sabkha conditions. The transitional contact zone between the lower limestone and the dolomitized limestone consists of fine-grained, < 50 µm sized, dolomite, LMC and HMC (listed from core to rim) deposited in single grains in the alternate mode. EMP analyses of the dolomite cores, ~10-15 µm in diameter, revealed excess of Ca and a significant amount of structural sulfate (up to 2500 ppm of SO_3), expressed as $(Ca_{0.99-1.13}Na_{0.002-0.004}Sr_{0-0.001})_{0.99-1.13}(Mg_{0.86-1}Fe_{0-0.02}Mn_{0-0.006})_{0.86-1.03}[(C_{0.96-0.995}S_{0.004-0.08})O_3]_2$.

Interestingly, sulfate was not detected in the subsequently deposited LMC, $(Ca_{0.86-0.99}Mg_{0.006-0.05}Fe_{0-0.004}Na_{0-0.002}Mn_{0-0.001})_{0.96-0.97}CO_3$, and HMC, $(Ca_{0.64-0.78}Mg_{0.19-0.32}Fe_{0-0.004}Na_{0-0.003}Mn_{0-0.002})_{0.91-0.99}CO_3$. The adjoining massive and almost "pure" dolostone (2.2 to 1.7‰ of $\delta^{18}O$, VPDB and 1.7 to -0.1‰ of $\delta^{13}C$, VPDB) has a composition of $(Ca_{1.03-1.24}Na_{0.001-0.006}Sr_{0-0.001})_{1.03-1.25}(Mg_{0.76-0.95}Fe_{0-0.02}Mn_{0-0.002})_{0.76-0.95}[(C_{0.98-0.998}S_{0.001-0.02})O_3]_2$. The dolostone comprises of euhedral dolomite crystals with a grain size of 2-50 µm, which show few microns thick, alternate growth zones of S and Fe. The XRD analyses confirmed the dolomite to be non-stoichiometric, with 51-54 mol% of $CaCO_3$. The degree of cation order in dolomite, in respect to ideal dolomite, decreases from 83% to 38% with increasing sulfur content, from 0.02 to 0.013 S atoms per formula unit, respectively.

The variation in the isotopic composition ($\delta^{18}O$ and $\delta^{13}C$) and in particular in the distribution and concentrations of Mg, Sr, Fe, and S in calcite and/or dolomite indicates cyclic and abrupt changes of the interstitial solution chemistry occurred

during carbonate mineral precipitation. The plausible scenario of carbonate evolution involves a decrease in sea level coupled with high evaporation rates, which led to increasing Mg/Ca ratios in the dolomitization fluids and thus alteration of primary LMC to HMC, subsequently transformed to dolomite.

Zusammenfassung

In rezenten aquatischen Milieus ist die direkte Ausfällung von Dolomit hauptsächlich durch die Bildung von Magnesium Aquokomplexen stark limitiert. Dieser Faktor scheint in anoxischen, Organik-reichen Sedimenten, unter Anwesenheit von Sulfat-reduzierenden Bakterien, weniger stark ausgeprägt zu sein.

Um den Prozess der Dolomitisierung in (Mg, S)-reichen Ablagerungsmilieus besser verstehen zu können, wurde in dieser Arbeit eine teilweise dolomitisierte oberjurassische Karbonatsequenz (~153 Ma) untersucht. Die Karbonate wurden in einem flachmarinen Becken, unter Sabkha-Bedingungen, in Oker (Langenberg, Deutschland) gebildet. Um die genauen Ablagerungsbedingungen und in weiterer Folge auch die diagenetischen Abläufe während der Dolomitisierung von Kalkstein zu rekonstruieren, wurden petrographische, geochemische und mineralogische Untersuchungsmethoden wie Dünnschliffanalyse, Röntgendiffraktometrie- (RDA), Mikrosonden- (EMPA), Röntgenfluoreszenz- (RFA) und Kathodolumines-zenzanalysen, sowie $\delta^{18}O$ bzw. $\delta^{13}C$ Isotopenmessungen durchgeführt. Auf Grundlage der Analytik konnten auf mikroskopischer und makroskopischer Ebene unterschiedliche Kalzitgenerationen (Hoch- und Niedrig-Mg-Kalzit) und zwei Dolomittypen (Matrixdolomite Typ A und Typ B) unterschieden werden.

Das untersuchte lithologische Profil beginnt im Liegenden mit einem massiven Kalkstein, welcher zum Hangenden zunehmend dolomitisiert ist. Auf den anschließenden massiven Dolomithorizont folgt ein weiterer dickbankiger Kalkstein. Die unterste Einheit der Sequenz besteht aus flachmarinem, mikritischen Kalkstein mit einer Isotopenzusammensetzung von -1.7 bis -2.9‰ $\delta^{18}O$ (VPDB) und 1.3 bis -0.7‰, $\delta^{13}C$ (VPDB). Die Kalzite der unteren Kalksteineinheit haben eine chemische Zusammensetzung von $Ca_{0.93-0.996}Mg_{0.003-0.03}Mn_{0-0.054}Sr_{0-0.001}Na_{0-0.001}Fe_{0-0.001})_{0.99-1.0}[(C_{0.94-1}S_{0-0.004})O_3]_2$. Die obere Kalksteineinheit hat eine Isotopenzusammensetzung von -1.8 to -3.4‰ $\delta^{18}O$ (VPDB) und -1.6 to -4.0‰ $\delta^{13}C$ (VPDB), was auf eine Ablagerung unter randmarinen Bedingungen hindeutet. Die Kontaktzone zwischen dem unteren Kalkstein und dem massiven Dolomitgestein, besteht aus partiell dolomitisiertem Kalkstein. Die Karbonatkristalle aus diesem Übergangshorizont besitzen einen Dolomitkern, welcher von Niedrig-Mg-Kalzit und Hoch-Mg-Kalzit gesäumt ist. Der ca. 10-15 μm große Dolomitkern zeigt einen deutlichen Ca-Überschuss und eine signifikante Anreicherung von Sulfat, ausgedrückt als $(Ca_{0.99-1.13}Na_{0.002-0.004}Sr_{0-0.001})_{0.99-1.13}(Mg_{0.86-1}Fe_{0-0.02}Mn_{0-0.006})_{0.86-1.03}[(C_{0.96-0.995}S_{0.004-0.08})O_3]_2$.

Interessanterweise konnte Sulfat weder in den nachfolgend präzipitierten Niedrig Mg-Kalziten mit einer Zusammensetzung von $(Ca_{0.86-0.99}Mg_{0.006-0.05}Fe_{0-0.004}Na_{0-0.002}Mn_{0-0.001})_{0.96-0.97}CO_3$, noch in den Hoch-Mg-Kalziten $(Ca_{0.64-0.78}Mg_{0.19-0.32}Fe_{0-0.004}Na_{0-0.003}Mn_{0-0.002})_{0.91-0.99}CO_3$, nachgewiesen werden.

Die im Hangenden anschließenden, „reinen" Dolomitgesteine haben eine chemische Zusammensetzung von $(Ca_{1.03-1.24}Na_{0.001-0.006}Sr_{0-0.001})_{1.03-1.25}(Mg_{0.76-0.95}Fe_{0-0.02}Mn_{0-0.002})_{0.76-0.95}[(C_{0.98-0.998}S_{0.001-0.02})O_3]_2$ und eine Isotopensignatur von 2.2 bis 1.7‰ $\delta^{18}O$ (VPDB) und 1.7 bis -0.1‰ $\delta^{13}C$ (VPDB). Die Dolomite bestehen aus euhedralen

Kristallen mit einem Durchmesser von 2-50 µm und zeigen teilweise eine Fe- und S-Zonierung. Die RDA-Analyse bestätigt, dass die Dolomite einen Ca-Überschuss (51-54 mol% $CaCO_3$) aufweisen und somit nicht stöchiometrisch sind. Der strukturelle Ordnungsgrad des Dolomits, bezogen auf stoichiometrischen und geordneten (idealen) Dolomit, sinkt von 83% auf 38% mit einem Anstieg der strukturgebundenen Schwefelkonzentration von 0.002 auf 0.013 Atome pro Einheitszelle.

Die Variation der Isotopensignaturen (δ^{18}O und δ^{13}C) und die Verteilung und Konzentration von Mg, Sr, Fe, und S im Kalzit bzw. Dolomit weisen auf sowohl zyklische als auch abrupte Änderungen der chemischen Zusammensetzung des Dolomitisierungsfluids hin. Ein plausibles Szenario, in welchem die Ausfällung der Karbonatsequenz bzw. die Umwandlung dieser stattgefunden haben könnten, beinhaltet das Absinken des Meerwasserspiegels, verbunden mit erhöhten Evaporationsraten, was zu einem Anstieg des Mg/Ca-Verhältnis und in weiterer Folge zu einer Umwandlung von Niedrig-Mg-Kalzit zu Hoch-Mg-Kalzit und letztlich zu Dolomit führte.

1. Introduction

Carbonates are of particular interest in Earth Science, mainly because of their broad occurrence on the Earth surface and their role in the global carbon cycle, where carbonates act as an atmospheric CO_2 buffer (e.g. Fenter *et al.*, 2007). Although the fundamental processes leading to carbonate mineral formation, transformation and/or dissolution in natural surroundings are considered to be generally understood, several individual reaction paths and controlling factors in the above reactions remain uncertain. One of the biggest ambiguities is related to the formation of dolomite at low temperatures, because even though modern seawater is supersaturated in respect to dolomite by one to two orders of magnitude, recent dolomite-forming environments are rare. In contrast, dolomite is abundant in many ancient (marine) sedimentary deposits (Fenter *et.al.*, 2007; Arvidson & Mackenzie, 1999). In the literature this paradoxon is often referred to as "the dolomite problem". (e.g. Fenter *et al.*, 2007). In the past, a huge number of dolomitization models were developed to explain the formation of dolomite throughout Earth history, but based on the study of recent dolomitization environments a set of (locality specific) parameters such as the importance of microbial activity in the dolomitization process were discovered (e.g. Deelman, 2011). However, because most of these models do not suit a large number of dolomite-forming environments, some scientists doubt the correctness of any of the postulated dolomitization models (e.g. Deelman 2011). Until now, the synthesis of stoichiometric and ordered dolomite in the laboratory (without microbial mediation) was only successful under extreme conditions such as high temperatures up to 200°C and/or high pressures (e.g. Kaczmarek & Sibley, 2011).

The aim of this work is to shed light on the individual reaction paths and ambient environmental controls of dolomitization of limestone that proceeded on an Upper Jurassic carbonate platform setting at Oker (Langenberg, Central Germany). Although dolomitization in ancient marine environments was apparently quite different regarding the distribution and scale of dolomitization events, some key factors that control the formation of dolomite in such settings can be reconstructed and extrapolated to understand the fundamental processes in modern dolomite-forming environments. For this purpose, a partly dolomitized limestone sequence from Oker was investigated. Different geochemical and mineralogical methods were applied to gain a better understanding of how the dolomitization reaction took place and what the depositional environment looked like.

1.1. Structure of dolomite

Dolomite, $CaMg(CO_3)_2$, is a water-free carbonate mineral that represents the Mg-rich member in the dolomite-ankerite group. The crystal system of dolomite is trigonal-rhombohedral (crystal class 3, space group R 3 - C2 3i, according to Wyckoff & Merwin, 1924). Figure 1 shows the structure of stoichiometric (ideal) dolomite, as indicated by the 1:1 ratio between subsequently deposited $MgCO_3$ and $CaCO_3$ layers in dolomite. However, the mineral type dolomite is not a simple (physical) mixture of calcite and magnesite layers deposited in the alternate mode, it is considered to be a double salt, built of alternating monolayers of Ca^{2+}, Mg^{2+}, and CO_3-layers that are arranged parallel to the [0001] dolomite layer plane. The random substitution of Mg^{2+} ions by larger Ca^{2+} ions often results in the precipitation of non-stoichiometric dolomites in many modern dolomite-forming environments. These Ca-excess dolomites typically show no superstructure reflections and thus are better represented as "proto-dolomites".

1.2. Formation of dolomite

For the formation of dolomite four different reaction mechanisms were postulated by Chilingar *et al., 1979:*
1.) Primary: dolomite is directly precipitated from an oversaturated solution.
2.) Diagenetic: dolomite is formed by the replacement of $CaCO_3$ precursors in the post-depositional but pre-lithification phase of sediment diagenesis. This process typically takes place during the earliest stage of diagenesis, but can also proceed during epigenesis.
3.) Epigenetic or catagenetic: dolomite is a replacement product of lithified $CaCO_3$-rich sediments or rocks. Post-orogenic dolomite can develop under special tectonic conditions.
4.) Metamorphic or metasomatic: recrystallization of early diagenetic dolomite and/or unstable $CaCO_3$ phases takes place at elevated temperatures and pressure conditions.

ad 1.): the direct precipitation of dolomite from a solution is hard to prove, as it is difficult to distinguish between primary formation and early diagenetic origin of dolomite.
ad 2.) and 3.): the difference between diagenetic and epigenetic dolomite formation, as defined by Chilingar *et al.* 1979, is not used widely; only a dolomite classification based on different stages of diagenesis (early to late) is common. Mostly, the term diagenetic is used for both processes.
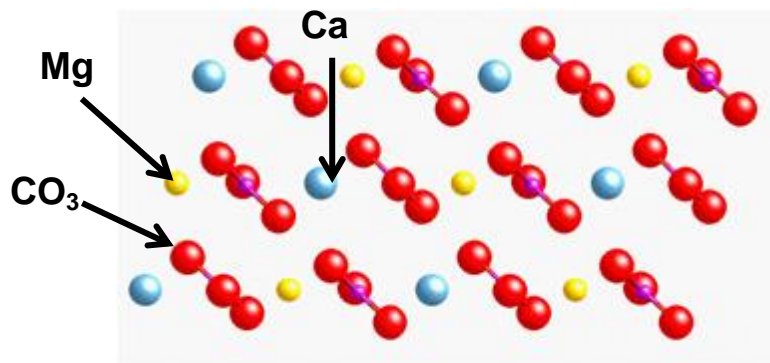
Figure 1: Ideal structure of dolomite, $CaMg(CO_3)_2$, showing the alternate Mg^{2+}, Ca^{2+}, and CO_3^{2-} layers that are arranged parallel to the [0001] dolomite layer plane (after Fenter *et. al.*, 2007).

Although modern seawater is supersaturated in respect to dolomite the formation of recent (stoichiometric and ordered) dolomite is often limited to highly localized environments, where it typically accounts only for a small percentage of the total sediment mass (Mackenzie, 2006). The formation of dolomite hence does not occur via direct precipitation in open marine environments, but can proceed by microbial assisted replacement of carbonate precursors in diagenetic (mostly hypersalinar and more rarely brackish) environments. Here, dolomitization is often restricted to the innermost areas of a stable carbonate ramp, especially in close contact to adjacent lagoons and/or shallow sabkha basins. For example, the formation of modern dolomite was observed to occur in the Persian Gulf sabkhas, in the Coorong district in South Australia, on Bonaire Island in the Caribbean Sea, in the Sugarloaf Key in Florida, in the supratidal sediments on Andros Island in the Bahamas, and in the Deep Springs Lake sediments in California (Mackenzie, 2006). The conditions in the above environments are known to differ significantly and hence numerous models were developed to explain the formation of recent sedimentary dolomite (see chapter 1.4.). Besides early diagenetic dolomite formation by a selective carbonate replacements process, direct dolomite precipitation was postulated to take place in the Brejo do Espinho Lagoon in Brazil (Sánchez-Román et al., 2012), assisted by sulfate-reducing bacteria. In summary, most recently formed dolomites are non-stoichiometric and poorly ordered, and only occur in small quantities.

1.3. Dolomitization reaction

In the last decades, several reaction pathways have been introduced to explain the origin and abundance of sedimentary dolomite throughout the geological record. These reactions are described in detail in Budd (1997) and Warren (2000). Here, only the two (most widely accepted) dolomitization reactions are summarized briefly:

(i)   Dolomitization is the process of selective/stepwise replacement of calcite and/or aragonite precursors by secondary dolomite. This replacement

reaction can be achieved via an exchange of Ca^{2+} ions by Mg^{2+} ions, derived from a Mg-rich dolomitization fluid following equation 1:

$$Mg^{2+}+2(CaCO_3) \rightarrow CaMg(CO_3)_2+Ca^{2+} \qquad (eq.\ 1)$$

(ii)   Dolomitization can occur by direct precipitation from an (over)saturated dolomitizing fluid, which delivers the required Mg^{2+} and CO_3^{2-} ions after equation 2:

$$CaCO_3+Mg^{2+}+CO_3^{2-} \rightarrow CaMg(CO_3)_2 \qquad (eq.\ 2)$$

Both dolomitization models postulate that dolomitization of limestone most likely proceeds through early to late diagenesis, by dissolution/replacement of unstable carbonate mineral precursors and re-precipitation as dolomite through intense interaction with a coexisting fluid at high Mg/Ca ratios. Some of the most common models are briefly discussed in the following chapter.

1.4. Dolomitization models

1.4.1.   Dolomites associated with Evaporates

The sabkha evaporative model is used for explaining the broad occurrence of ancient dolomites in supratidal areas (Flügel, 2010). The formation of dolomite is linked to intensive evaporation, which causes a successive change in seawater chemistry to more hypersalinar (brine) solutions. Here, dolomite replaces pre-existing metastable carbonates. The dolomitizing fluid typically has a high Mg/Ca-ratio, because Ca^{2+} ions are selectively reduced by initial aragonite, gypsum and/or anhydrite precipitation, whereas the more heavily complexed Mg^{2+} ions become progressively enriched in the residual solution.

In the Holocene, tidal flat dolomitization was observed in the Persian Gulf sediments, in the Florida Keys and in the Bahamas. The precipitating dolomites are mostly microcrystalline, non-stoichiometric and show a lack of structural ordering. These protodolomites occur in muddy carbonate-rich sediments and/or as surface crusts in supratidal flats.

In the seepage reflux model, dolomite precipitation is associated with the formation of evaporates (see model above).The dolomitizing fluid is a Mg^{2+}-rich hypersaline fluid, which is penetrating through the underlying carbonate-rich sediments causing a selective dolomitization reaction. The fluid develops through evaporation of seawater or pore waters in tidal flats.

The falling sea-level or evaporation model is used to explain the cyclic occurrence of dolomite and evaporates in intertidal and subtidal sediments. The dolomitization process is caused by sea-level changes (mostly related to major sea-level lowstands) and occurs beneath massive evaporate sequences.

In the Coorong model, the dolomitization is referred to ephemeral alkaline lakes, which are located behind the modern shoreface (e.g. South Australia). The lakes are fed by seawater and seaward-flowing continental groundwater. Due to evaporation of Mg^{2+}-rich groundwater, fine-grained dolomite is formed during coupled annual lake cycles, consisting of flooding and desiccation periods.

1.4.2.   Mixing-Water and Seawater Models

The Meteoric-marine mixing zone model or the Dorag-model refers to the mixing of meteoric and marine water masses, from which dolomites can precipitate through interaction of coastal unconfined or deep confined water bodies. The model is used to explain the occurrence of dolomite in subtidal, environments. Dolomitization occurs prior to, or during the early stages of diagenesis and related sediment compaction. In this model, dolomite is not associated with evaporates.

The Seawater dolomitization model postulates the formation of dolomite by precipitation from slightly modified seawater, associated with tidal pumping in platform, reef and pelagic environments.

The Kohout convection model postulates dolomitization to occur through mixing of cold marine water masses with ascending geothermally heated groundwater within the carbonate platform. The driving force of water mixing is convection. It is induced by the density difference between the two water types.

In the burial dolomitization model, dolomitization occurs during slow subsidence of intrabasinal mudstones. The immersion of sediments causes compaction and dehydration of the mudstone. Burial diagenetic transformation of the clay mineral smectite to illite with increasing burial pressure and temperature results in the generation of Mg^{2+}-rich fluids, which finally lead to the dolomitization of compacted limestone. Metamorphic or hydrothermal fluids can also serve as a Mg^{2+}-source.

2. Geological setting at Oker

The study area is located at Oker, Lower Saxony, in Central Germany.

For this thesis, samples were collected from an active limestone quarry (Langenberg at Oker) of the Rohstoffbetriebe Oker GmbH & Co. Figure 2 shows a geological map of Central and Northern Germany, where the location of the investigated outcrop is marked with an icon. The limestone quarry at Oker belongs to the northernmost part of the so-called "Aufrichtungszone", which is located in the south of the Western Harz foreland basin (Baldermann & Nickel, 2012). The latter feature bounds the Central German High Mountains, which belongs to the Harz Mountains, to the north. The Harz is a Variscian mountain arc, which has a dimension of roughly 30x90 km in Central Europe (Kulke, 1997). It can be subdivided into three geological and morphological subunits: The Upper Harz (Westharz), the Middle Harz and the Subharz (Eastharz).

At Oker, the overthrusting of the Harz foreland sediments during the development of the Harz Thrust Fault has led to an inversion of the bedding planes during the Upper Cretaceous (Coniac/ Santon boundary at about 85 Ma) (Baldermann & Nickel, 2012). Thus, the inverted Langenberg sediments dip now 50-70 degrees S and cover a sedimentary sequence from the Late Oxfordian to the Upper Kimmeridgian (Upper Jurassic).

During the Lower Jurassic to Upper Cretaceous, the Harz foreland basin was a shallow marine basin (Baldermann & Nickel, 2012). At this time, the Langenberg area at Oker was a shallow bay-like basin or an estuary and partly connected to the Thetys Ocean (Fischer, 1991; Baldermann & Nickel, 2012). In the North, the water inflow towards this basin was limited by the Pompecki´sche Schwelle and the Rheinisches Massiv confined it towards the South (Fischer, 1991). The overall depositional environment at Oker was likely to be a stable, flat-angled carbonate ramp (Baldermann & Nickel, 2012).
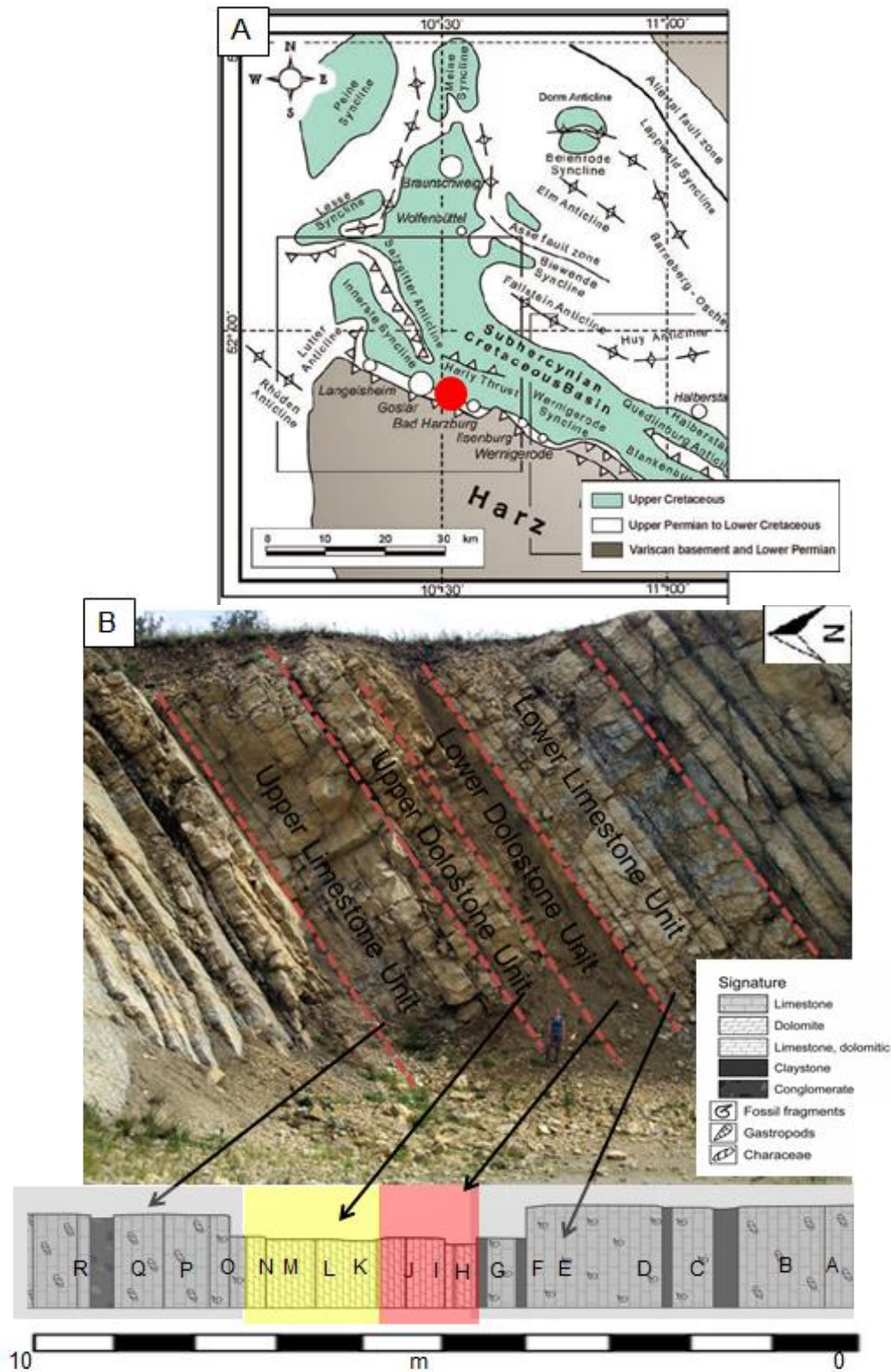
Figure 2: A: Geological map of Central and Northern Germany showing the location of the study area at Oker (after Voigt *et. al.*, 2006). B: Optical photograph showing the investigated sedimentary section, located on the northernmost flank of the Langenberg profile. Below, the rock classification and the location of sampled intervals are reported. Person for scale is about 1.7 m tall.

During the Kimmeridgian (155.6 Ma to 150 Ma), the carbonate platform was stepwise closed up by the development of an open-marine barrier reef facies of type Exogyra, which resulted in the establishment of a stable inner-reef carbonate platform setting, characterized by a proximal lagoonal facies. Due to a freshwater inflow in the Lower to Middle Kimmeridgian from the Mitteldeutsches Festland, the restricted lagoon became seasonally brackish, which caused intense facies changes of argillite-limestone-dolostone alternations. Progressive evaporation in this lagoonal setting subsequently led to aggradation and partial islanding. This caused an increase in salinity and progressive carbonate mineral precipitation. During the Upper Kimmeridgian, a sea level regression finally resulted in a shift back to open-marine conditions (Baldermann & Nickel 2012).

2.1. Description of the sequence

For this thesis, a ~10 m thick calcareous sequence was studied bed by bed. This sequence dates back from the Middle Kimmeridgian to the Upper Kimmeridgian (~153 Ma). The overall depositional environment at Oker at this time was a restricted lagoonal environment. Progressive evaporation of the lagoonal water masses caused an increase in salinity (indicated by the occurrence of normal marine to hypersaline faunal elements) and led to progressive carbonate mineral precipitation (indicated by the occurrence of thick dolostone and partly dolomitized limestone beds).

2.2. Sampling strategy

Based on previous work of Baldermann & Nickel (2012) and Fischer (1991) an approximately 10 m thick sedimentary sequence within the Langenberg quarry at Oker (Germany) was investigated in order to determine the environmental controls and reaction paths associated with the progressive dolomitization of limestone during the Upper Jurassic.

In total 18 orientated specimens were collected from the above section. Characteristic and representative samples from every single bed from the sequence (samples were chosen mainly after morphology and color) were collected for further petrographic, mineralogical and (isotope)geochemical analyses. The sequence includes the so-called upper dolomite or "Wasserbank" (Fischer, 1991), which was named after its high porosity and related high water content.

3. Methods

3.1. Optical Microscopy of thin sections

Thin sections were prepared from orientated rock specimens of freshly broken surfaces. Eleven thin sections were polished to a thickness of about 20-30 µm. These thin sections were then analyzed with a LEICA DMLP optical microscope. For documentation, photomicrographs of the thin sections were taken with an Olympus DP26 camera. Optical microscopy of thin sections is a basic tool to study e.g. mineral content, rock texture, and microfacies. This method is often used in sediment petrographic analysis to reconstruct the depositional environment and the degree of diagenetic alteration of sedimentary rocks.

3.2. Cathodoluminescence (CL) microscopy

CL-microscopy of polished thin sections was done to decipher various calcite cement generations and zonation patterns in dolomite and calcite spar. The analysis was performed at the Karl-Franzens University Graz on a HC5-LM, a hot cathode CL-microscope, equipped with a high sensitivity CCD kappa camera. Prior to the CL analysis, the thin sections were sputtered with carbon to make them electric conductive. The measurements were performed at a maximum electric current of 0.6 mA and a maximum voltage of 14 KeV.

3.2.1. CL characteristics of carbonates

In the dolomite and calcite crystal lattice, Mn^{2+} ions and trivalent rare earth elements (REE) serve as activator elements, whereas Fe^{2+} and Cu^{3+} ions operate as quencher elements (they reduce the fluorescence effect). In case of calcite, Mn^{2+} can substitute for the Ca^{2+} ion. This substitution causes a yellow-orange luminescence color. In case of the dolomite structure, Mn^{2+} can occur in two emission bands and this can cause either a red (Mn^{2+} substitution at the Mg^{2+} position) or a yellow luminescence color (Mn^{2+} substitution for Ca^{2+}). Significant reduction of the emitted photons occurs at Fe^{2+} contents of >2000 ppm in calcite and >1500 ppm in dolomite. The self-quenching effect starts at an amount of >1000 ppm Mn^{2+}, which also causes a reduction of the luminescence (Zorlu, 2007).

3.3. Electron Microprobe Analysis (EMPA)

EMPA is widely used to acquire precise chemical composition data of minerals, besides providing high resolution information about the distribution of elements in crystals (down to 1 µm), and is therefore very convenient for the analysis of calcite and dolomite.

The measurements were performed by Mag. Dr. Artur Deditius (University of Technology Graz) on a Jeol JXA-8200 "Superprobe" Electron Probe Microanalyzer at the Montan University at Leoben. Prior to the chemical analysis, the thin sections were first sputtered with carbon and imaged in the scanning electron mode of the microscope, and afterwards element distribution maps of Ca, Mg, S, Sr, Fe, Mn, Si and V were acquired using wavelength-dispersive X-ray spectrometers (WDS detectors). The elemental mappings of 1000 x 1000 pixels resolution were collected using a focused beam ~1 µm in size, an accelerating voltage of 20 kV, 20 nA beam current, and a dwell time of 20 milliseconds per step (see Appendix for elemental data, Table A-4).

For chemical analyses, the microprobe was operated at an accelerating voltage of 15 kV using a beam current of 10 nA and a focused beam diameter of ~1 µm over a raster of 4 µm x 6 µm. The quantitative chemical analyses were standardized against natural and synthetic crystals, and included following elements with characteristic spectral lines: Ca Kα, and Mg Kα (dolomite); Fe Kα (almandine), Mn Kα (rhodonite), Sr Lα and S Kα (celestine), and Na Kα (albite). The counting times for single spot analyses were: (i) 20 s for Ca, Mg, Fe, Mn, and Na and 10 s for determining the background position on each side of these peaks; and (ii) 40 s for Sr and S measurements plus 20 s on background positions, respectively. Only the analyses with an analytical error of < 5 % were used. The lower analytical totals (< 100 wt.%) are due to the presence of CO_2, and porosity (see Table A-4 for data summary).

3.4. X-ray diffraction (XRD) analyses

For the XRD analysis, the samples were crushed in an agate mill for 10 min, together with 10 wt % zincite (ZnO) powder as internal standard. This standard is necessary to correct the peak positions of in particular carbonate minerals to receive information about their mineralogical composition (e.g. Mg content in calcite) and stoichiometry (in case of dolomite). The powdered samples were then carefully filled into XRD sample holders using the top loading technique to avoid preferential particle order effects.

The XRD measurements were conducted at the TU Graz with the Panalytical X`Pert PRO diffractometer equipped with a Co- tube (40 kV, 40 mA), automatic sample changer, 0.5° divergence and antiscattering slits and a Scientific X`Celerator detector. Samples were X-rayed over the range 3-85° 2θ with a step size of

0.008 °2θ s^{-1}. The counting time per step was set to 40 s. The mineral identification was conducted with the Panalytical Highscore Plus Software.

3.4.1. XRD characteristics of carbonates

XRD analysis is used to determine the mineralogical composition of bulk samples, besides providing information about the Mg-content of calcite as well as on the stoichiometry and degree of cation order in dolomite. Moreover, the relative abundance of those two minerals can be determined.

For calcite and dolomite, the Mg-content can be calculated based on the position of the $d_{(104)}$-peak, according to the equation 3 after (Lumsden & Chimahusky, 1980):

$$Mg - content \ (mol\%) = 100 - \left(333.33 * d_{(104)} - 911.11 \right) \qquad (eq.3)$$

Ideal calcite, without any Mg incorporated, has its $d_{(104)}$-peak at 3.035 Å. The $d_{(104)}$-peak for ideal dolomite is at 2.883 Å. In both cases, incorporation of smaller Mg^{2+} ions for larger Ca^{2+} ions shifts the crystal lattice to higher 2θ values. This means that the higher the Mg-content in calcite and dolomite the lower are their corresponding d-values. Furthermore, the intensity ratio of the $d_{(110)}$-peak and the superstructure $d_{(105)}$-peak provides information about the degree of cation order in dolomite. If the superstructure reflection is absent, such –highly disordered (near-stoichiometric) Ca-Mg carbonates are often referred to as "protodolomites" (Fürchtbauer & Goldschmidt, 1965). Finally, if both, calcite and dolomite, coexist in a sample, the ratio of the two minerals can be calculated based on their $d_{(104)}$-peak intensities, following equation 4:

$$calcite \ \% = \frac{Idol}{Idol+Icc} * 100 \qquad (eq. \ 4)$$

3.5. Isotope-ratio mass spectrometry (IR-MS)

The oxygen and carbon isotope measurements were performed by Dr. Albrecht Leis at the Joanneum Research on a DELTA plus XP mass spectrometer using the common phosphoric acid method (after Révész and Landwehr, 2002; Spötl and Vennemann, 2003; Paul and Skrzypek, 2007; Dietzel, et.al, 2009). The oxygen and carbon isotopic composition of the Oker carbonates are reported in terms of δ-notation via the international V-PDB standard. The analytical error was determined to be <0.1‰ for $δ^{13}C$ and $δ^{18}O$, respectively.

The sample material was crushed with an arcade mile and measured together with NBS18 and NBS19 standards. After sample homogenization, 300-600 µg of the sample was filled into a high purity glass vessel previously cleaned with phosphoric

acid and rinsed three times with ionized water (18.2 MΩ cm, ELGA PURELAB Maxima), and then dried overnight at 70°C. Prior to the IR-MS analysis, phosphoric acid was injected into the vessels and reacted with the carbonates for 82 minutes at 72 ±0.1°C.

The $\delta^{13}C$ and $\delta^{18}O$ isotope signatures of carbonates are often used to reconstruct the depositional environment and temperature conditions during carbonate mineral formation, but they can also provide proper information about the diagenetic history of rocks (e.g., degree of diagenetic alteration, burial temperatures, intensity of water-rock interaction).

3.6. X-ray fluorescence (XRF) spectrometry

The XRF analyses were conducted by Dipl.-Ing. Judith Jernej, on a PANalytical PW 2404 X-ray fluorescence spectrometer at the TU Graz. Sample (pre-)treatment was the same as in Brown (1973). The analytical error was determined to be < 2 wt.% for major components and < 0.5 wt.% for minor components, respectively. This method is routinely used to determine the geochemical composition of bulk samples.

4. Results

4.1. Petrographic description of limestone and dolostone horizons

The classification of the main limestone microfacies types was done according to the scheme of Dunham (1962); the classification of the calcite cement based on Flügel (2010).

The studied section starts with massive micritic limestone, denoted as the Lower Limestone Unit (LLU), which is only slightly weathered. The rock color is light grey, but some intercalated (disaggregated and unconsolidated) clayey layers are somewhat darker. The LLU is followed by a dolomitic limestone, denoted as the Lower Dolostone Unit (LDU). Beds from the LDU are greyish to yellowish-brown and their surfaces are intensively weathered. The LDU is followed by the massive Upper Dolostone Unit (UDU), which consists of almost pure dolomite. This unit is followed by another massive limestone: the Upper Limestone Unit (ULU). Single beds from these four superunits do not differ significantly in petrography, and thus their characteristics are summarized below.

Note that samples A, C, D and E correspond to the LLU; samples H and I refer to the LDU, samples K, L and M reflect the UDU, and finally sample O and Q are representative for the ULU. Representative CL-images of the above superunits are provided in the appendix (Figure A4 - A6).

4.1.1. Lower Limestone Unit (LLU)

Samples from the LLU comprise greyish, yellow-brownish when weathered, wackestones to packstones. They form dense and massive limestone beds with a micritic fabric. Samples A and B consist of around 10-20% bioclasts, mostly crinoids and Mollusca. In thin section, quartz and undifferentiated clay minerals can be found. In samples C to G, the amount of bioclast debris increases to 20-30%, and some of them are filled with secondary calcite cement (see below). Single beds from the LLU have a vertical thickness from 0.5-1 m.

Most of the fossils from this section are recrystallized and filled with different calcite cement generations, which also replace micritic matrix and/or occupy voids. Three types of calcite spar were identified in sample C:

- Granular calcite cement consists of void-filling calcite crystals, about 5 to 20 µm in size, which fill former pores.

- Fibrous calcite cement is typically fine- to medium-sized, but single crystals extend up to a few millimeters in length. Most calcite crystals thus show a length elongation, usually parallel to the c-axis. The shape of the crystals is needlelike to columnar (the aspect ratio is >6:1).
- Blocky (equant) calcite cement consists of medium- to coarse-grained crystals without any preferential orientation. These crystals typically replace primary aragonite shells or clog remaining pore space. Their grain size is >20 µm.

In sample D, two additional calcite cement types were detected:

- Micritic calcite-envelopes occur as microcrystalline calcite around a progressively recrystallized bioclast or peloid.
- Dogtooth calcite cement forms scalenohedral or rhombohedral calcite crystals with an acute-angled side. The crystals are a 10-100 µm in length with an acute top.

4.1.2. Lower Dolostone Unit (LDU)

The LDU consists of massive, partly dolomitic, limestone and some (but rather thin) dolostone beds. Sample H consists mainly of dolomite, only small amounts of quartz can be found and no calcite was detected. The dolomite grains are rhombic, euhedral, and ~10-20 µm in size. The fabric is a sleeve to peloidal mosaic (after Flügel, 2010). Figure 4 displays the fine-grained and highly porous dolostone from the lower part of the LDU. The above bed is a calcitic dolostone (sample I), which consists of a fine-grained dolomitic matrix that is interrupted by a ~200 µm thick calcite vein. The calcite vein consists of blocky calcite spar, which is surrounded by Fe(hydr-)oxides (see Figure 4). The samples from the LDU are highly porous, intensively weathered and have a bright grayish to yellow color.
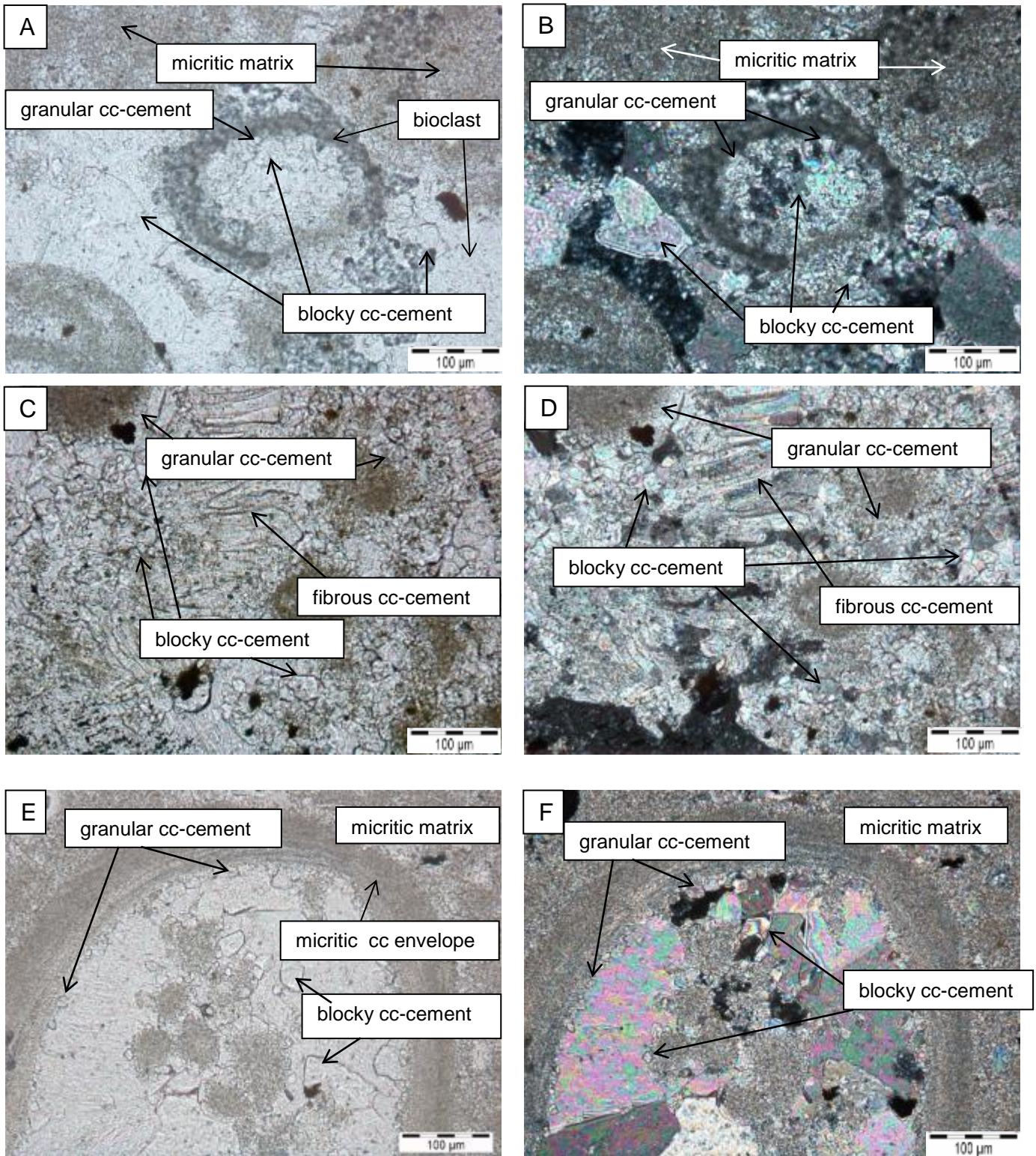
Figure 3: Thin section photomicrographs of samples from the LLU. Wackestones and packstones with undifferentiated bioclast debris and different generations of calcite cement (cc-cement) are visible: granular, blocky and fibrous cc-cement (A, C, E) occur together with micritic matrix. Crossed Nicols are on the right (B, D, F).
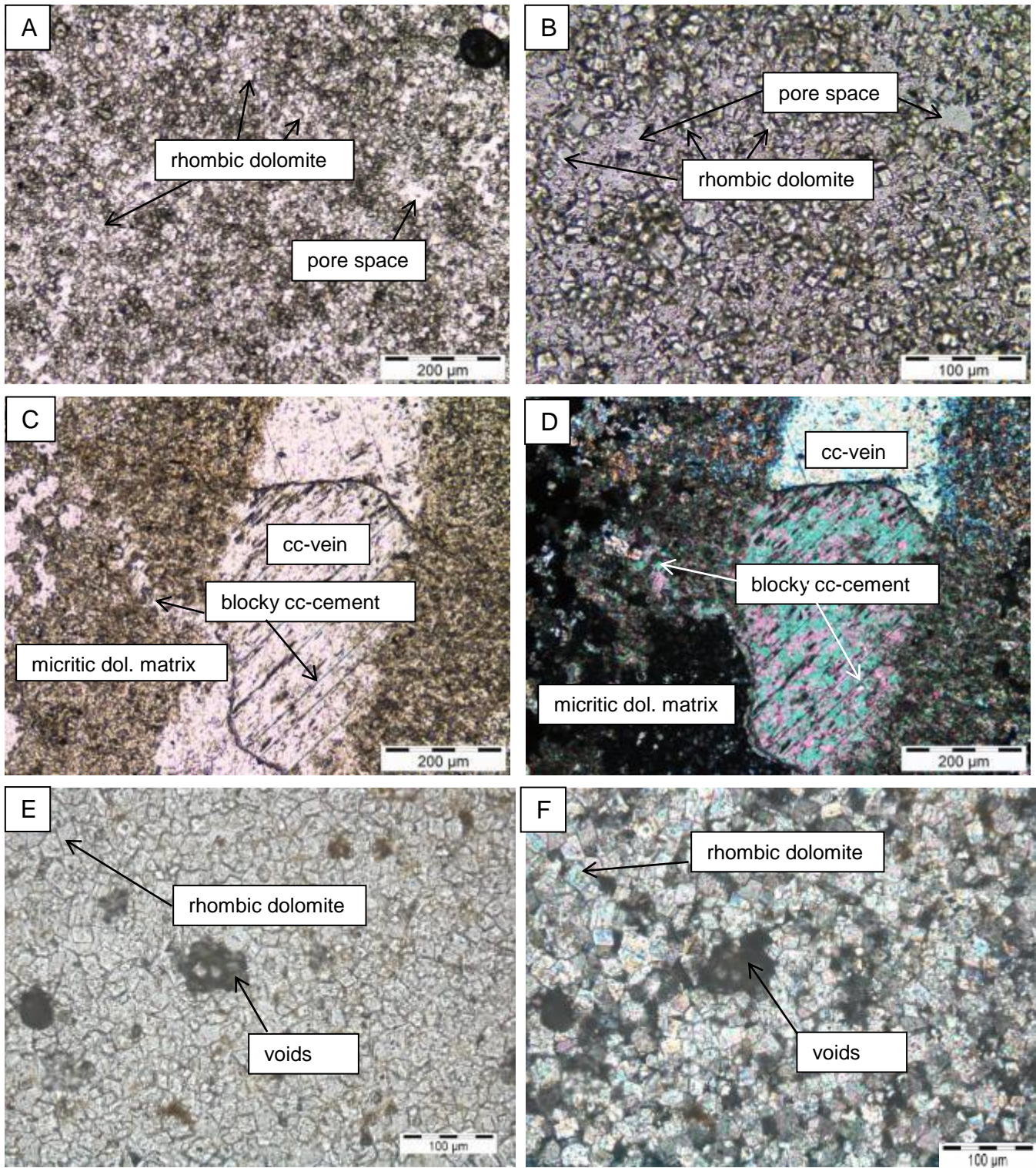
Figure 4: Thin section photomicrographs of representative samples from the LDU and UDU. Rhombic dolomite crystals (~10 μm) dominate in the lower part of the LDU (A, B). Calcite veins can be rarely found in fine-grained dolomite on top of the LDU (C), 2N (D). Rhombic dolomite grains with an average size of about 20 μm dominate towards the top of the UDU (E) and 2N (F).

16

4.1.3. Upper Dolostone Unit (UDU)

This unit covers dense and massive dolostone beds that are cut (on top) by a 4 cm thick clayey layer. Optical microscopy revealed that the almost pure dolostone consists mainly of equigranular dolomite crystals within a size of ~30 μm (Figure 4). Calcite, Fe(hydr-)oxides and quartz are scarce.

Above the clayey layer the main dolostone occurs, with a thickness of about 40 cm. This thick horizon is termed "Wasserbank" (Fischer, 1991) - a highly porous rock. It consists mainly of dolomite. On the bottom of the "Wasserbank" sequence, the euhedral dolomite grains are around 20-30 μm in size, whereas the dolomite grains in the top layers are around 20-50 μm in their largest dimension.

Samples from the UDU have a brownish to pink color, and a weathered surface. Individual dolostone beds have a slightly smaller thickness (0.2-0.5 m) compared with the beds from LLU and ULU.

4.1.4. Upper Limestone Unit (ULU)

The ULU consists, similar to the LLU, of micritic limestone (mainly packstones and to a minor amount wackestones) that contain bioclast debris in various quantities. Single beds from this unit show slightly weathered surfaces. The thickness of the beds is around 0.5-0.8 m. Abundant secondary calcite spar was identified in thin sections, and here micritic envelopes as well as granular and blocky cc-cements dominate. The transitional contact zone between the UDU and the ULU is characterized by a sharp (partly erosive) surface. Thus, it is not surprising that samples from the ULU do not contain dolomite. Besides different generations of calcite spar, some quartz grains and undifferentiated clay minerals were found.

4.2. Mineralogical composition of Oker carbonates

The quantitative mineralogical composition of the investigated samples, estimated by the relative peak height of the XRD-patterns is given in the appendix (Table A-2) – detailed qualitative calculations of the mineral composition were done by Andre Baldermann, MSc. The corresponding powder XRD patterns are shown in Figure A-1 (Appendix). The samples from the LLU consist mainly of low-Mg calcite (> 95 wt.%), in addition to small amounts of quartz and detrital clay minerals such as illite, chlorite and kaolinite (each <3 wt.%). This almost pure limestone section is followed by the LDU, which starts with a thin but almost pure dolostone comprising >80 wt.% of non-stoichiometric dolomite. Above this single dolostone layer, partly dolomitized limestone occurs, which generally consists >80 wt.% of low-Mg calcite and 5-10 wt.% of Ca-excess dolomite, with minor proportions of quartz (2-6 wt.%), clay minerals (< 5 wt.%) and Fe-(hydr)oxides (<2 wt.%) (samples I and J). The UDU contains >90 wt.%

of non-stoichiometric dolomite and 5-10 wt.% of quartz and clay minerals (samples K-N). Samples from the ULU finally consist of 90-95 wt.% of low-Mg calcite and 5-10 wt.% of quartz, clay minerals and Fe-(hydr)oxides (samples O-R).

The Mg-content in calcite as well as the dolomite stoichiometry was calculated after equation 3 (see above). These data are reported in Table A-3 (Appendix). It was recognized that the LLU and the ULU comprise of low-Mg calcite (0.4-2.3 mol% $MgCO_3$). The dolomites from the LDU and UDU show Ca-excess (44.8 to 45.4 mol% $MgCO_3$) and are thus non-stoichiometric. The degree of cation order in dolomite, in respect to dolomite superstructure, ranges from 0.38 to 0.86.

4.3. Geochemical composition of Oker carbonates

The EMPA were conducted on 7 samples. The following samples were analyzed from their respective superunits: (i) LLU (C, D and E), (ii) LDU (I), (iii) UDU (K and M) and (iv) ULU (Q). On 5 of these 7 samples, elemental spot analysis was conducted.

4.3.1. Lower Limestone Unit

Backscattered electron (BSE) images of mud- to wackestones show bioclasts and surrounding matrix as well as different calcite cement generations that occupy former pore spaces and voids in partly recrystallized bioclast debris. The BSE image of sample C (see Appendix Figure A-7) shows three calcite generations: cc_1 is a blocky calcite, which replaces biogenic calcite (e.g., shells from bioclasts), cc_2 is a fibrous calcite cement, which is not part of the bioclast material but occurs as a vein filling and cc_3 is a micro-sparite that replaces the primary shell material and in particular (organic-rich) peloids. Besides these calcite generations, Fe(hydr-)oxides were identified. In the element distribution maps of Ca and Mg, these three calcite generations are also visible, as evident from the varying Mg/Ca ratio in the calcite cement phases. For example, Mg is partly depleted in cc_1 in respect to the micrite, cc_2 and cc_3.

A representative BSE image and related element distribution maps of sample D are shown in Figure 5. Similar to sample C, two calcite cement types were detected: granular and blocky calcite, which occur together with micrite and primary (largely unaltered) shell material. The primary shell material is porous and slightly enriched in Fe, similar to the matrix. The latter also shows a Si enrichment that reflects small occurrences of clay minerals.

Sample E shows a negative correlation between the Ca and S distribution. Areas which are S enriched, are Ca poor and vice versa (see Appendix Figure A-8). The blocky calcite cement seems to be enriched in Ca, compared with the primary shell material. However, this effect can be explained by the different grain sizes and high

porosity, as the composition of calcite phases is largely homogenous, $(Ca_{0.93-0.996}Mg_{0.003-0.03}Mn_{0-0.054}Sr_{0-0.001}Na_{0-0.001}Fe_{0-0.001})_{0.99-1.0}[(C_{0.94-1}S_{0-0.004})O_3]_2$.

4.3.2. Lower Dolostone Unit

The element distribution maps of Fe and S of fine-grained dolomites from the LDU (sample I) clearly show that the dolomite crystals are zoned (Figure 6). They have a Mg-rich core indicative of dolomite, $(Ca_{0.99-1.13}Na_{0.002-0.004}Sr_{0-0.001})_{0.99-1.13}(Mg_{0.86-1}Fe_{0-0.02}Mn_{0-0.006})_{0.86-1.03}[(C_{0.96-0.995}S_{0.004-0.08})O_3]_2$, followed by a Mg-poor inner rim (low-Mg calcite) and a subsequently deposited Mg-rich outermost zone (high-Mg calcite), $(Ca_{0.49-0.97}Mg_{0.02-0.50}Mn_{0-0.003}Sr_{0-0.001}Na_{0-0.003}Fe_{0-0.01})_{0.51-1.484}[(C_{0.92-1}S_{0-0.19})O_3]_2$. Calcite occurs as a vein, which cuts the fine-grained dolomite. The calcite cement seems to be blocky. The Ca distribution map virtually shows no chemical heterogeneities in single calcite grains, whereas the Mg distribution is not completely homogeneous. It seems that some areas, dominated by calcite spar, are slightly enriched with respect to Mg. The dolomitic area is highly porous.

4.3.3. Upper Dolostone Unit

Samples from the dolomitic "Wasserbank" show the transitional contact zone between limestone and dolostone (in sample K). Two calcite cement generations were distinguished based on their Mg contents. The dolomite, $(Ca_{1.004-1.11}Na_{0.001-0.006}Sr_{0-0.001})_{1.005-1.11}(Mg_{0.86-0.98}Fe_{0-0.04}Mn_{0-0.002})_{0.86-0.99}[(C_{0.86-0.996}S_{0-0.003})O_3]_2$, does not show zonation. Some Fe-oxides and pyrite grains were identified based on the BSE images and element distribution maps of Fe and S. The dolomite grains are somewhat larger than those from the LDU, they are about 20 µm in size.

Samples L and M, which are located above the contact zone between the dolomitic limestone and the pure dolostone, consists mainly of dolomite, $(Ca_{0.97-1.14}Na_{0-0.006})_{0.97-1.14}(Mg_{0.86-0.99}Fe_{0-0.03}Mn_{0-0.01})_{0.76-0.99}[(C_{0.92-0.999}S_{0-0.2})O_3]_2$ and $(Ca_{1.03-1.24}Na_{0.001-0.006}Sr_{0-0.001})_{1.03-1.25}(Mg_{0.76-0.95}Fe_{0-0.02}Mn_{0-0.002})_{0.76-0.95}[(C_{0.98-0.998}S_{0.001-0.02})O_3]_2$, respectively. Calcite was not identified in this horizon. As shown in Figure 7, the dolomite grains are up to 40 µm in size, and have a rhombic crystal shape. Abundant pore space occurs between single grains. The dolomite grains typically have a Na- and S-rich core, which is followed by partly Fe-rich and S-rich rims, deposited in the alternating mode within single dolomite rhombs.

4.3.4. Upper Limestone Unit

Sample Q also comprises of different calcite cement generations that show many similarities to the samples from the LLU. The overall composition of calcite phases is $(Ca_{0.96-0.995}Mg_{0.004-0.03}\ Mn_{0-0.054}\ Sr_{0-0.008}Na_{0-0.002}Fe_{0-0.005})_{0.99-1.0}\ [(C_{0.995-1}S_{0-0.005}\ )O_3]_2$. Figure 8 shows a BSE image and different element distribution maps of sample Q. Especially the Mg distribution can differ significantly between Mg-rich micrite and biogenic calcite and Mg-poor calcite spar. Moreover, the matrix is enriched in Sr in respect to the recrystallized bioclasts. Granular calcite cement occurs within these bioclasts. Interestingly, Mg-poor areas within secondary calcite also seem to be S-enriched. In the BSE image, some peloids and "spongy" aggregates (probably biogenic material) can be detected.

4.3.5. Dolomite and calcite composition

Overall, 360 single spot analyses were conducted by EMP on the above samples. In the following chapter, the compositional data (see appendix Table A-4 for data summary) are presented and compared with structural formulae that were calculated each for calcite and dolomite.

Figure 9 shows a Mg/Ca cross plot that comprises all chemical data collected for the individual samples from the entire Langenberg sequence. Note that this Figure shows the calculated structural formulae and thus the axes are reporting the number of atoms (in this case Ca versus Mg) per formula unit (a.p.f.u.). Based on this correlation, a classification of the carbonates into low-Mg calcite (LMC), high-Mg calcite (HMC), and non-stoichiometric (Ca-excess) dolomite can be done. Ideal calcite and ideal (stoichiometric) dolomite are included for comparison. Most single spot analyses from the LLU and ULU plot well in the LMC field, a feature confirmed by the petrographic (thin section analysis) and mineralogical (XRD) data. Sample I (LDU: from the transitional contact zone between limestone and the pure dolostone), contains LMC, HMC, and non-stoichiometric dolomite. The pure dolostone horizon (samples K to M) comprise of non-stoichiometric dolomite, as also indicated by the XRD data. A slight tendency towards more stoichiometric dolomite is evident with the increasing thickness of the dolostone beds.

Interestingly, a negative, but linear correlation between the degree of cation order in dolomite (calculated on the basis of the XRD data) and the structural sulfur content in dolomite (derived from EMP data) was observed (Figure 10): This relationship indicates that structural sulfur (which is likely present as sulfate) can substitute for the CO_3^{2-} ion in the dolomite crystal lattice, thereby causing disordering effects, which lower the degree of cation order in dolomite. This might explain why most sedimentary dolomites formed in sulfate-loaded environments (e.g. seawater derived pore waters) are better represented by poorly ordered, non-stoichiometric proto-dolomites.
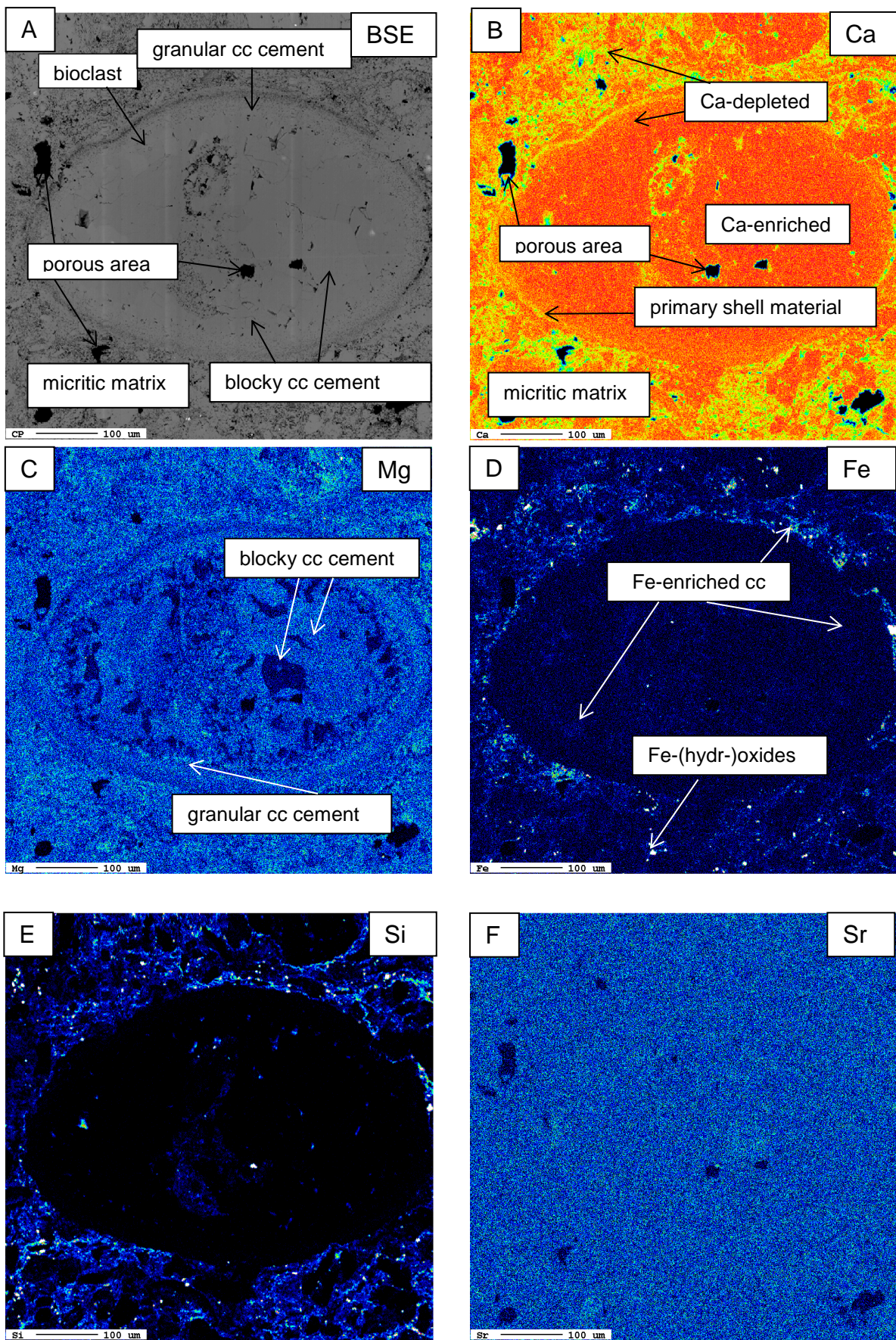
Figure 5: BSE image and element distribution maps of sample D: A) bioclast in micritic matrix, the bioclast is partly recrystallized and filled with various calcite (cc) cement generations. B) the micritic matrix contains more Ca than the recrystallized bioclast, the shell as well as the granular cc cement contain more Ca than the blocky cc cement. C) the blocky cc cement is Mg-depleted. D-E: Fe and Mg maps showing the presence of clay minerals and Fe(hydr)-oxides in the micritic matrix. F: Sr is homogenously distributed in sample D.
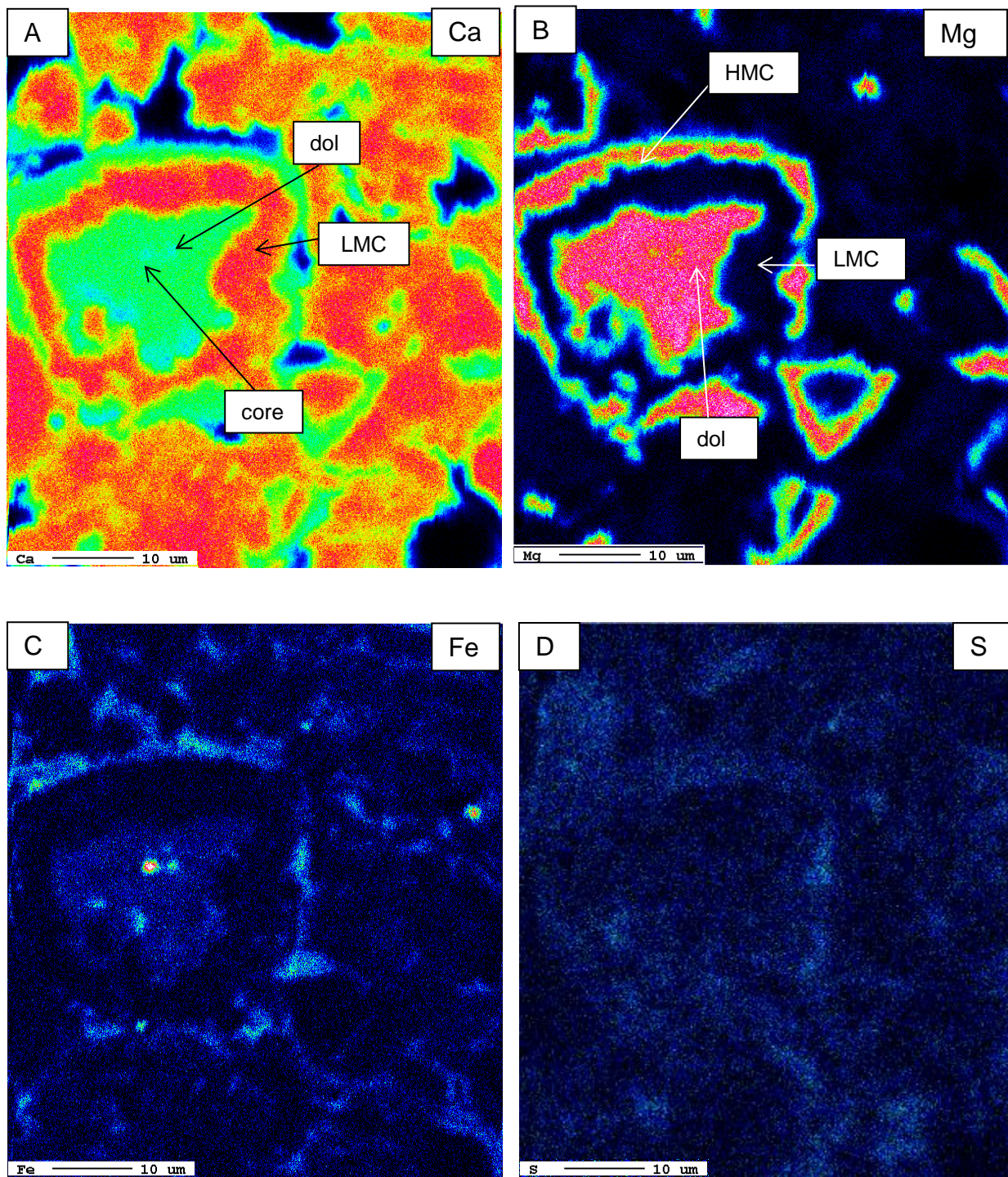
Figure 6: Element distribution maps of sample I: note the zoning of the grains, as evident from the Ca and Mg maps (A and B). A dolomite core is followed by a LMC rim and a subsequently deposited HMC rim. C-D) The Fe and S distribution coincides with the Mg distribution. The Fe and S enrichment in HMC may be caused by its higher porosity.
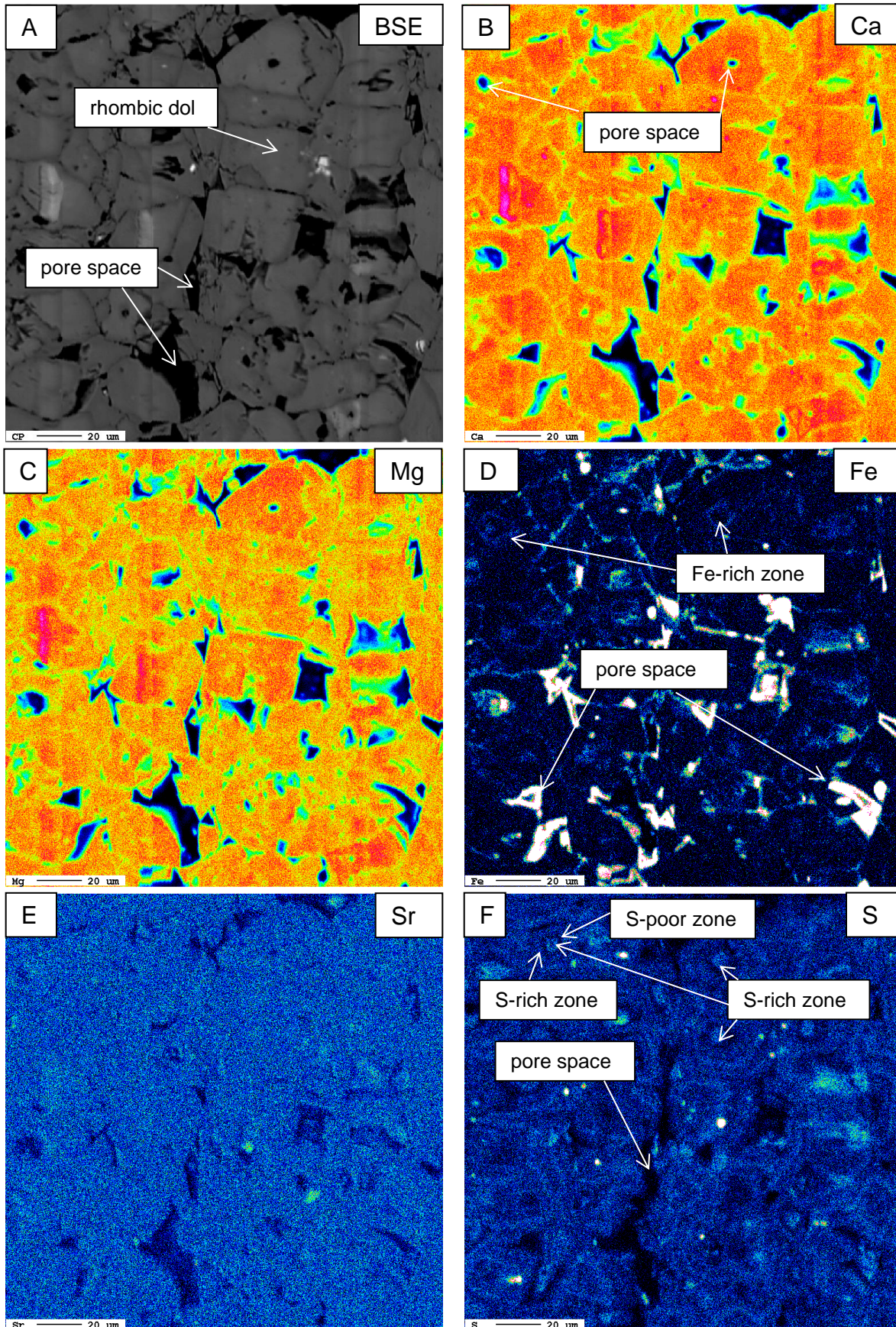
Figure 7: BSE image and element distribution maps of sample M: (A) Fine-grained, euhedral dolomite (dol) with high porosity. (B), (C) and (E) show the homogenous distribution of Ca, Mg and Sr with single dolomite grains. (D) and (F) Fe and S distribution; Note the enrichment of S in the dolomite cores and the alternating growth zoning of S and Fe in the dolomite rims. The higher amount of Fe in the pores is due to abundant Fe-(oxides)hydrates.

23
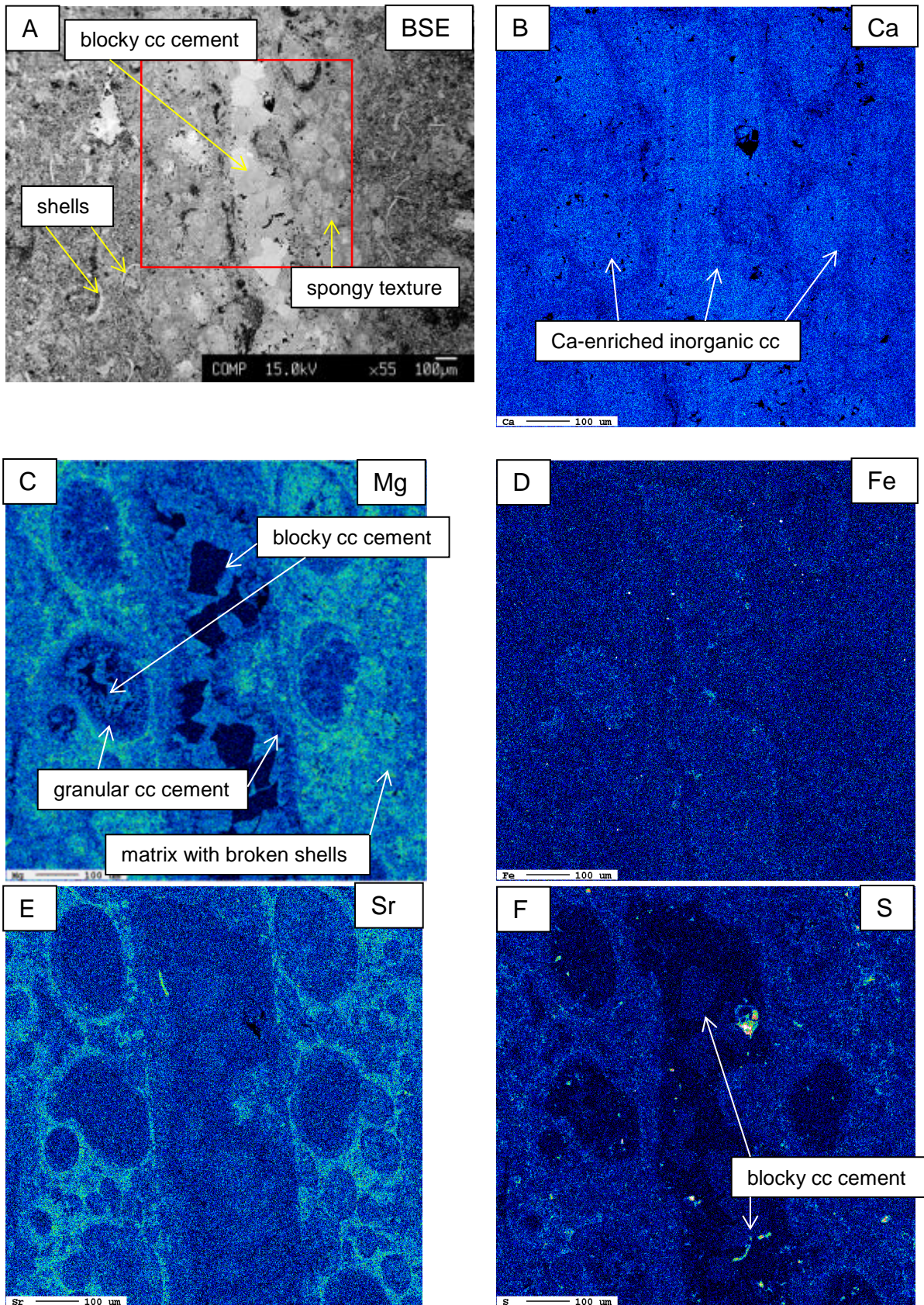
Figure 8: BSE image and element distribution maps of sample Q: A) micritic matrix occurs together with biogenic material (spongy textures) and secondary veins. Note two different cc-types: (1) blocky cc cement and (2) granular cc cement. B), D) and F) the calcite spar is Ca/Fe-enriched, but S-poor, in contrast to the micrite and biogenic calcite. C) and E) the blocky cc is Mg/Sr-poor and the matrix is rich in Mg and Sr.

4.3.6. Clay content

The clay mineral content in all samples was calculated based on the measured Al_2O_3 and SiO_2 concentrations, determined by EMPA. The clay mineral content varies only slightly throughout the investigated sequence, but is generally lower in the LLU and ULU (pure limestone) compared to the LDU and UDU (dolomitized limestone and pure dolostone). Especially in sample I (ULU), the proportion of detrital clay minerals is moderate to high, in contrast to the ULU, where detrital silicates are almost absent. Based on a correlation between the Al_2O_3 amount of roughly 0.02 wt.% and SiO_2 amount of 0.04 wt.% (Figure 11), most of the clay minerals incorporated in the micritic matrix and dolomite cores should refer to mixtures of kaolinite- and illite-type clay minerals. However, the sum of clay minerals present (as identified in the single spot analysis) in all samples does not exceed 0.8 wt.% (0.1-0.2 wt.% on average) and thus the calcite and dolomite compositional data reported above are not biased towards clay mineral contamination.
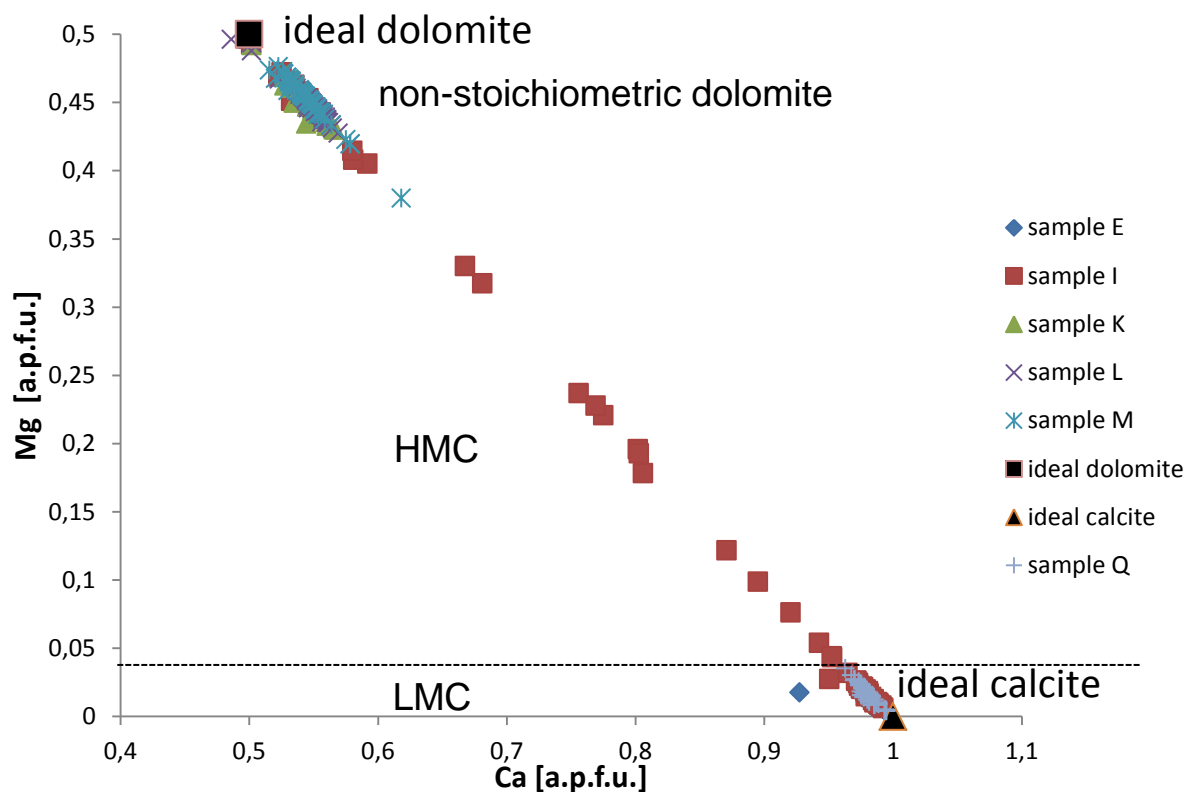
Figure 9: Ca vs Mg cross plot showing a variety of carbonate minerals from the investigated samples. Ideal calcite and ideal dolomite are implemented for comparison. Note the complexity of sample I (UDU: limestone-dolostone contact).
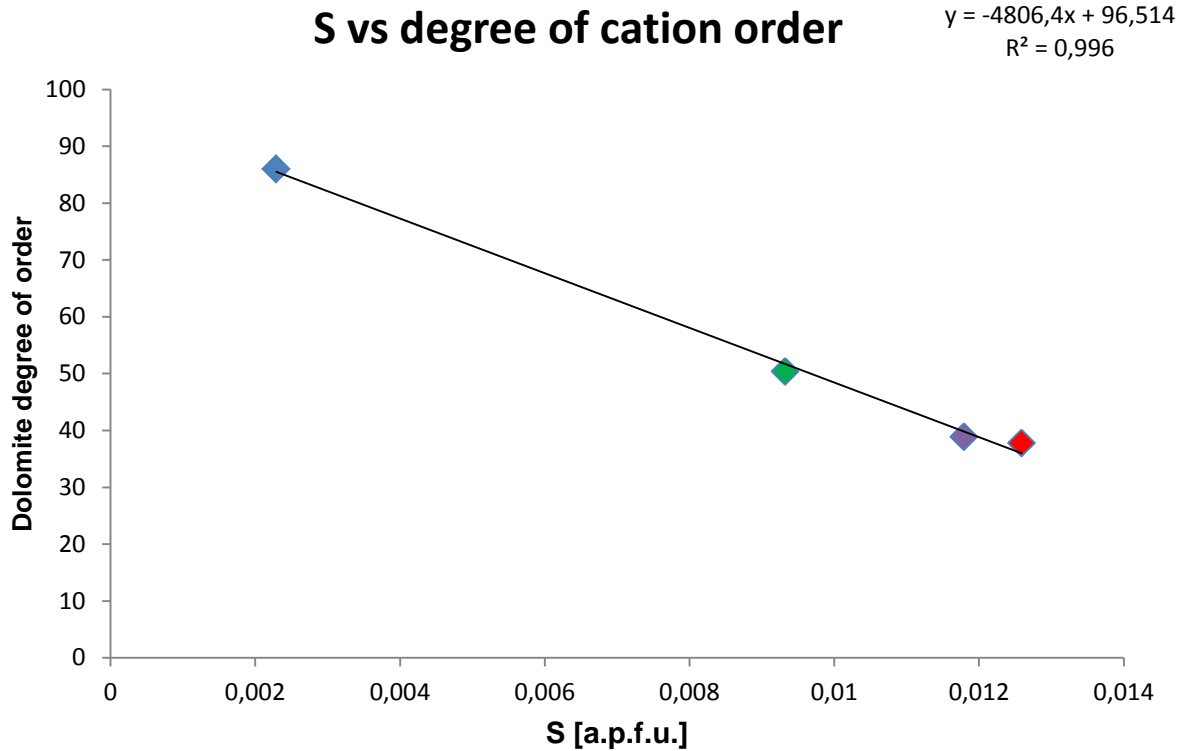
Figure 10: Correlation between the degree of cation order in dolomite based on XRD data and averaged S concentration, calculated from the EMP data. The blue icon shows the data from sample I, the red shows sample K, the green is L and the purple one is sample M.
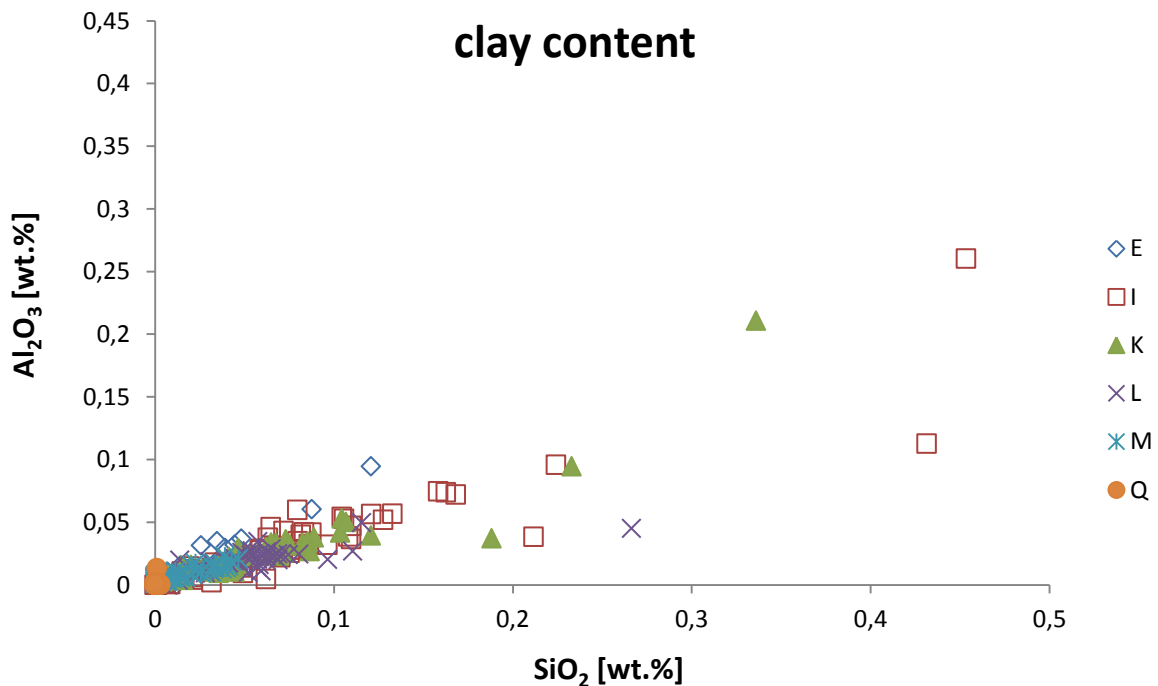
Figure 11: SiO_2 vs Al_2O_3 plot illustrating the effect of clay mineral contamination in the EMP spots. Sample E and Q from the LLU and ULU have low concentrations in these minerals. Especially I and K from the LDU and the lower part of the UDU respectively, have the highest amount of clay minerals. Corresponding data can be found in the Appendix (Tab. A-4).

4.4. Bulk chemical composition of Oker carbonates

The XRF results confirm the previous results from both the XRD analysis and the EMP analysis. Based on the anti-correlation of MgO and CaO contents (Figure 12), dolomitized limestone (LDU) and dolostone beds (UDU) can be easily distinguished from almost pure limestone (LLU and ULU). Moreover, the SiO_2 and Al_2O_3 contents (and to a minor amount the K_2O and Fe_2O_3 contents) correspond to the amount of silicates and Fe-(hydr)oxides present in the bulk samples. The silicates occur mainly in the form of quartz.

The CaO/MgO ratio shows that the LLU and the ULU are basically consisting of low-Mg calcite. The dolostone unit can be divided into two subgroups, namely the LDU and the UDU. The LDU, starts with a single dolostone bed, which is followed by two dolomitic limestone beds (Sample I and J). The LLU and the ULU show a rather similar chemical composition, except for the elevated Sr content of sample Q (from the ULU), which is attributed to comparatively high amounts of (Sr-rich) biogenic calcite. This slightly increased Sr content was also detected by EMPA. In addition, a clear dependence between the increasing MgO+CaO contents and high LOI and $SiO_2+Al_2O_3+K_2O+Fe_2O_3$ contents was detected. These relationships can be best explained by the coexistence of dolomite ± minor amounts of calcite, Fe-oxyhydrates and silicates in particular in the partly dolomitized samples and pure dolostone. Especially in the LDU the silicate phase content is comparatively high, but decreases gradually towards the UDU and ULU. SO_3 only occurs in more relevant amounts (the average SO_3 content ranges from 0.1-0.3 wt.%) in sample H, where it is related to the occurrence of pyrite (FeS_2); as identified by optical microscopy.

4.5. Oxygen and carbon isotopic composition of Oker carbonates

Figure 13 shows a $\delta^{18}O/\delta^{13}C$ cross plot that also includes average values and/or ranges for Upper Jurassic limestone, Upper Jurassic seawater and Upper Jurassic sabkha dolomite. The samples from the LLU have $\delta^{18}O$ values from -2.87 to -1.66‰, VPDB and $\delta^{13}C$ values between -0.65 and 1.30‰, VPDB, similar to Upper Jurassic platform carbonates (Reinhold, 1998). Overall, no systematic trend in the isotopic signatures was observed throughout the Langenberg sequence. The dolomitic limestone of the LDU comprises the lightest isotopic signals of the whole sequence, they range from -1.22 to -1.12‰, VPDB, of $\delta^{13}C$ and from -5.55 to -5.07‰, VPDB, of $\delta^{18}O$. In contrast, the isotopic signatures of dolomite from the UDU range between -0.11 and 0.69‰, VPDB, of $\delta^{13}C$ and 1.65 to 2.22‰, VPDB, of $\delta^{18}O$, and thus they plot well in the range of Upper Jurassic platform dolomites and modern sabkha dolomites (e.g. Budd, 1997, Reinhold, 1998, Warren, 2000). The samples from the

ULU finally show similar $\delta^{18}O$ values than the LLU, but the $\delta^{13}C$ values are slightly lower. The $\delta^{13}C$ values range from -3.96 to -1.64‰, VPDB, and the $\delta^{18}O$ values are between -3.40 and -1.79‰, VPDB. The $\delta^{13}C$ values decrease from the bottom to the top of this interval; the $\delta^{18}O$ signals do not show any trend.
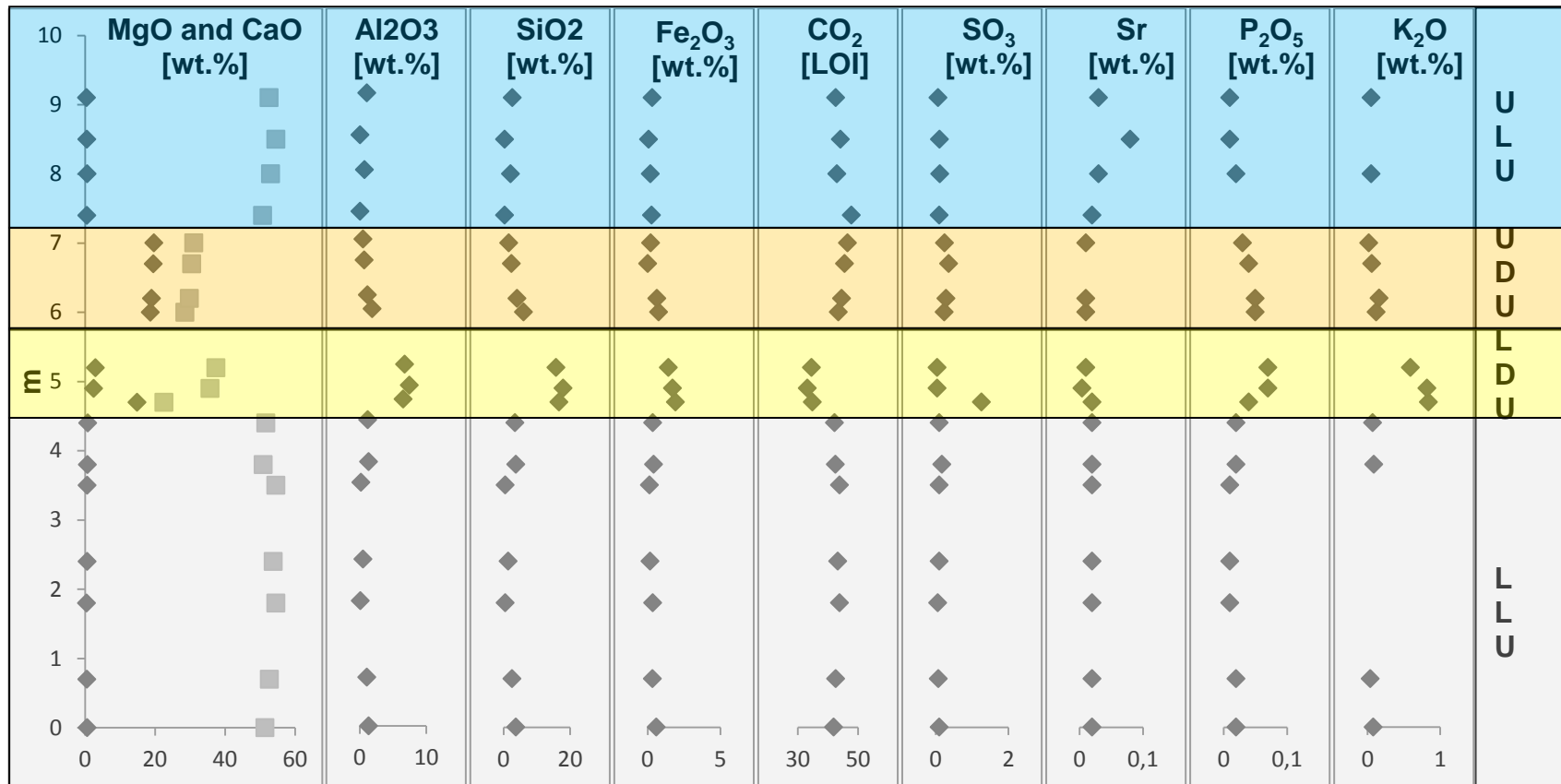
Figure 12: Compilation of bulk rock geochemical data, received from the XRF analysis. The MgO (rhombs) and CaO (squares) data were summed up as they directly reflect the dolomite and calcite content of bulk rock samples. The data are given in weight percent (wt. %) and CO_2 is given in loss on Ignition (LOI).
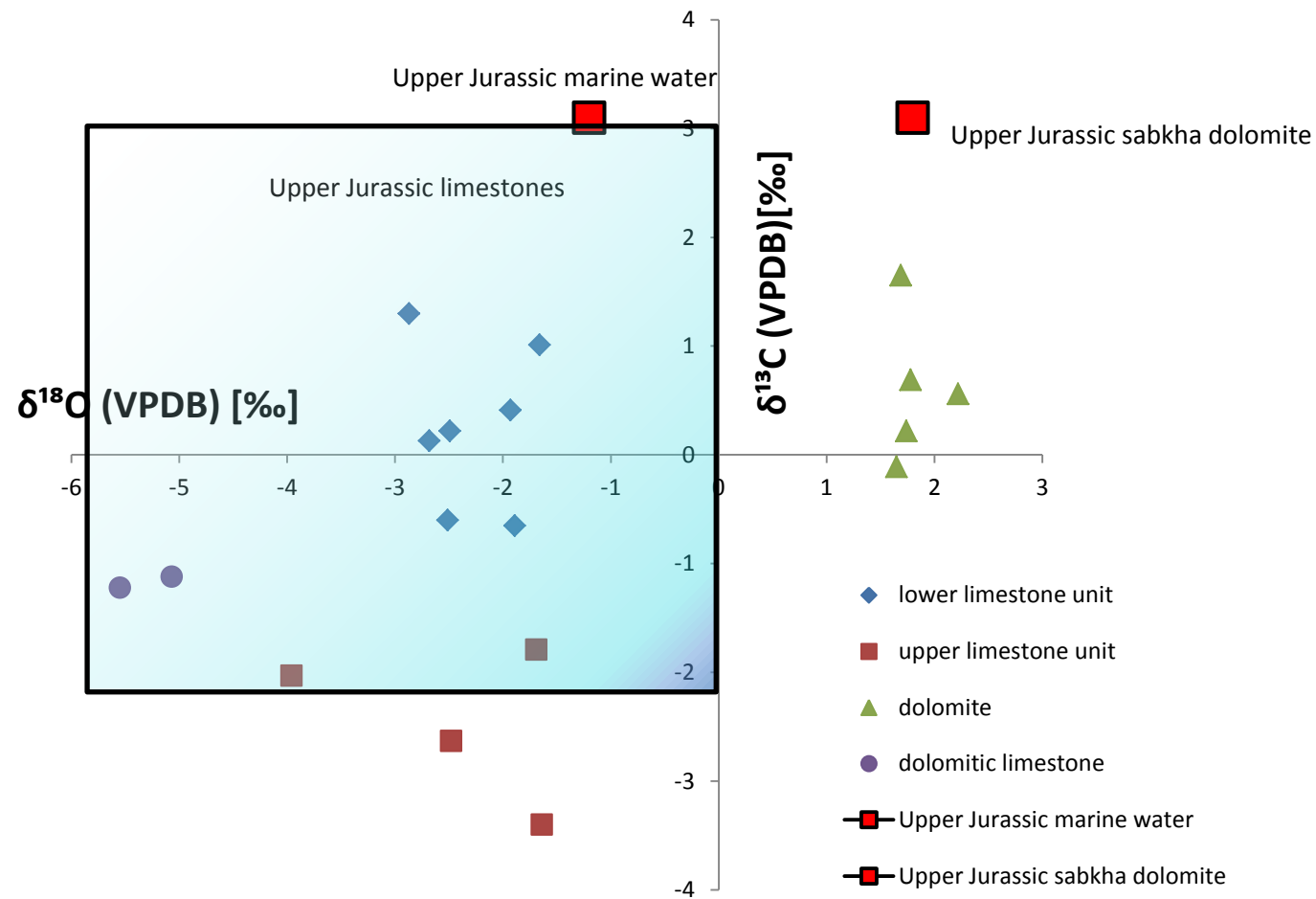
Figure 13: Comparison of the $\delta^{18}O$ and $\delta^{13}C$ data. The light blue square marks the field of Jurassic limestones (Reinhold, 1998). Most of the limestone samples from Oker plot well in this area. The Oker dolomites show similar $\delta^{18}O$ values compared to Upper Jurassic sabkha dolomites. The dolomitic limestones from the LDU (sample I and J) have the lowest $\delta^{18}O$ values, suggesting alteration of the carbonates occurred during burial diagenesis.

5. Discussion

Combined petrographic, mineralogical, geochemical and stable isotopic data support evidence that cyclic and abrupt changes in the depositional environment occurred during carbonate mineral formation at Oker, followed by a highly complex diagenetic history. These relationships are discussed in the following chapters.

5.1. The depositional environment at Oker

At the Oxfordian/Kimmeridgian boundary, Central Europe was covered by a (shallow) marginal sea, partly connected to the Upper Jurassic Thetys Ocean, wherein stable carbonate platforms and numerous (semi-confined) shallow-water basins existed (Hug, 2003; Thierry, 2000). The formation of these shallow carbonate platforms was triggered by a worldwide transgression of the Thethys Ocean during the Early and Late Kimmeridgian. These shallow-marine basins provided important accommodation space for carbonate mineral deposition; and carbonate production in the Kimmeridgian was highly effective due to the location of the Oker carbonate platform at tropical to subtropical latitudes. During the Lower to Late Kimmeridgian, a stable carbonate platform setting at Oker evolved, where alternating beds of argillite, limestone and dolostone were deposited (Thierry, 2000).

The beds from the LLU consist of micritic limestone (wacke- to packstones) that were formed in a shallow-water environment, characterized by an overall low hydrodynamic regime as it occurs in the inner barrier reef setting of a carbonate ramp (Baldermann & Nickel, 2012). The barrier reef (Exogyra micro-reefs) and ooid shoal facies developed during the Lower Kimmeridgian and their occurrence in the Langenberg profile denote the abrupt transition from high-energetic to low-energetic hydrodynamic conditions. However, during the Middle Kimmeridgian, a shallow lagoonal setting was established, as indicated by the deposition of (partly clay mineral rich) micritic calcite. The severely destroyed bioclast material indicates minor winnowing action and related reworking of the fine-grained sediments. Due to the strong disintegration of bioclasts it is often problematic to identify primary fauna in thin section. However, most of the fossils are strictly marine (Fischer, 1991) and comprise of diverse mollusks, brachiopoda, and echinoderms (although some of them were reworked from the open marine barrier reef facies and thus represent allochthonous biogenic components). During the Middle to Upper Kimmeridgian, intense evaporation took place in the lagoonal environment at Oker resulting in a salinity increase, as indicated by hypersaline faunal elements, like internal moulds of Trigonia (Fischer, 1991). High evaporation degrees might have also caused an elevated Mg/Ca ratio in the artificial seawater solutions, conditions that are well-known to cause alteration of limestone and subsequent transformation into dolomite

(Deffeyes et al., 1965), in a sabkha-like depositional environment. Although only few primary rock textures and microfacies features (e.g. lamination) of limestone precursors are preserved in the LDU and the UDU, the secondary dolomite was likely formed by early diagenetic replacement of limestone, rather than being formed by direct precipitation from (slightly) evaporated seawater under sabkha conditions. Finally, during the Upper Kimmeridgian the shift back to more open-marine conditions is indicated (Fischer, 1991; Baldermann & Nickel, 2012) by the deposition of micritic limestone with Skolithos of the ULU.

5.2. Diagenetic history and evolution of Oker carbonates

5.2.1. Limestone (micrite and calcite spar)

To understand the ambient environmental conditions of carbonate mineral formation as well as potential diagenetic alteration features of the sequence, early diagenetic rock textures and (isotope)geochemical signatures need to be distinguished from later diagenetic overprinting. Soon after the deposition of sediments, metastable phases like aragonite (although not observed at Oker) and HMC are dissolved through intense interaction with seawater derived pore fluids that are typically undersaturated with respect to those carbonate phases. This process takes place during the earliest stage of diagenesis and is often influenced by mixing of marine and meteoric waters (Flügel, 2010). Despite inducing dissolution phenomena, the above water mixing causes micritization, which is considered to be one of the first diagenetic processes that occurs directly at the sediment-water interface (Mahboubi *et al.,* 2010). At Oker, micritic matrix but also micritic envelopes were formed around the (decaying) bioclast debris and originally organic-rich peloids. In marine-diagenetic environments and lagoonal sediments, micrites (LMC carbonates) are most abundant (Schlager and James, 1978).

During the more advanced stages of marine diagenesis, calcite cement is typically formed, particularly when the pore water becomes oversaturated with respect to calcite (Flügel, 2010). In the limestone beds (LLU and ULU) at Oker, fibrous, granular and blocky cements were detected. These cc-cement types are indicators for carbonate mineral precipitation during meteoric-phreatic diagenesis. Micritization and calcite cement formation in a shallow burial environment are also supported by the chemical composition of the carbonates: they are Fe- and Mn-poor and Na- and Sr-rich, the opposite trend would indicate formation during deep burial diagenesis.

Another argument supporting the idea of shallow-diagenetic calcite cement formation at Oker is the occurrence of granular to blocky calcite spar that occupies former pore space in bioclasts. In particular, variations in the Ca and Mg contents in the subsequently deposited calcite cement generations indicate precipitation from

chemically highly dynamic (and still evolving), seawater-derived pore water solutions. As seen in the EMP data, no "homogenization" of the chemical composition of the calcite cement types took place, suggesting preservation of pristine signatures, which is also typical for shallow-burial diagenesis.

Another approach to decipher early and late diagenetic processes is based on $\delta^{18}O$ and $\delta^{13}C$ isotopic signatures of carbonates. The $\delta^{18}O$ and $\delta^{13}C$ values of the different beds from the LLU and ULU are nearly identical. In the LLU, the $\delta^{18}O$ values ranges from -2.87 to -1.66‰, VPDB, and in the ULU ranges from -3.40 to -1.79‰, VPDB. The $\delta^{13}C$ values ranges in the LLU between -0.65 and 1.30‰, VPDB, and in the ULU from -3.96 to -1.64‰, VPDB. This suggests direct carbonate mineral precipitation from Upper Jurassic seawater. According to e.g. Husinec & Read (2010), Reinhold (1998), and Price and Sellwood (1994), the $\delta^{18}O$ composition of the Jurassic mean seawater is slightly lighter than modern seawater: a $\delta^{18}O$ value from -1 to -1.2‰, VSMOW, is widely accepted and seems to be also applicable for Oker. This lower $\delta^{18}O$ isotopic composition of Upper Jurassic seawater can be explained by a "greenhouse-like" climate (and ice-free polar caps) during the Kimmeridgian (e.g. Colombié et al., 2011). In the literature, the $\delta^{18}O$ values of diagenetically unaltered marine platform carbonates typically range between -1.85 and 0‰, VPDB, (Ribeloulleau et al., 1998; Wierzbowski, 2004), similar to the Oker limestones. On the other hand, Colombié et al. (2011) showed that $\delta^{18}O$ values from -8.7 to -2.2‰ VPDB indicate burial diagenetic overprinting.

In summary, both the $\delta^{18}O$ and $\delta^{13}C$ signatures of most of the Oker limestones fall within the range of unaltered Upper Jurassic marine platform carbonates (e.g. Reinhold, 1998 and Husenic and Read, 2010). Only the samples from the transitional contact zone between the lower limestone unit and the dolomitized limestone (UDU) show some indications of local alteration that occurred during (late diagenetic) and/or meteoric diagenesis, as their $\delta^{18}O$ and $\delta^{13}C$ signatures range from 1.65 to 2.22‰, VPDB, and -0.11 to 0.69‰, VPDB, respectively.

It can be concluded that the pure limestone (LLU and ULU) from Oker largely preserved its pristine isotopic signatures.

The formation temperature of limestone was calculated, based on the $\delta^{18}O$ values. For the limestones from the LLU and ULU consisting basically of calcite, the equation by Kim & O'Neil (1997), corrected for conventional CO_2-calcite acid fractionation factor of 1.01025 was used. For the calculation a $\delta^{18}O$ value (V-SMOW) of the ancient precipitating seawater of -1‰ was assumed. For the LLU carbonates, the formation temperature ranges between 18.8 and 24.4°C. In the ULU the formation temperatures were calculated to be slightly higher 19.4 and 26.9°C.

5.2.2. Dolostone

Due to high evaporation degrees in the (confined) lagoonal setting at Oker during the Middle to Upper Kimmeridgian, the Mg/Ca ratio of the dolomitization fluid became progressively higher, resulting in partial (LDU) to almost complete (UDU) dolomitization of the pre-existing limestone under generally reducing conditions. The dolomites are non-stoichiometric (54.5 to 55.2 mol% $CaCO_3$) and generally poorly ordered (0.38 to 0.83), characteristics that are indicative of sedimentary dolomite formed in low-temperature environments. The single dolomite grains are euhedral, about ~10-50 μm in size, and often show distinct growth zonation patterns, comprising of Na/S-rich cores and partly Fe-rich rims.

In thin sections, small amounts of recrystallized micrite and euhedral pyrite were found especially in the LDU, suggesting local alteration of the limestone and dolomite occurred (a feature confirmed by the significantly lower $\delta^{18}O$ signatures, see above). The EMP analyses proof the coexistence of dolomite cores and subsequently deposited LMC and HMC layers in this altered bed. It is most likely that calcite veining during late burial diagenesis caused the alteration of fine-grained dolomite (Figures 4 and 6).

Biogenic material (e.g. shells) is absent in the pure dolostone from the UDU, indicative of almost complete dolomitization of limestone by early diagenetic replacement. The $\delta^{18}O$ values of these dolomites range from 1.65 to 2.22‰, VPDB, and their $\delta^{13}C$ values range from -0.11 to 1.65‰, VPDB, respectively. This isotopic composition and the small grain size of the dolomites indicate that dolomitization proceeded soon after limestone deposition during shallow-burial diagenesis (Reinhold, 1998). Moreover, the relatively high $\delta^{18}O$ values of Oker dolomite agree well with that of Upper Jurassic sabkha dolomites (Husinec & Read, 2010), formed in sabkha-like environments. If the dolomites had been formed simultaneously with the calcite from the LLU, (the oxygen equilibrium fractionation between co-precipitating calcite and dolomite is 3‰) (Budd, 1997), one would need to explain why the $\Delta\delta^{18}O_{Cc-Dol}$ is ~3-5‰. The latter feature clearly indicates that the dolomites precipitated from an evaporitic brine (Rameil, 2008).

The formation temperature of the Oker dolomite was calculated after Friedman and O´Neil (1977), assuming a $\delta^{18}O$ value of -1‰, SMOW, for Jurassic seawater:

$$1000\ln(\delta^{18}O_{dol} - \delta^{18}O_{water}) = (2.78x10^6/T^2) - 2.89 \qquad \textit{(eq. 5)}$$

For the LDU and for the ULU a temperature of 28 °C was obtained.

Since the dolomitizing fluid was likely a brine, the formation temperature of the dolomites might have been somewhat higher than the above calculated values.

The zonation patterns of the dolomites indicate that cyclic and abrupt changes in the chemical composition of the dolomitization fluids occurred during the progressive dolomitization of limestone.

The occurrence of pyrite in the dolomitized sequence and the relicts of lamination indicate that the dolomitization reaction of pre-existing limestone took place under reducing conditions. In summary, the dolomites from the LDU and UDU are considered to be an early replacement product of pre-existing (Mg-)calcite (and aragonite) precursors (Malone *et.al.*,1994).

5.2.3.   Dolomite classification

Reinhold (1998) describes six types of dolomite based on the study of sedimentary rocks from the Swabian Alps. The two relevant dolomite types are outlined below. Matrix dolomite type A is a non–stoichiometric, zoned dolomite that occurs together with calcite. It is comparable to the Oker dolomite from the LDU. However, matrix dolomite type A, as described by Reinhold (1998), is fine- to coarse-grained (~50-800 µm in size) and thus generally coarser than the dolomites from the LDU that range from 5 to 20 µm in size.

The second relevant dolomite type (Reinhold, 1998) is the so-called matrix dolomite type B, which shows some similarities to the dolomites from the UDU such as the stable isotopic signatures, the chemical composition, the zonation patterns and the crystal habitus. The minor differences in the dolomite grain sizes observed in both locations can be explained by the deeper burial of the Swabian Alp dolomites. The overall depositional environment during dolomitization, however, is considered to be quite similar.

Gallucio (2009) also distinguishes two dolomite types (A and B) in her study of Upper Jurassic dolomites from the Sorrento peninsula (Southern Appenins, Italy). The environmental conditions for dolomite formation seem to be similar to those proposed for the dolomites from Oker. However, saddle dolomite (found by the above two authors) was not detected in the Oker sequence. Saddle dolomite is typically formed during late burial diagenesis, and the lack of this dolomite type at Oker supports the idea of dolomitization during shallow burial.

Finally, comparing the characteristics of the Oker dolomites to the recently formed dolomites from Abu Dhabi (McKenzie, 1981), dolomitization by replacement of limestone precursors in a sabkha-like environment is most likely. The proposed hydrogeological model designed for the recent dolomitization in Abu Dhabi has to be slightly modified for the setting at Oker, but the general conditions might have been relatively similar. A (diagenetically modified) seawater-derived pore water solution served as the most likely dolomitization fluid.

5.3. The role of sulfur in the dolomitization process

The anti-correlation of the S content and the degree of cation order in dolomite suggests that bacterial sulfate-reduction can play a key role in the dolomitization process (Figure 10). Although several studies have already discussed the lowering effect of high sulfate concentration on the dolomitization rates, Morrow & Rickets (1986) and Morrow & Abercrombie (1994) found, based on their geochemical modelling, no influence of sulfate concentration on the dolomitization process under low-temperature conditions (<80°C). At higher temperatures, however, (100-200°C) abundant sulfate can significantly reduce the dolomitization rate. On the other hand, Brady et al. (1996) propose a promotion of the dolomitization rate within sulfate-rich environments. Yet, the role of sulfate in the dolomitization process might have been overrated in some previous works (e.g. Galluccio, 2009), but my observations on the ordering ratio in dolomite and its sulfur concentration indicates that abundant sulfate-reduction can trigger the dolomitization process of limestone. With an increase of the S concentration in dolomite, its stoichiometry decreases notably. Morrow & Rickets (1986) and Morrow & Abercrombie (1994) explain this relationship (at higher temperatures) by an indirect correlation: the degree of calcite undersaturation correlates inversely with the sulfate concentration. This means that with an increasing sulfate concentration, the calcite dissolution decreases and subsequently lowers the dolomitization rate as well. This observation might serve as an explanation for the lower degree of cation order of the Oker dolomites that are enriched in sulfate.

6. Summary and conclusions

Limestone, partly dolomitized limestone and dolostone beds from an Upper Jurassic stable carbonate platform setting at Oker (Central Germany) were investigated. A multi-method approach comprising of thin section analyses, XRD, EMP and XRF analyses as well as $\delta^{18}O$ and $\delta^{13}C$ isotope analyses were used in order to shed light on the reaction paths and environmental controls of dolomitization of limestone. The following conclusions can be drawn:

(i) The dolomitization process and burial history at Oker was highly complex but the obtained data reveal that present dolomites are not a primary precipitate from seawater. The dolomites, were most likely formed by early diagenetic replacement of limestone precursors through intense interaction with a Mg-rich dolomitization fluid. The occurrence of various calcite cement types and dolomite within single beds indicate unstable environmental conditions during early-marine diagenesis, causing cyclic and abrupt changes in the pore fluid chemistry.

(ii) The depositional environment at Oker during the Middle to Upper Kimmeridgian was a shallow-lagoonal environment, characterized by high evaporation degrees and restricted water circulation. The latter caused at least seasonally suboxic to anoxic conditions that resulted in pyrite formation and deposition of organic-rich clayey sediments in an overall carbonate dominated sequence.

(iii) Combined chemical and isotopic data of calcite and dolomite lead to the conclusion that the Oker carbonates largely preserved their pristine signatures and were only slightly modified during shallow burial diagenesis. Thus, the lagoonal limestone was formed at around 20°C. The formation temperature of the dolomites was calculated to be around 30°C, a feature confirmed by the small crystal size (~10-50 μm in size) of the euhedral dolomite rhombs

(iv) The Lower Dolomite Unit is the most complex one. Here, the coexistence of the fine-grained dolomite cores and subsequently deposited LMC and HMC rims leads to the idea that (during late burial diagenesis) partial de-dolomitization took place, but only on a local scale.

(v) The negative correlation between the S concentration and the degree of cation order in dolomite suggests that (microbial mediated) sulfate reduction could play an important role in the dolomitization process.

7. Acknowledgements

8. References

Arvidson, R. S., and F. T. Mackenzie. "The dolomite problem: Control of precipitation kinetics by temperature and saturation state." American Journal of Science 299 (1999). 257-88.

Baldermann, A., and C. Nickel. "Kartierbericht: Oberjurassische Schichtenfolge und sedimentärer Ablagerungsraum vom Langenberg von Oker (westliches Harzvorland, Deutschland)." Ernst-Moritz-Arndt-Universität Greifswald, (2012).

Brown, G, C., D, J. Hughes, and J. Esson, "New X.R.F. data retrieval techniques and their application to U.S.G.S. standard rocks." Chemical Geology 11 (1973): 223-29.

Budd, D.A. "Cenozoic dolomites of carbonate islands: their attributes and origin." Earth Sci. Rev. 42, (1997). 1-47.

Brady P.V., Krumhansi J.L., and Papenguth H.W. "Surface complexation clues to dolomite growth." *Geochimica et Cosmochimica Acta*, 60, (1996). 727-731.

Chilingar, G. V., D. H. Zenger, H. J. Bissell, and K. H. Wolf. "Diagenesis in sediments and sedimentary rocks" Chapter 7, Dolomite and Dolomitization. Elsevier Science, (1979). 423-536.

Colombié, C., C. Lécuyer, and A. Strasser. "Carbon- and oxygen-isotope records of palaeoenvironmental and carbonate production changes in shallow-marine carbonates (Kimmeridgian, Swiss Jura)." Geol. Mag. 148.1 (2011). 133-53.

Deelman, J C. "Low-temperature formation of dolomite and magnesite- A comprehensive revision." Compact Disc Publications Geology Series, Eindhoven, (2011). 3-23

Deffeyes, K.S., F.J. Lucia, and P.K. Weyl." Dolomitization of Recent and Plio and Pleistocene sediments by marine evaporite waters on Bonaire, Netherlands Antilles." Dolomitization and limestone diagenesis. SEPM Spec. Pub. (1965). 71-88.

Dietzel, M., J. Tang, A. Leis, and S. J. Köhler. "Oxygen isotopic fractionation during inorganic calcite precipitation - Effects of temperature, precipitation rate and pH." Chemical Geology 268 (2009). 107-15.

Dunham R. J. "Classification of carbonate rocks according to depositional texture." *AAPG Mem.*, 1, (1962). 108-121.

Fenter, P., Z. Zhang, C. Park, N. C. Sturchio, S. R. Higgins, and X. M. Hu. "Structure and reactivity of the dolomite (104)–water interface: New insights into the dolomite problem." Geochimica et Cosmochimica Acta 71 (2007). 566-79.

Fischer, R. "Die Oberjura-Schichtfolge vom Langenberg bei Oker." Arbeitskreis Paläontologie Hannover 2 (1991). 21-52.

Flügel, Erik. „Microfacies of Carbonate Rocks- Analysis, Interpretation and Application". 2nd ed.: Springer-Verlag Berlin Heidelberg, (2010). 267-332.

Friedman, I., O'Neil, J.R. "Compilation of stable isotope fractionation factors of geochemical interest. U.S. Geol. Surv.Prof. Pap. 440-KK. (1977).12.

Fürchtbauer, H., and H. Goldschmidt. "Beziehungen zwischen Calcium-Gehalt und Bildungsbedingungen der Dolomite." Geol. Rdsch. Stuttgart 55 (1965). 29-40.

Galluccio, L. "Dolomites within the mesozoic carbonates of Sorrento Peninsula(Southern Apennines - Italy): Genetic models and reservoir implications." PhD-Thesis - University of Naples "Federico II", (2009). 25-29.

Hug, Wolfgang A. "Sequenzielle Faziesentwicklung der Karbonatplattform des schweizer Jura im späten Oxfordium und frühesten Kimmeridge." Geofocus 7 Diss. Universität Freiburg (Schweiz), (2003). 17-20

Husinec, A., and F. J. Read. "Sequence Stratigraphy, Carbon Isotopic Signature, and Dolomitization of a Late Jurassic Greenhouse Platform, Croatia*." Search and Discovery Article #50345 (2010).

Kaczmarek, S. E., and D. F. Sibley. "On the evolution of dolomite stoichiometry and cation order during high-temperature synthesis experiments: An alternative model for the geochemical evolution of natural dolomites." Sedimentary Geology 240 (2011). 30-40.

Kim S.T. and O'Neil J. R. "Equilibrium and nonequilibrium oxygen isotope effects in synthetic carbonates." Geochim. Cosmochim. Acta 61. (1997). 3461–3475.

Kulke, H. "Der Harz (Norddeutschland): Geologisch-Lagerstättlenkundlicher Überblick, Historische Baumaterialien (Natursteine, Gipsmörtel, Schlackensteine, Blei)." Mitt. Österreich. Miner.ges. 142 (1997). 43-84.

Lumsden, D.N. and Chimahusky, J.S. "Relationship between dolomite non-stoichiometry and carbonate facies parameters." in: Dunham, J.B. and Ethington, R.L. (Eds.) Concepts and Models of dolomitization. Society of Economic Paleontologist and Mineralogists (SEPM) Special Publication, (1980) 28, 87-110.

Malone, M. J., Baker, P.A. and Burns S.J. "Recrystallization of dolomite: evidence from the Monterey Formation (Miocene), California." Sedimentology 41 (1994). 1223-1239.

Mackenzie, F. T. "Sediments, Diagenesis, and Sedimentary Rocks:" Treatise on Geochemistry. 7th ed. Vol. 2, Elsevier, (2006). 35-49.

Mahboubi, A., R. Moussavi-Harami, S. J. Carpenter, A. Aghaei, and L. B. Collins. "Petrographical and geochemical evidences for paragenetic sequence interpretation of diagenesis in mixed siliciclastic–carbonate sediments: Mozduran Formation (Upper Jurassic), south of Agh-Darband, NE." Carbonates Evaporates 25 (2010). 231-46.

McKenzie, J. A. "Holocene dolomitisation of calcium carbonate sediments from the coastal sabkhas of Abu Dhabi, U.A.E.: A stable isotope study." J. Geol. Chicago 89 (1981). 185-98.

Morrow, W. D., and B. D. Rickets. "Chemical controls on the precipitation of mineral analogues of dolomite: the sulphate enigma." Geology 14 (1986). 408-10.

Morrow, W. D., and H. J. Abercrombie. "Rates of dolomitization: the influence of dissolved sulphate." In Purser B.H., Tucker, M.E. & Zenger, D.H. (eds) Dolomites – A Volume in Honour of Dolomieu. 21st ed. International Association of Sedimentologists, (1994). 377-86.

Price, G. D., and B. W. Sellwood. "Palaeotemperatures indicated by Upper Jurassic (Kimmeridgian-Tithonian) fossils from Mallorca determined by oxygen isotope composition." Palaeogeography, Palaeoclimatology, Palaeoecology 110 (1994). 1-10.

Rameil, N. "Early diagenetic dolomitization and dedolomitization of Late Jurassic and earliest Cretaceous platform carbonates: A case study from the Jura Mountains (NW Switzerland, E France)." Sedimentary Geology 212 (2008). 70-85.

Reinhold, C. "Multiple episodes of dolomitization and dolomite recrystallization during shallow burial in Upper Jurassic shelf carbonates: eastern Swabian Alb, southern Germany." Sedimentary Geology 121 (1998). 71-95.

Sánchez-Román, M., C. Vasconcelos, R. Warthmann, M. Rivadeneyra, and J. A. McKenzie. Microbial Dolomite Precipitation under Aerobic Conditions: Results from Brejo do Espinho Lagoon (Brazil) and Culture Experiments. ETH, Geological Institute, 8092 Zürich, Switzerland and Dept. of Microbiology, Faculty of Pharmacy, University of Granada, Spain, (2012).

Schlager, W., and N. P. James. "Low-magnesian calcite limestones forming at the deep-sea floor Tongue of the Ocean, Bahamas." Sedimentology 25 (1978). 675-702.

Spötl, C., Vennemann, T.W. "Continuous-flow isotope ratio mass spectrometric analysis of carbonate minerals." Rapid Communications in Mass Spectrometry 17, (2003).1004–1006.

Thierry, J., S.Cresquin cord. "Atlas Peri-Tethys Palaeographic Maps. – Chapter 10.- Early Kimmeridgian (146 - 144 Ma)" Paris: Commission for the Geologic Map of the World, (2000). Explanatory Notes. –S.Cresquin cord. 85-89

Voigt, T., F. Wiese, Himar von Eynatten, H. Franzke, and R. Gaupp. "Facies evolution of syntectonic Upper Cretaceous deposits in the Subhercynian Cretaceous Basin and adjoining areas (Germany)." 157.2 (2006): 203-44.

Warren, J., Dolomite: occurrence, evolution and economically important associations. Earth Sci. Rev. 52, (2000). 1-81.

Wierzbowski, H. "Carbon and oxygen isotope composition of Oxfordian–Early Kimmeridgian belemnite rostra: palaeoenvironmental implications for Late Jurassic seas." Palaeogeography Palaeoclimatology Palaeoecology 203, (2004) 153–68.

Wyckoff, R. W. G., and H. E. Merwin. "The crystal structure of dolomite." Am. Jour. Sci. 8.5 (1924). 447-61.

Zorlu, J. "Sedimentpetrographische und geochemische Untersuchungen an unterschiedlich überprägten Triasdolomiten der Ost- und Südalpen." Dissertation: Ruhr- Universität Bochum, (2007). 22-25, 128-37

9. Appendix

Table A-1:Characteristics of calcareous samples from Oker.

Sample	Mineralogical composition	Methods	Type of rock	Mineral paragenesis	Fabric	Classification after Dunham (1962)	Comments
A	Calcite Quartz	Optical microscopy, SEM, XRD,	Limestone	Calcite, sparite, glaukonite Fe-Oxides	compact micritic matrix with components	Wackestone	organics: Mollusca, Foraminifera
B	Calcite Quartz	XRD	Limestone	Calcite, sparite, glaukonite Fe-Oxides	compact micritic matrix with some components	Wackestone	organics: Mollusca Foraminifera
C	Calcite Quartz	optical microscopy SEM, Microprobe, XRD	Limestone	Calcite (sparite)	micritic matrix with some components sparitic cements	Wakestone	Some components: Pelloids, Foraminifera Partly recrystallized Different cement phases
D	Calcite Quartz	optical microscopy, microprobe, SEM XRD	Limestone	Calcite (sparite)	micritic matrix with some components sparitic cements	Packstone	Little amount of components, mainly recrystallized Different cement phases
E	Calcite Quartz	Optical microscopy, microprobe, SEM	Limestone		micritic matrix with some components sparitic	Packstone	Little amount of matrix, many compononents Different cement

		XRD			cements		phases
F	Calcite, Quartz	XRD	Limestone			Packstone	
G	Calcite, Quartz	XRD	Limestone			Packstone	
H	Dolomite, Pyrite Clay minerals Quartz	Optical microscopy SEM microprobe XRD	Limestone		Very porous	Crystalline	Components are not identifiable very much recrystallized
I	Calcite, Dolomite, clay minerals Quartz	Optical microscopy XRD Microprobe SEM	Dolomite		Very porous	Crystalline	Components are not identifiable Soft material with small grain size
J	Calcite, Dolomite clay minerals Quartz	XRD	Dolomite			Crystalline	Soft material with little grain size
K	Dolomite, Calcite, Pyrite, Hematite Quartz	Optical microscopy, SEM, microprobe XRD	Dolomite			Crystalline	No components, totally recrystallized Soft material with small grain size
L	Dolomite Quartz	Optical microscopy XRD	Dolomite		Compact	Crystalline	Soft material with small grain size
M	Dolomite Quartz	Optical microscopy XRD	Dolomite		Compact	Crystalline	grains with a size of some µm
N	Dolomite Quartz	XRD	Dolomite		Compact	Crystalline	grains with a size of some µm
O	Dolomite Quartz	XRD Optical microscopy	Limestone		Compact	Grainstone	Grain size: some µm

P	Calcite, Quartz	XRD	Limestone		Compact	Grainstone	
Q	Calcite, Quartz	Optical microscopy Microprobe SEM XRD	Limestone		Compact	Packstone	Components Recrystallized
R	Calcite, Quartz	XRD	Limestone		Compact	Packstone	

Table A-2: Mineralogical composition of the investigated samples

Sample	Mineralogy	Formation
A	> 90% cc, < 10% qtz	
B	> 90% cc, < 10% qtz	
C	> 90% cc, < 10% qtz	
D	> 90% cc, < 10% qtz	**LLU**
E	> 90% cc, < 10% qtz	
F	> 90% cc, < 10% qtz	
G	> 90% cc, < 10% qtz	
H	10% clay, 80% dol, < 10% qtz	**LDU (Dolostone)**
I	10% clay, 70% cc, 10% dol, <10% qtz	**LDU**
J	10% clay, 70% cc, 10% dol, <10% qtz	**Dolomitic Limestone**
K	>90% dol, <10% qtz	
L	>90% dol, <10% qtz	**UDU**
M	>90% dol, <10% qtz	
N	>90% dol,<10% qtz	
O	> 90% cc, < 10% qtz	
P	> 90% cc, < 10% qtz	**ULU**
Q	> 90% cc, < 10% qtz	
R	> 90% cc, < 10% qtz	

Table A-3: XRD data showing the mineralogical composition of samples, the $MgCO_3$ content of dolomite and calcite, and dolomite stoichiometry. The ratio of the two dolomite peaks 015/110 in the XRD-pattern gives information about the degree of cation order of the dolomites in the sample. The higher the number, the better the cation order is.

Sample	CaCO₃ [mol%]	MgCO₃ [mol%]	015/110- ratio	Cc/dol -ratio	Main minerals
A	98.603	1.397			LMC
B	97.663	2.337			LMC
C	99.140	0.860			LMC
D	98.827	1.173			LMC
E	98.523	1.477			LMC
F	98.723	1.277			LMC
G	98.863	1.137		99.995:0.005	LMC
H	54.870	45.130	0.378		Dol, HMC
I	98.070	1.930	0.465	91.216:8.784	LMC, Dol
J	99.273	0.727	0.617	88.692:11.309	LMC, Dol
K	55.184	44.816	0.378		Dol
L	54.764	45.236	0.389		Dol
M	54.907	45.093	0.504	0.383:99.617	Dol
N	54.540	45.460	0.462		Dol
O	99.067	0.933			LMC
P	99.650	0.350			LMC
Q	98.803	1.197			LMC
R	99.003	0.997			LMC
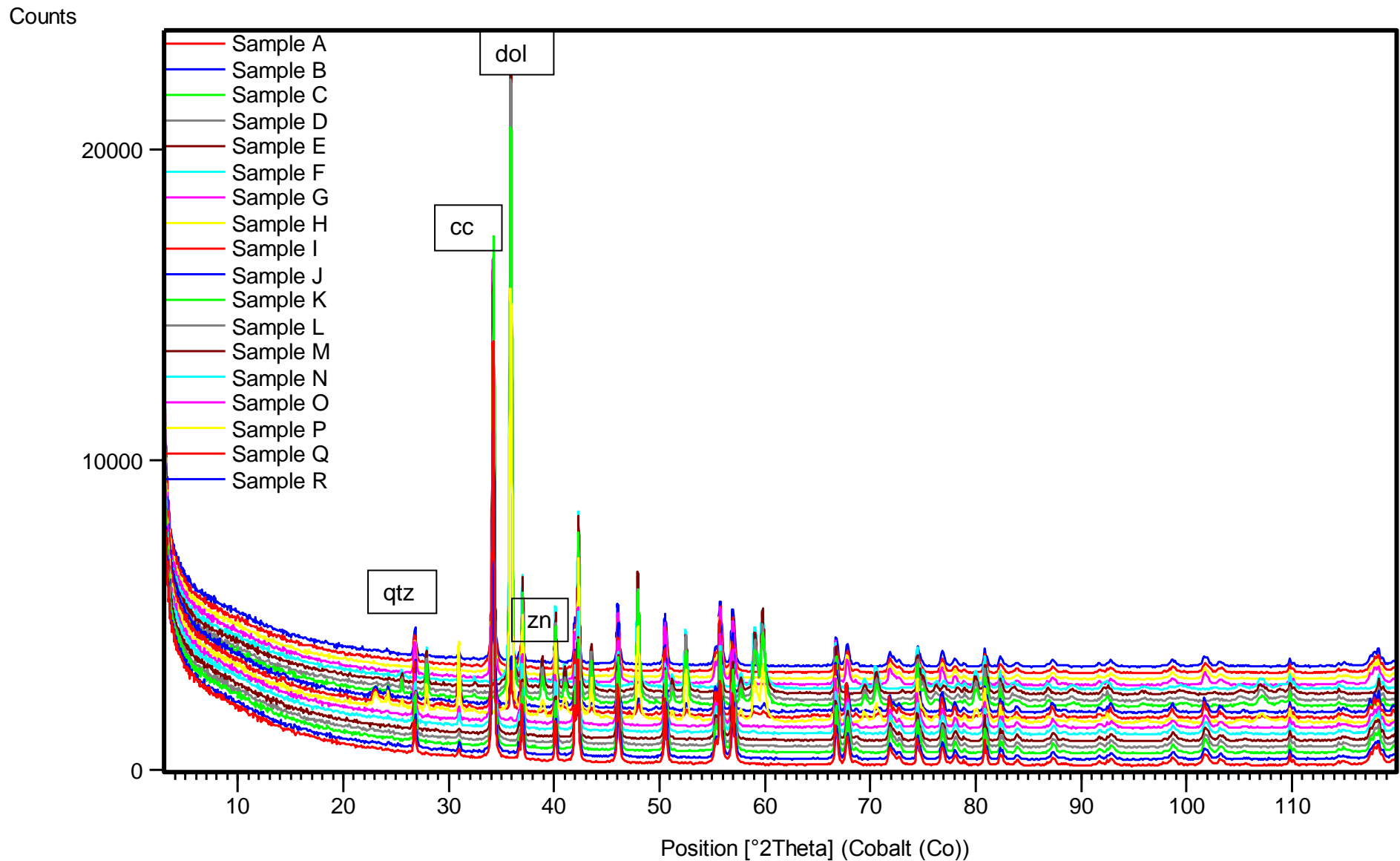
Figure A-1: Comparison of collected XRD patterns, from the investigated Oker sequence. Qtz, cc, dol zn are acronyms for quartz, calcite, dolomite zincite respectively.
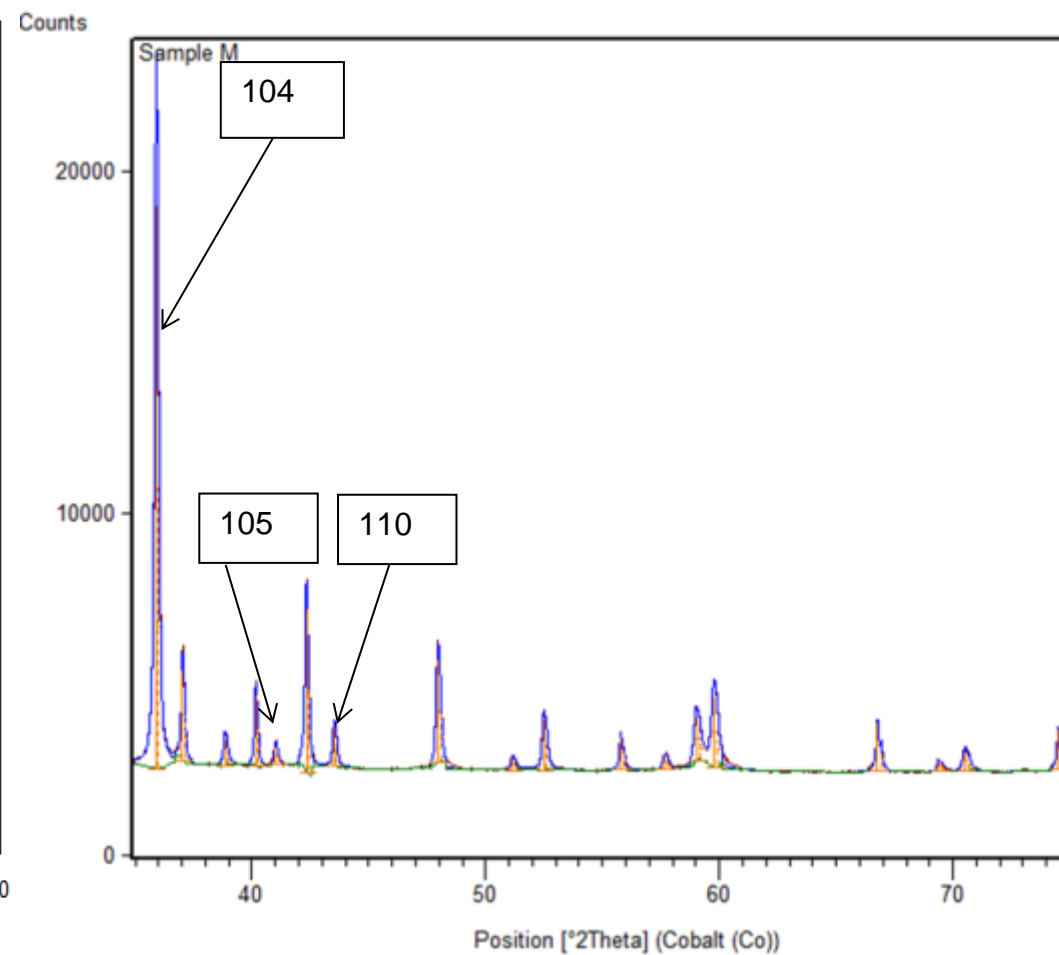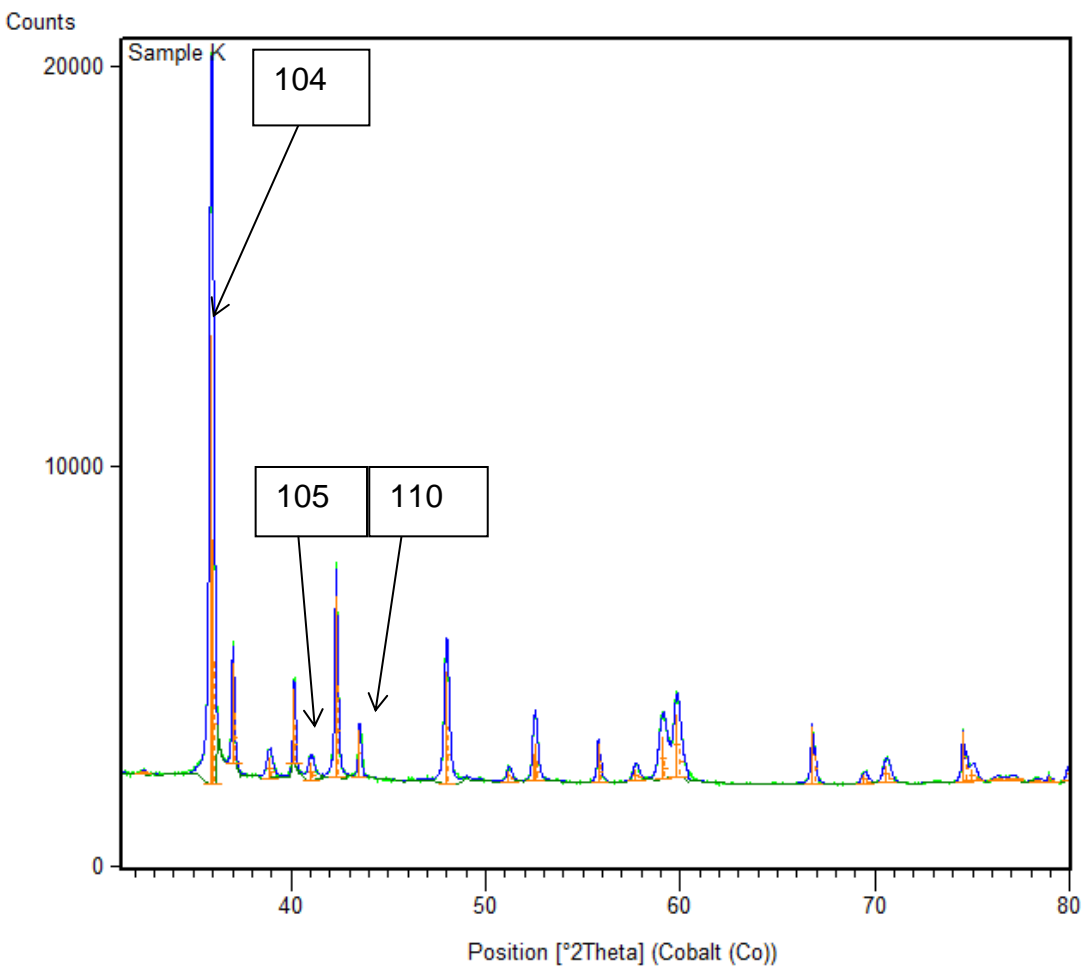
Figure A-2: Comparison of XRD patterns of the samples K and M from the UDU. The main dolomite peak (104 peak) can be used to calculate the dolomite stoichiometry. Zincite was added as an internal standard. The ratio of the 110/105 dolomite peak is indicative for the degree of cation order in the dolomite lattice structure.
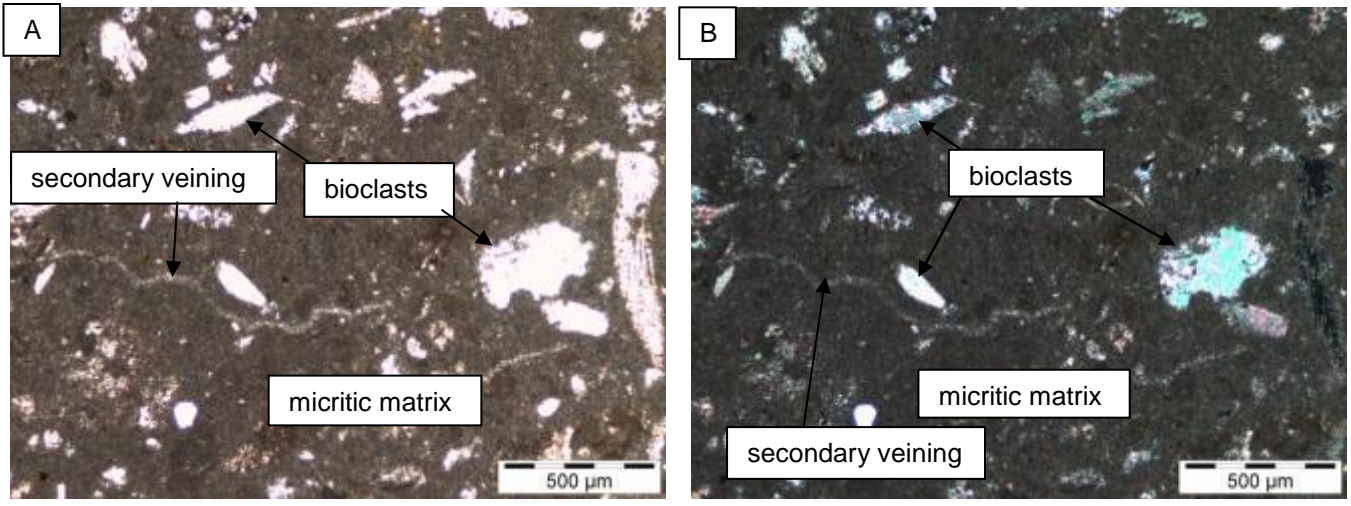
Figure A-3: Microphotograph of sample A: Wackestone with bioclast debris and secondary calcite veining in a micritic matrix (A), 2N on the right (B).
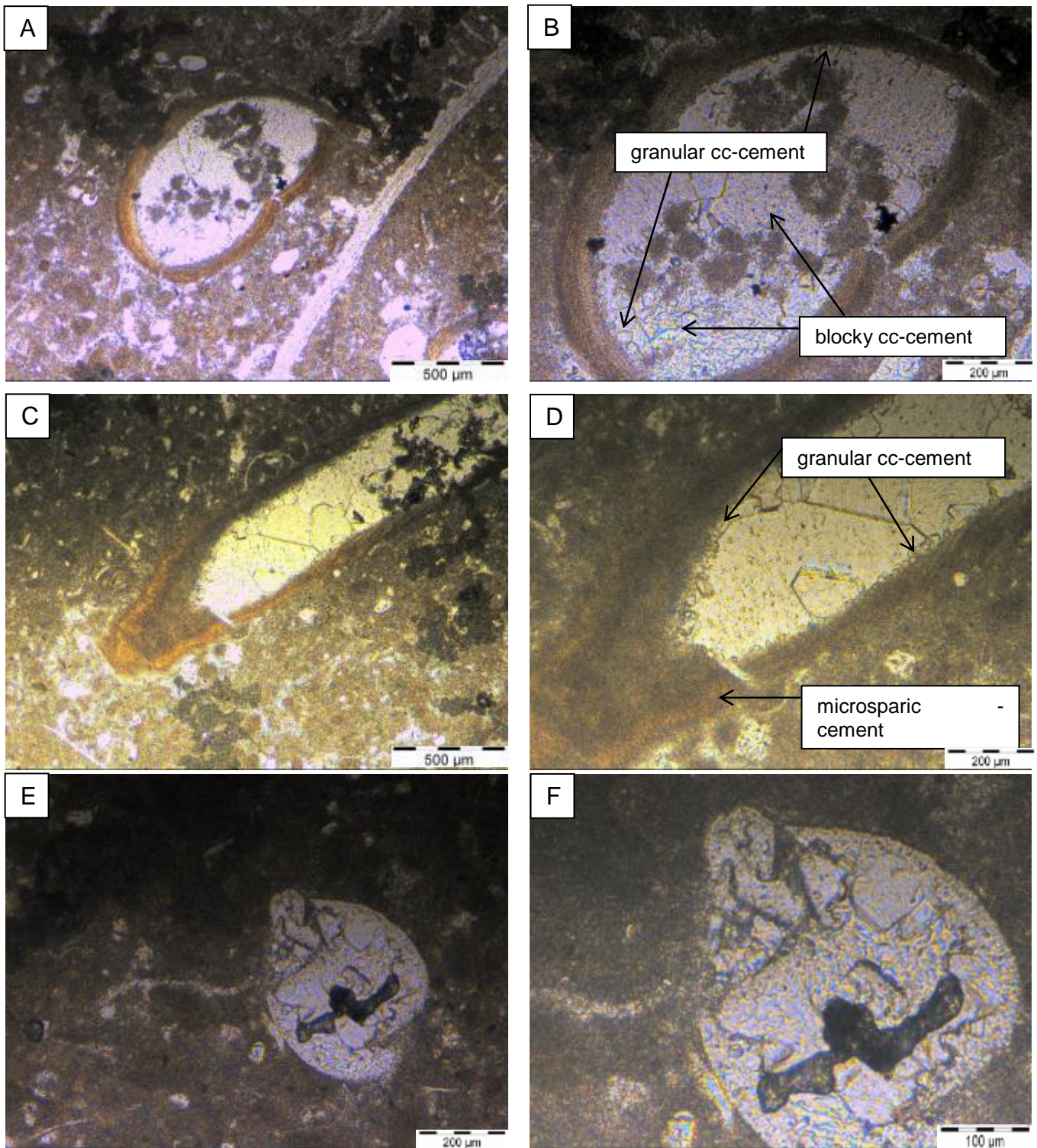
Figure A-4: CL-microphotographs of samples from the LLU: recrystallized bioclast material occurs in a micritic matrix. The CL color is mainly light yellow with some blue areas. The micritic cement is somewhat darker (A-F).
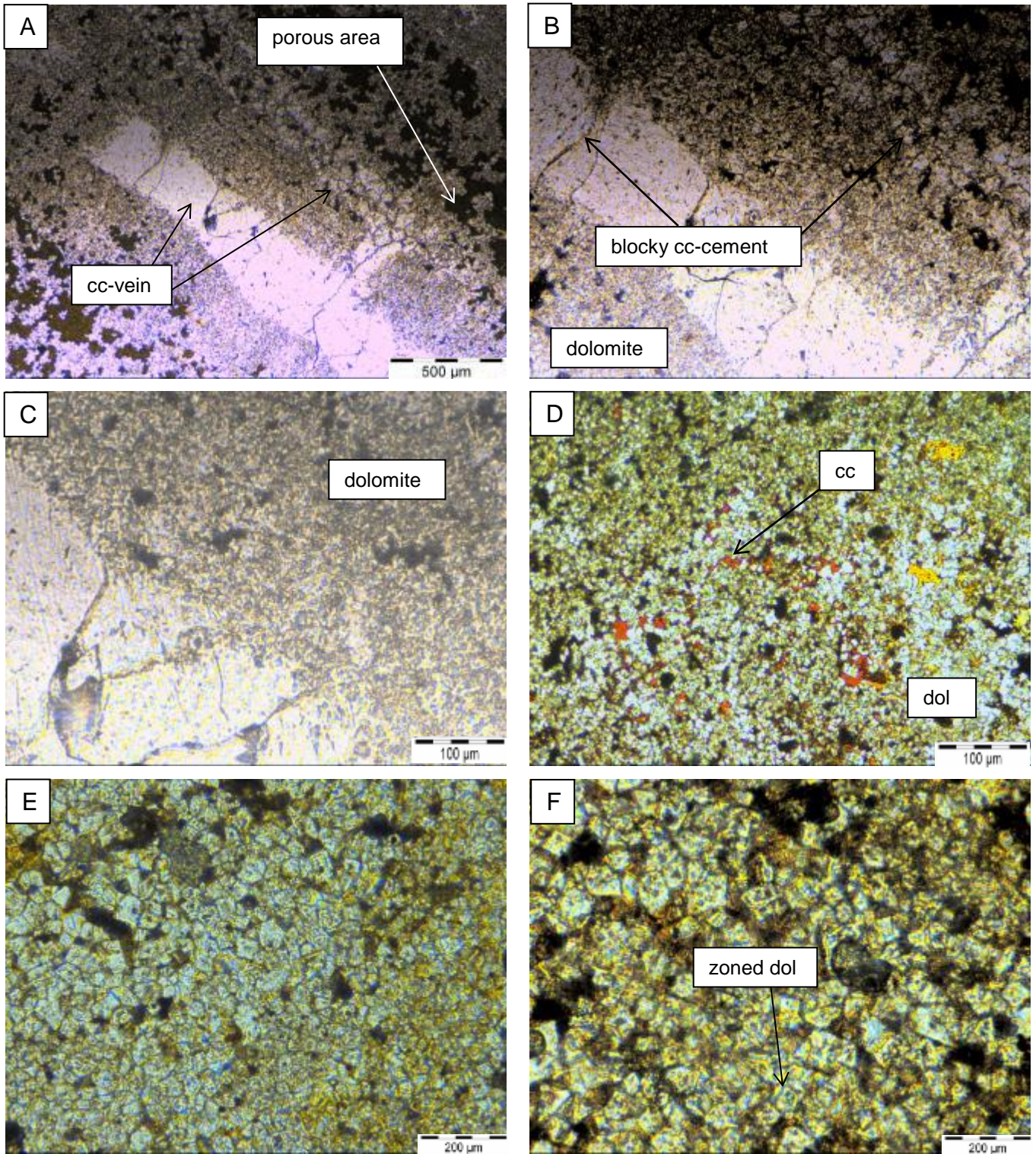
Figure A-5: CL-microphotographs of samples from the dolostone units: calcitic dolostone with a cc-vein in a micritic dolomite matrix (A-B); CL-photos of the cc-vein surrounded by fine grained dolomite, darker areas are porous areas. The CL-color is white to slightly yellow, small rhombic dolomite grains occur with some cc-grains.; Note the dark yellow to red color of the cc grains (C); zoned dolomite with yellow to blue CL-color (D), dolomite crystals from the UDU (E, F), 2N on the right (F).
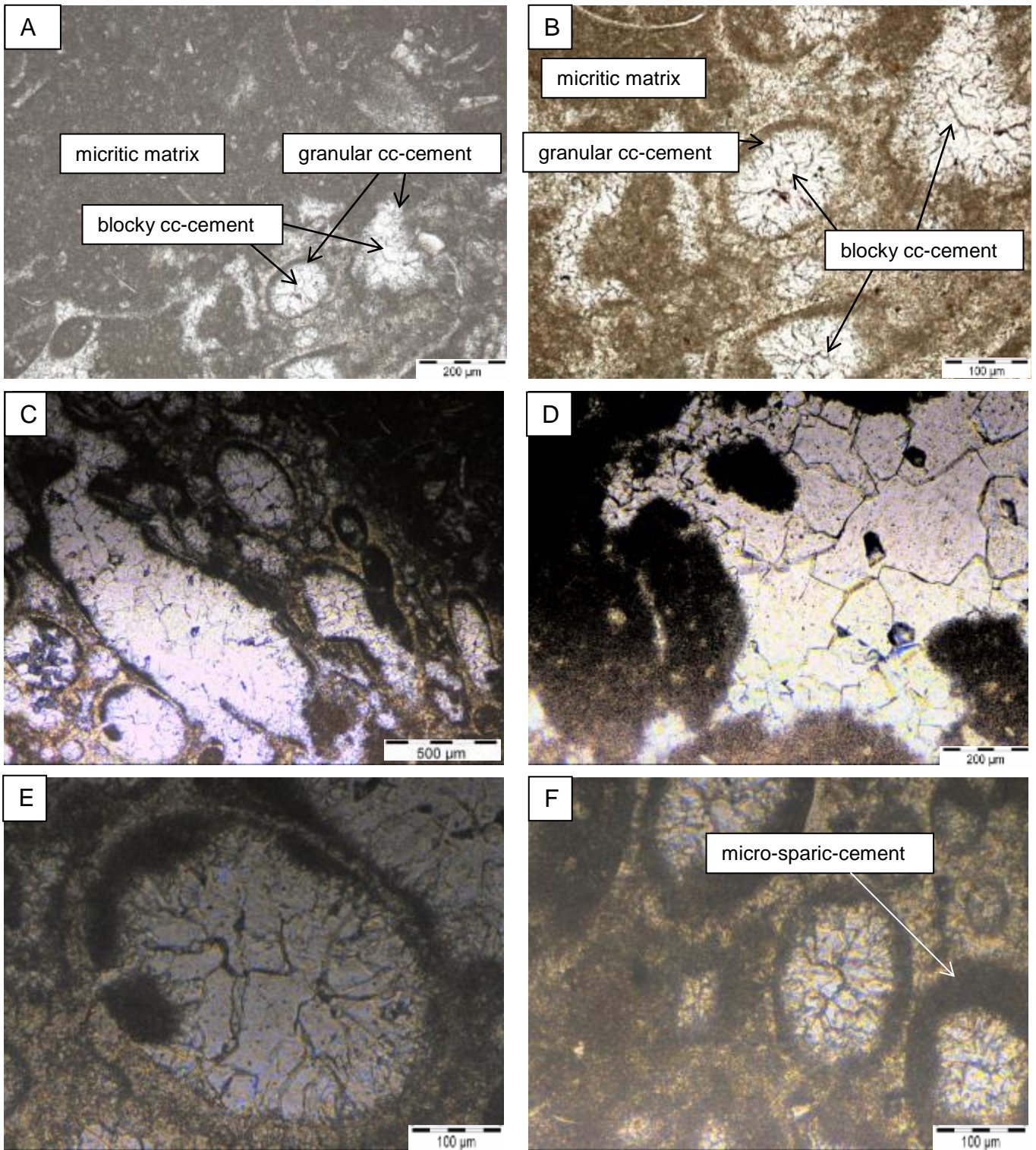
Figure A-6: Microphotograph and CL photos of samples from the ULU (sample Q): Wackestone with undifferentiated bioclasts that are frequently filled with different calcite (cc) cement generations, embedded in a micritic matrix (A), 2N on the right (B) C-H) CL color of cc is white to slightly yellow.
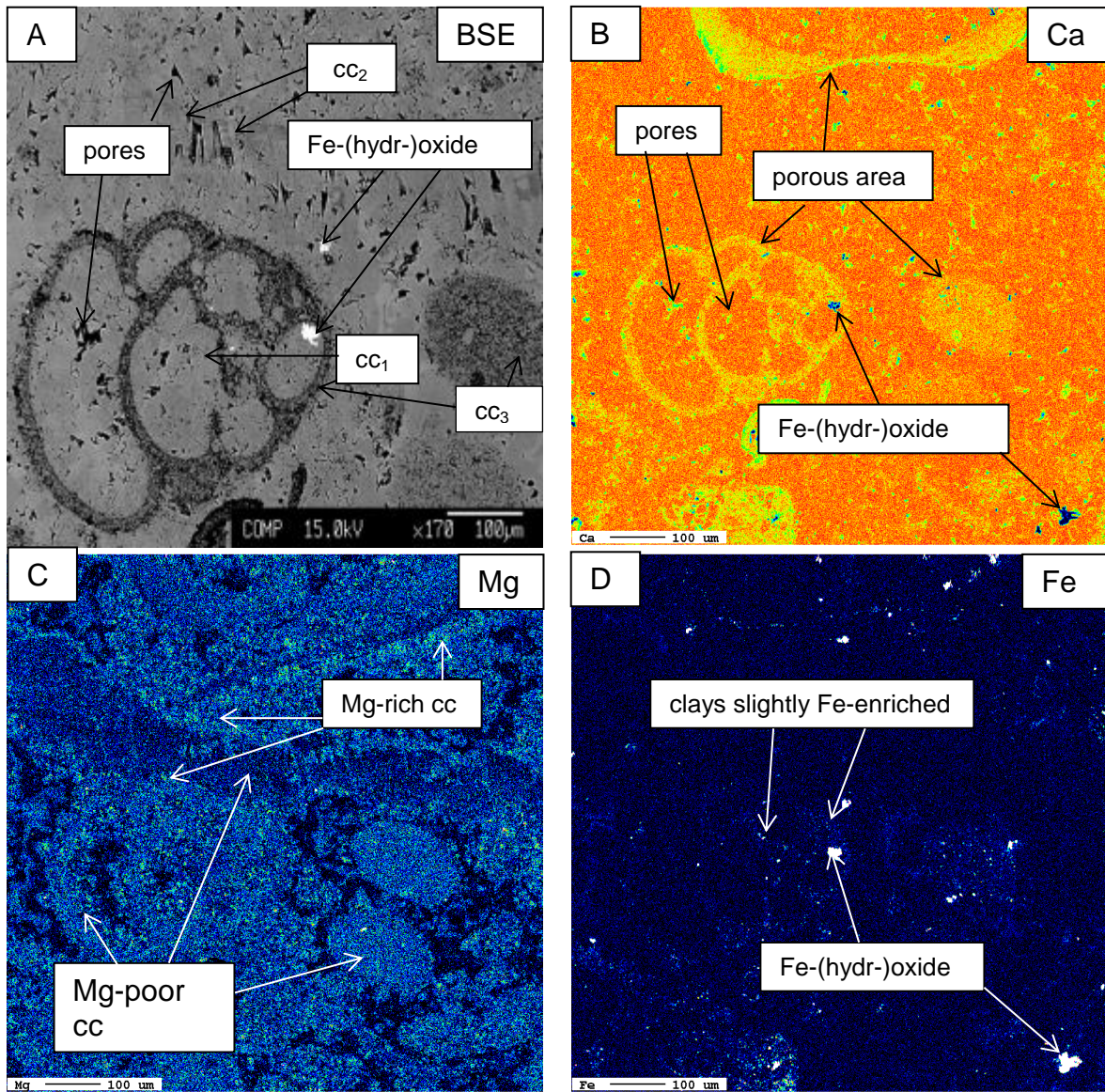
Figure A-7: Backscattered electron image and elemental mapping of sample C. (A) Bioclast filled with calcite spar (cc_1) and fibrous calcite (cc_2); (B) Distribution of Ca; the depletion of Ca in the matrix is due to porosity; (C) Elemental map of Mg; note the relative decrease in Mg content in cc_2 in comparison to the matrix; (D) Elemental map of Fe; note that Fe-(hydro)-oxides are present in the porous areas of the sample D) the matrix is more Fe enriched than the bioclast.
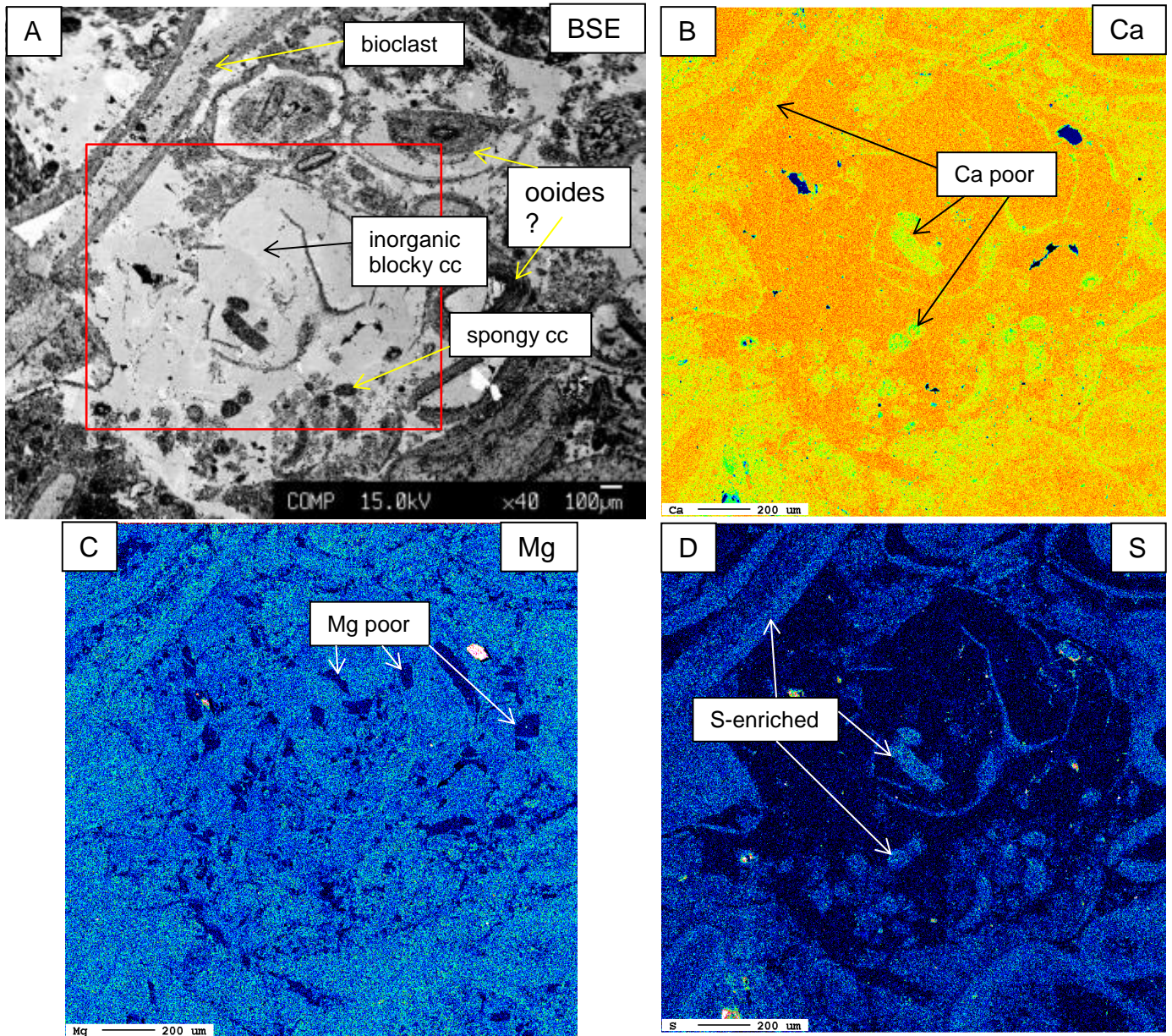
Figure A-8: BSE image and elemental mappings of sample E. (A) BSE image showing blocky calcite spar and relicts of bioclasts; the red square marks the area of elemental mappings. (B) Elemental map of Ca; the heterogeneous distribution of Ca is most probably due to the differences in the grain size. (C) Elemental map of Mg: the blocky calcite is somewhat poorer in Mg than the biogenic calcite. (D) Elemental map of S: S anti-correlates with the Ca distribution. The Ca rich areas are S poor.
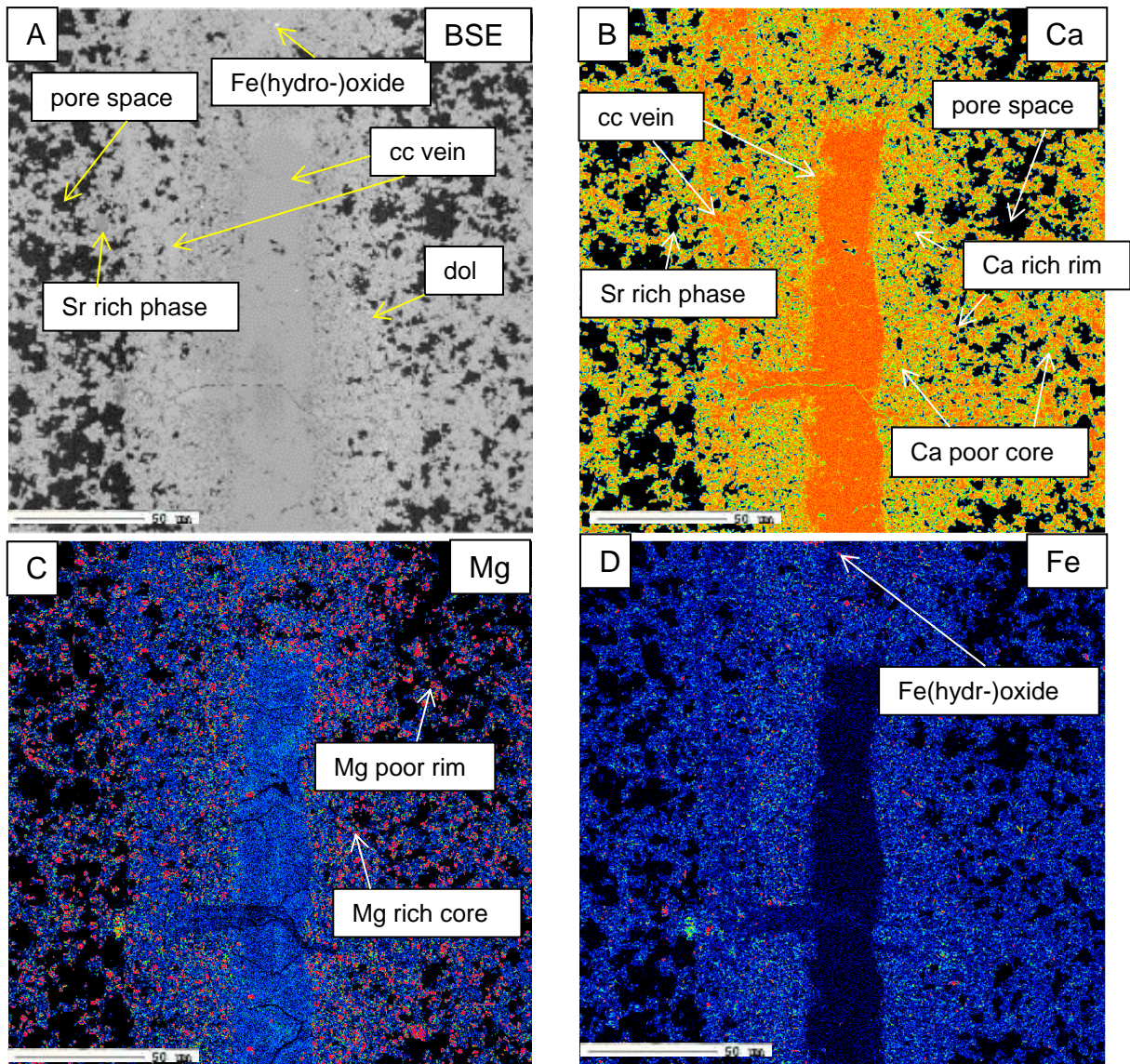
Figure A-9: Backscattered electron image and elemental mapping of sample I: A) Secondary calcite-vein (cc) cutting through aggregates of fine-grained dolomite and micro-sparite; (B) Elemental map of Ca; note the higher Ca content in the cc-vein; (C) Elemental map of Mg; note: (i) the increase in the Mg content in dolomite and (ii) the variable content of Mg in the cc-vein; (D) The elevated contents of Fe are due to Fe-(hydro-)oxide present in the matrix.
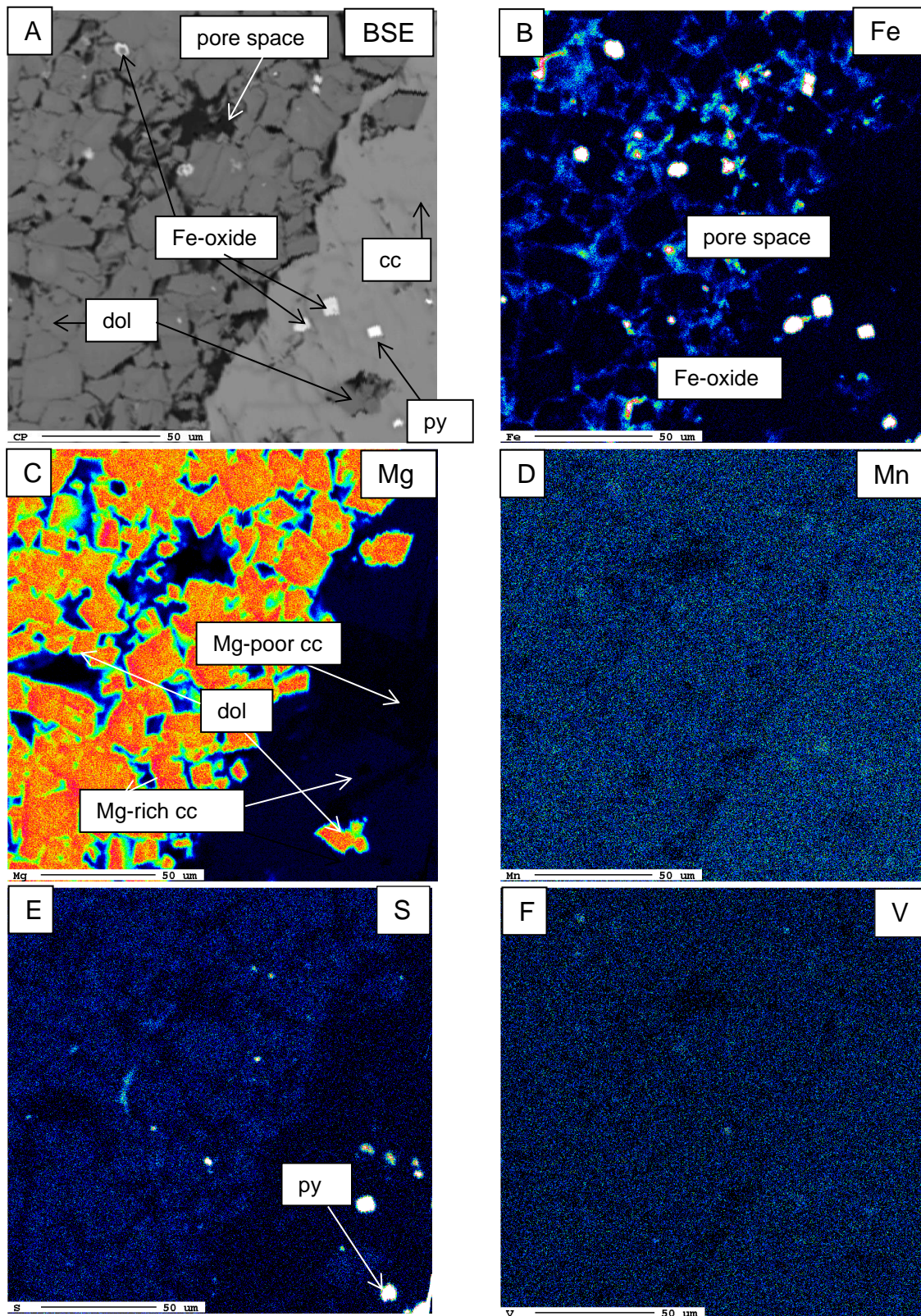
Figure A-10: Backscattered electron image and elemental mapping of sample K. A) Contact between fine-grained dolomite (dol) and coarse-grained calcite (cc); (B) Elemental map of Fe. The increase in the Fe intensity corresponds to present Fe-hydroxides and pyrite (py). (C) Elemental map of Mg; note two generations of Mg-rich and Mg-poor calcite spar; (D); Elemental map of S. Note the S-enrichment in dolomite in comparison to calcite, bright spots are inclusions of pyrite.
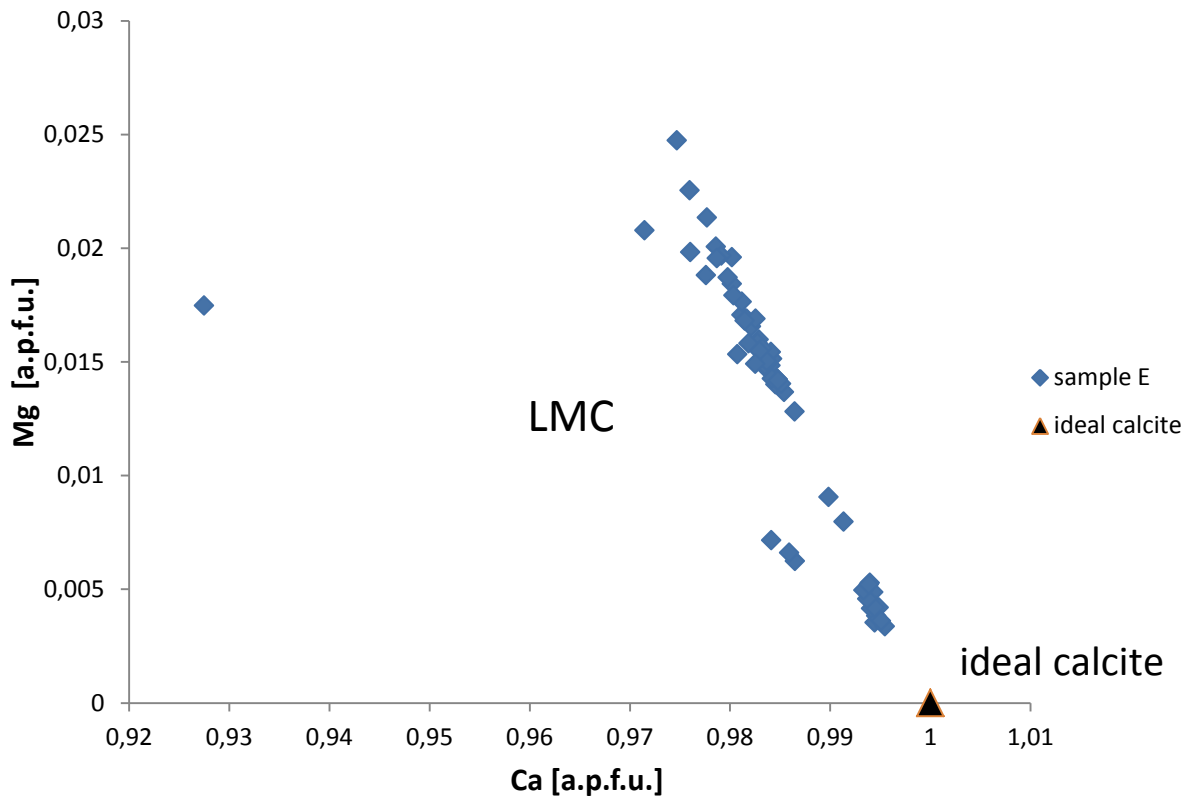
Figure A-11: Ca vs Mg plot of sample E from the LLU and the chemical composition of an ideal calcite. All analyses are located in the LMC field.
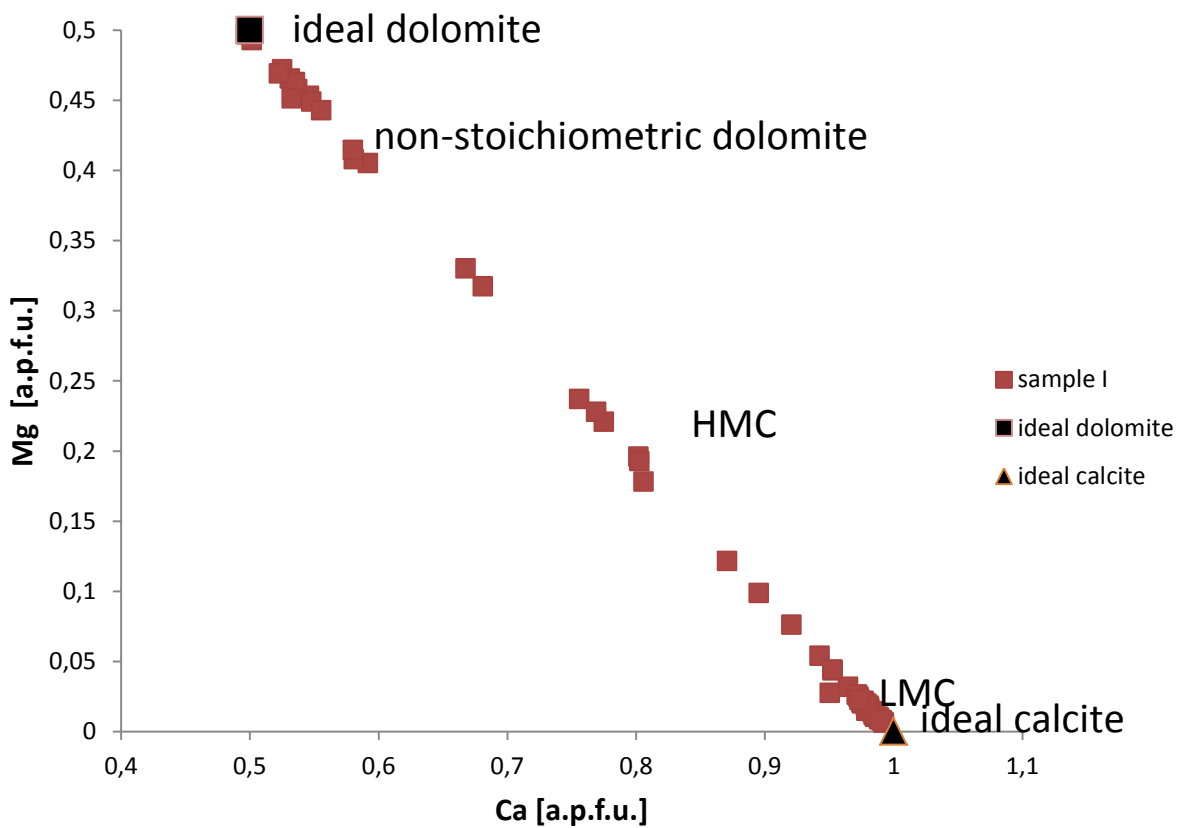
Figure A-12: Calcium vs Magnesium distribution in sample I from the LDU. LMC, HMC as well as dolomite can be found.
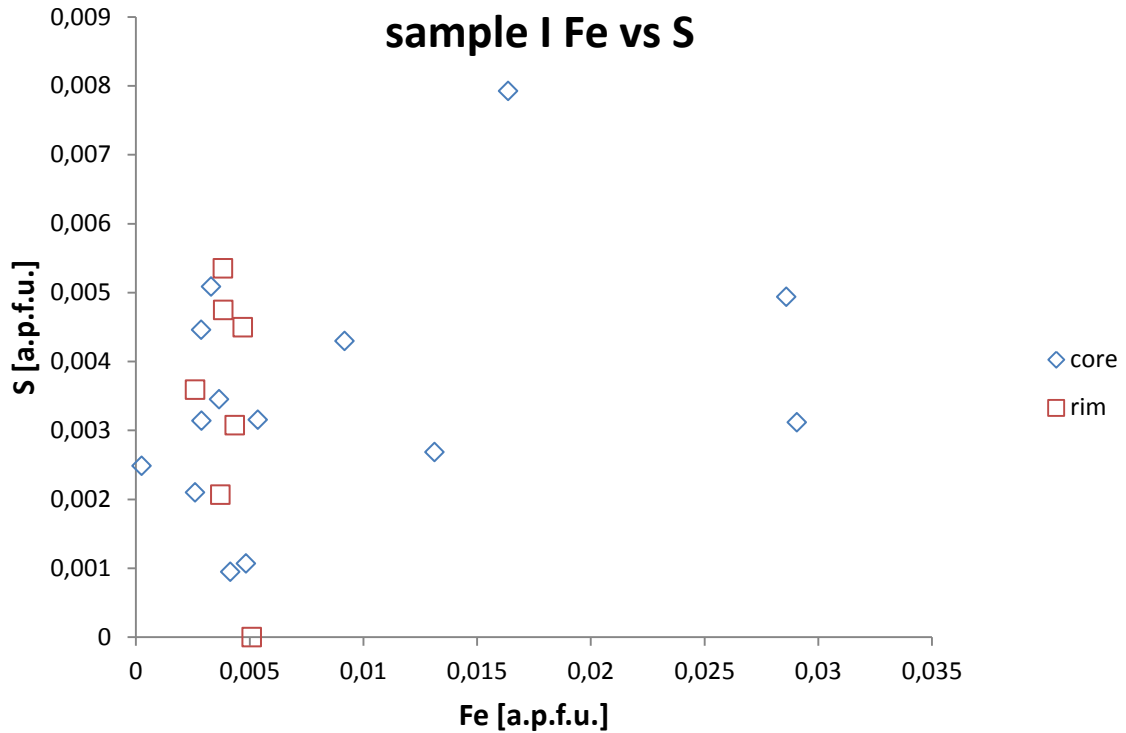
Figure A-13: Iron (Fe) versus sulfur (S) concentration in sample I from the LDU. Rim and core areas of the dolomites were analyzed seperatly. There is no difference in the sulfur concentration, but the Fe concentration in the cores is generally higher than that of the rims.
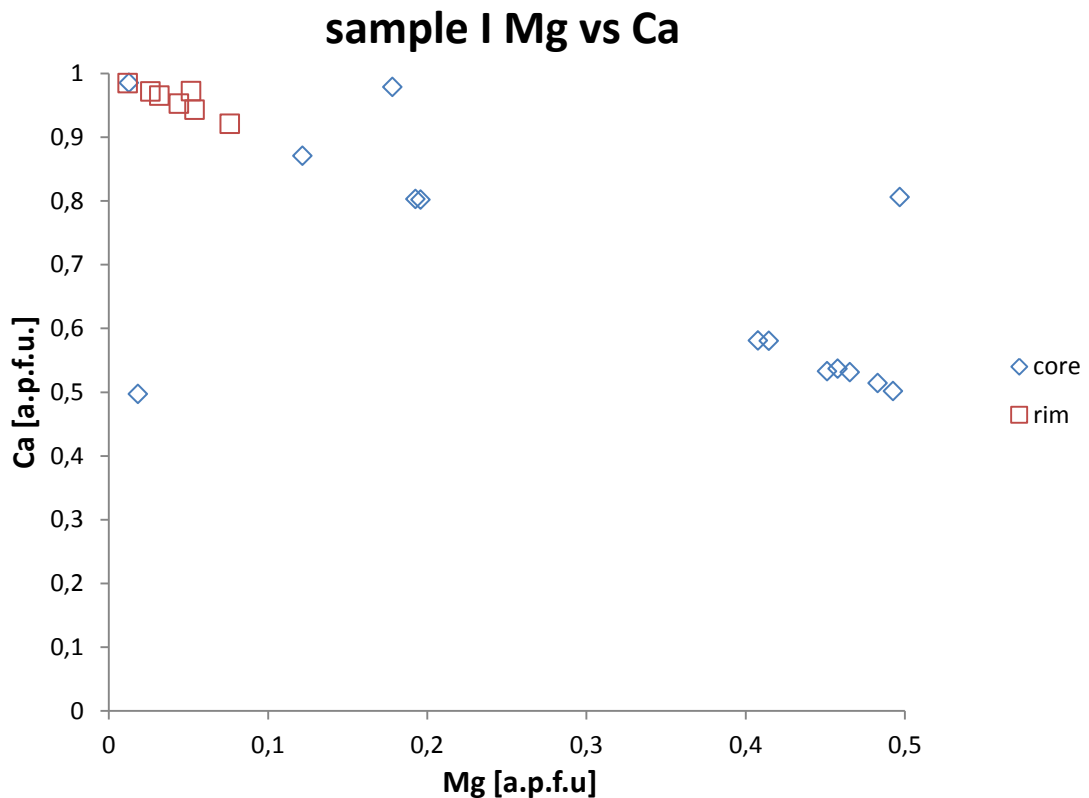
Figure A-14: Mg versus Ca concentration from sample I from LDU: notice the overall low Mg concentration the surrounding area of the dolomite, indicating a LMC and the Mg rich cores indicating dolomite.
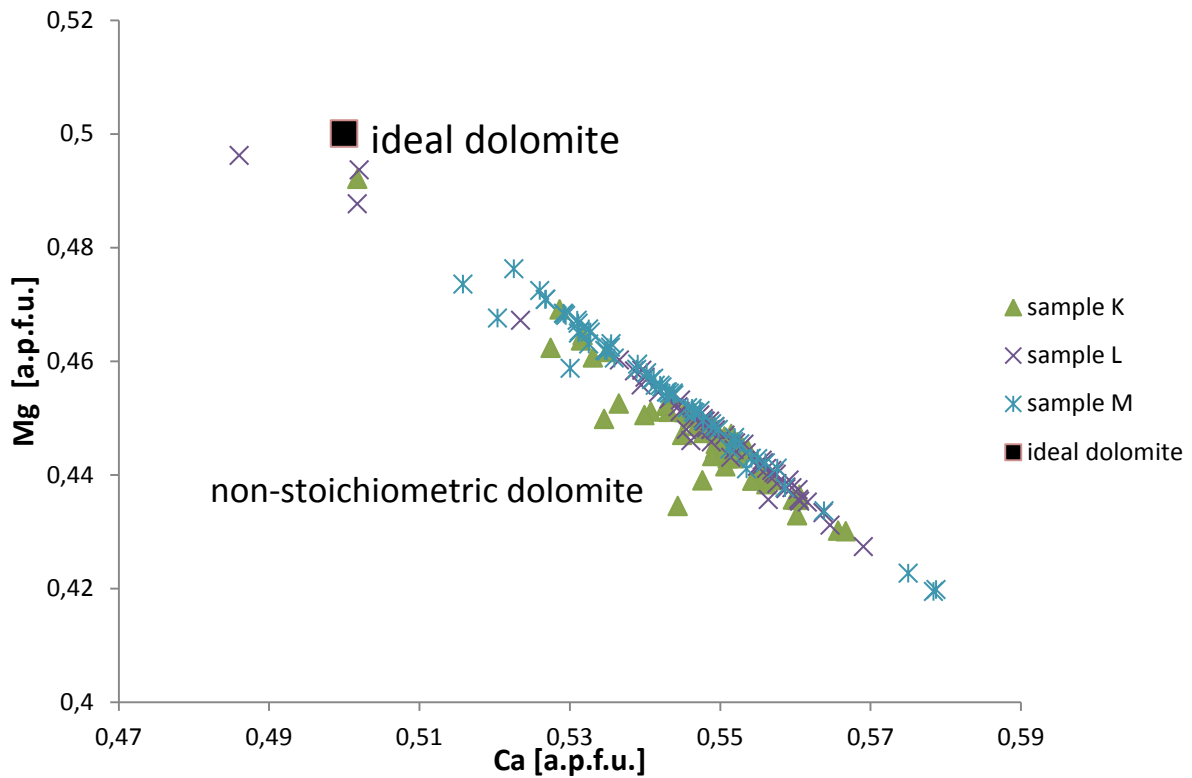
Figure A-15: Mg/Ca ratio from the UDU. The ratio of most of the chemical point analyses accord to non-stoichiometric dolomite.
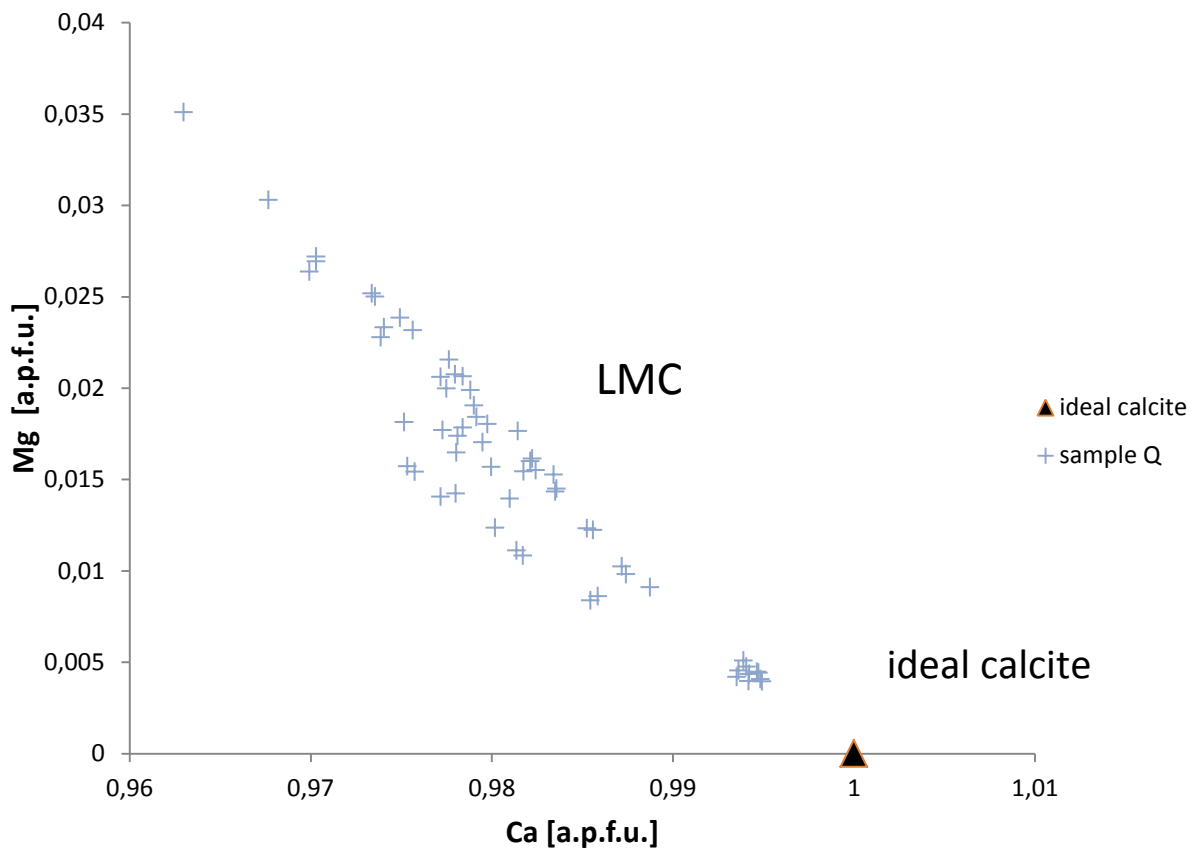
Figure A-16: Mg/Ca ratio of sample Q from the ULU. All chemical point analyses plot in the LMC field.
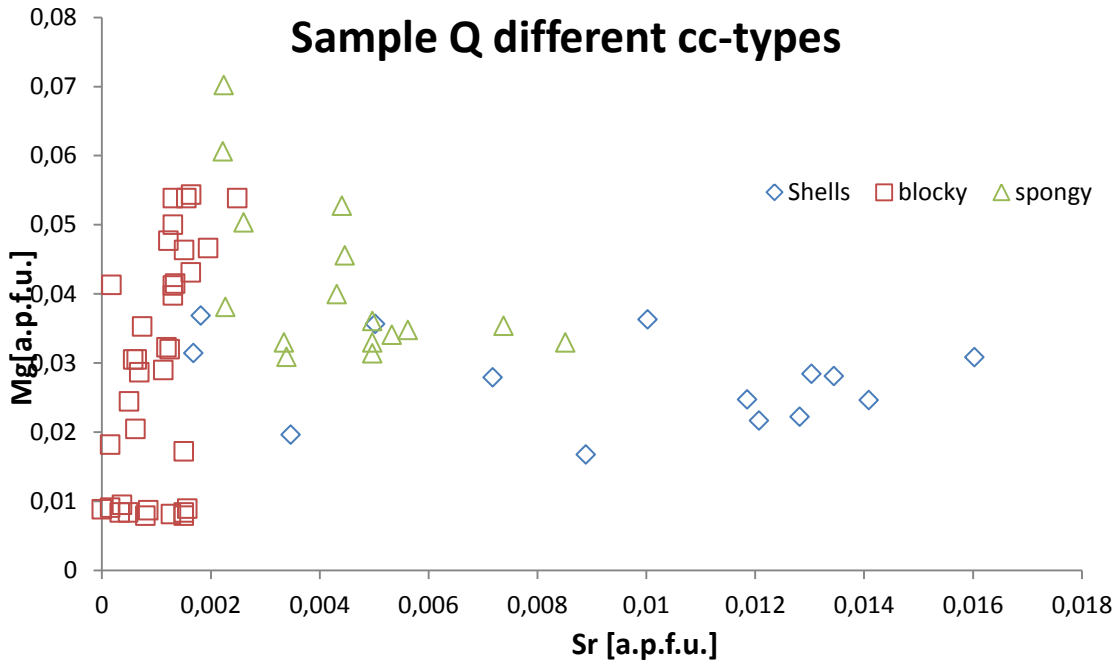
Figure A-17: in sample Q from the UDU, different calcite (cc) cement types can be found. The cc cement types show different enrichment in their Mg and Sr concentration. Note that the blocky cc incorporates small amounts of Sr, whereas the primary shell cc is more enriched in this element. The spongy cc has a higher Mg concentrations and an intermediate Sr content.
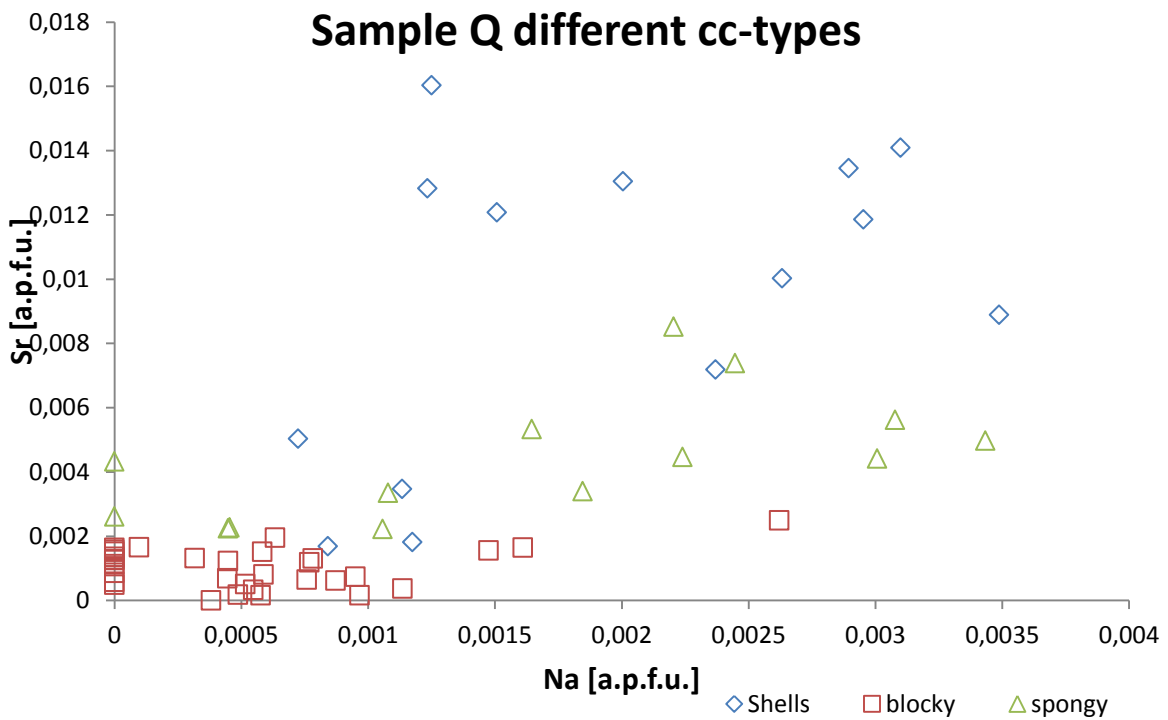
Figure A-18: in sample Q a trend in the Na concentration can be seen: the blocky cc has a very homogeneous Na concentration in general, whereas the Na concentration of the spongy cc varies strongly (as do the Sr concentrations). In the shells, the Na concentration also varies strongly, but low Na concentrations like in the blocky cc are rare.

Table A-4: Results of the EMPA chemical point analysis:

MgO [wt%]	Na₂O [wt%]	CaO [wt%]	SrO [wt%]	MnO [wt%]	Al₂O₃ [wt%]	SO₃ [wt%]	FeO [wt%]	SiO₂ [wt%]	Total	Sample
0,80	0,00	55,05	0,01	0,04	0,03	0,00	0,11	0,35	56,38	i1
19,51	0,03	31,82	0,01	0,22	0,17	0,04	0,14	0,23	52,17	i2
3,04	0,02	51,23	0,02	0,06	0,19	0,05	0,14	0,22	54,96	i3
8,84	0,03	43,18	0,01	0,04	0,71	0,01	0,23	1,26	54,30	i4
0,56	0,04	51,04	0,00	0,04	1,30	0,02	0,33	2,68	56,01	i5
3,82	0,03	48,24	0,00	0,04	1,00	0,06	0,34	1,88	55,41	i6
9,78	0,06	43,41	0,00	0,12	0,51	0,03	0,33	1,25	55,48	i7
19,05	0,02	31,94	0,00	0,03	0,06	0,07	0,03	0,05	51,24	i8
17,17	0,02	34,88	0,00	0,02	0,77	0,07	0,18	1,58	54,69	i9
13,36	0,03	39,89	0,01	0,04	0,08	0,06	0,04	0,13	53,63	i10
0,42	0,00	54,01	0,00	0,01	0,39	0,01	0,12	0,76	55,71	i11
0,26	0,01	55,12	0,01	0,00	0,02	0,00	0,08	0,04	55,53	i12
0,36	0,00	54,68	0,02	0,04	0,06	0,00	0,09	0,18	55,44	i13
1,69	0,02	51,46	0,02	0,03	0,37	0,01	0,19	0,89	54,69	i14
0,25	0,03	55,17	0,00	0,03	0,01	0,01	0,03	0,07	55,59	i15
7,86	0,02	44,75	0,01	0,05	0,36	0,02	0,09	0,69	53,85	i16
1,27	0,01	53,44	0,00	0,06	0,28	0,05	0,17	0,79	56,06	i17
20,34	0,06	31,47	0,01	0,03	0,57	0,06	0,11	1,00	53,65	i18
0,80	0,00	54,03	0,02	0,07	0,49	0,02	0,22	2,37	58,01	i19
0,46	0,00	53,05	0,02	0,05	0,48	0,00	0,18	1,27	55,50	i20
19,73	0,08	31,31	0,03	0,02	0,74	0,06	0,13	1,27	53,37	i21
0,89	0,00	55,26	0,03	0,06	0,01	0,00	0,07	0,00	56,32	i22
0,86	0,00	54,88	0,00	0,05	0,00	0,04	0,08	0,01	55,93	i23
0,87	0,01	54,82	0,00	0,05	0,00	0,02	0,06	0,00	55,83	i24
0,79	0,01	55,04	0,00	0,04	0,00	0,01	0,05	0,00	55,95	i25
19,99	0,08	32,15	0,01	0,01	0,39	0,05	0,07	0,71	53,44	i26
0,80	0,00	52,20	0,01	0,05	0,97	0,01	0,22	1,90	56,16	i27
18,65	0,03	31,64	0,00	0,02	0,84	0,05	0,18	0,98	52,38	i28
13,76	0,05	38,71	0,02	0,02	0,58	0,03	0,09	0,85	54,10	i29
0,75	0,00	55,34	0,00	0,02	0,01	0,00	0,05	0,09	56,25	i30
17,37	0,04	28,53	0,00	0,08	1,69	0,06	0,98	5,70	54,44	i31
17,51	0,07	27,15	0,02	0,03	4,00	0,06	0,43	6,16	55,43	i32
4,79	0,01	47,74	0,01	0,06	0,29	0,03	0,46	0,60	53,98	i33
16,13	0,09	31,95	0,01	0,11	0,55	0,09	0,58	0,81	50,30	i34
0,99	0,02	54,33	0,04	0,01	0,20	0,02	0,11	0,54	56,25	i35
0,40	0,02	55,21	0,00	0,04	0,06	0,01	0,05	0,69	56,46	i36
0,51	0,01	54,91	0,00	0,05	0,05	0,03	0,10	0,24	55,90	i37
21,24	0,00	31,47	0,00	0,21	0,03	0,03	0,01	0,05	53,03	i38
0,40	0,00	52,87	0,00	0,04	0,74	0,00	0,23	1,40	55,69	i39
0,31	0,00	55,08	0,01	0,00	0,12	0,00	0,06	0,55	56,14	i40
17,70	0,02	34,45	0,00	0,22	0,24	0,01	0,16	0,40	53,18	i41
1,02	0,00	53,12	0,00	0,03	0,33	0,02	0,13	0,86	55,51	i42
0,47	0,00	53,80	0,00	0,05	0,54	0,02	0,17	0,99	56,03	i43
0,67	0,00	53,34	0,00	0,05	0,42	0,01	0,13	0,99	55,61	i44
7,95	0,06	46,03	0,02	0,06	0,30	0,03	0,20	0,58	55,22	i45
0,56	0,01	54,39	0,00	0,08	0,21	0,01	0,10	0,50	55,85	i46
0,68	0,00	54,52	0,01	0,01	0,08	0,00	0,11	0,23	55,64	i47
0,62	0,01	53,09	0,03	0,05	0,45	0,02	0,12	0,92	55,30	i48
21,26	0,05	30,10	0,02	0,02	0,44	0,05	0,35	1,16	53,45	i49
1,04	0,01	53,62	0,01	0,05	0,59	0,04	0,09	0,73	56,17	i50

0,90	0,01	43,14	0,01	0,04	5,85	0,03	1,22	14,89	66,08	i51
0,71	0,00	52,71	0,00	0,05	0,52	0,01	0,17	0,95	55,11	i52
9,38	0,00	44,07	0,00	0,04	0,30	0,03	0,19	0,79	54,81	i53
0,34	0,03	54,84	0,02	0,03	0,15	0,00	0,08	0,32	55,81	i54
7,41	0,03	46,62	0,02	0,05	0,36	0,03	1,08	0,92	56,52	i55
2,09	0,03	50,73	0,02	0,03	0,96	0,03	0,15	1,97	56,01	i56
21,36	0,08	29,73	0,06	0,22	0,19	0,05	0,11	0,59	52,38	i57
1,69	0,00	50,92	0,02	0,09	0,63	0,06	0,13	1,30	54,83	i58
19,95	0,07	34,82	0,02	0,01	0,14	0,06	0,04	0,17	55,26	i59
0,88	0,00	53,23	0,05	0,03	0,67	0,00	0,20	1,45	56,51	i60
19,53	0,09	32,17	0,01	0,00	0,17	0,08	0,03	0,46	52,53	m1
19,81	0,09	31,91	0,00	0,00	0,17	0,07	0,06	0,28	52,39	m2
18,94	0,06	33,31	0,01	0,00	0,06	0,08	0,02	0,03	52,50	m3
19,28	0,08	33,15	0,02	0,00	0,04	0,09	0,00	0,04	52,72	m4
19,20	0,10	33,07	0,00	0,05	0,13	0,08	0,02	0,02	52,66	m5
20,47	0,02	31,24	0,02	0,01	0,12	0,08	0,05	0,17	52,17	m6
19,47	0,07	32,44	0,01	0,01	0,13	0,10	0,06	0,16	52,45	m7
20,27	0,16	32,20	0,01	0,03	0,10	0,04	0,04	0,00	52,86	m8
19,42	0,10	32,09	0,03	0,04	0,19	0,12	0,04	0,40	52,42	m9
19,45	0,15	33,86	0,01	0,01	0,08	0,09	0,03	0,17	53,85	m10
20,14	0,13	31,65	0,01	0,02	0,08	0,08	0,02	0,01	52,11	m11
20,14	0,12	32,43	0,04	0,02	0,03	0,06	0,02	0,02	52,88	m12
18,25	0,10	34,54	0,03	0,03	0,10	0,08	0,01	0,08	53,21	m13
19,85	0,02	31,91	0,01	0,02	0,06	0,01	0,82	0,02	52,71	m14
19,05	0,10	33,27	0,01	0,08	0,05	0,06	0,21	0,01	52,84	m15
20,43	0,08	31,66	0,02	0,01	0,06	0,08	0,00	0,01	52,35	m16
18,50	0,11	35,48	0,02	0,03	0,05	0,09	0,00	0,02	54,29	m17
20,15	0,06	31,20	0,00	0,04	0,30	0,02	0,82	0,47	53,06	m18
19,50	0,08	32,39	0,02	0,03	0,14	0,12	0,06	0,38	52,72	m19
19,21	0,10	33,50	0,00	0,00	0,13	0,09	0,05	0,30	53,38	m20
16,19	0,08	36,65	0,01	0,00	0,10	0,08	0,05	0,25	53,41	m21
20,01	0,07	32,20	0,00	0,00	0,07	0,08	0,03	0,05	52,50	m22
20,43	0,04	30,95	0,00	0,03	0,23	0,03	0,75	0,27	52,72	m23
18,61	0,08	33,67	0,03	0,01	0,07	0,13	0,07	0,11	52,78	m24
19,24	0,12	33,20	0,05	0,02	0,05	0,13	0,13	0,02	52,95	m25
19,63	0,10	32,62	0,04	0,02	0,02	0,12	0,03	0,02	52,59	m26
19,49	0,09	32,80	0,02	0,01	0,05	0,07	0,02	0,02	52,58	m27
20,27	0,12	31,88	0,02	0,02	0,07	0,08	0,02	0,01	52,49	m28
19,95	0,13	32,12	0,02	0,04	0,06	0,08	0,06	0,00	52,46	m29
19,36	0,08	33,05	0,04	0,02	0,08	0,11	0,03	0,09	52,86	m30
19,86	0,12	32,00	0,02	0,03	0,19	0,14	0,08	0,40	52,83	m31
19,94	0,09	31,91	0,04	0,03	0,02	0,07	0,18	0,01	52,29	m32
19,02	0,11	31,64	0,01	0,01	0,29	0,18	0,04	0,57	51,86	m33
19,91	0,10	31,72	0,02	0,02	0,18	0,14	0,03	0,48	52,59	m34
19,60	0,10	33,03	0,03	0,00	0,04	0,13	0,05	0,09	53,07	m35
19,79	0,07	32,31	0,04	0,00	0,02	0,13	0,00	0,01	52,38	m36
19,44	0,07	32,80	0,00	0,01	0,09	0,15	0,02	0,18	52,76	m37
20,00	0,06	31,67	0,01	0,00	0,26	0,14	0,09	0,52	52,75	m38
20,19	0,09	31,92	0,03	0,02	0,04	0,12	0,01	0,00	52,41	m39
17,96	0,07	34,44	0,01	0,01	0,08	0,15	0,02	0,10	52,83	m40
19,52	0,10	31,61	0,00	0,01	0,15	0,10	0,14	0,14	51,76	m41
19,12	0,11	33,46	0,01	0,00	0,01	0,14	0,01	0,00	52,87	m42
19,72	0,10	32,37	0,03	0,00	0,08	0,12	0,00	0,04	52,45	m43

19,17	0,06	32,67	0,03	0,04	0,08	0,13	0,05	0,21	52,43	m44
19,21	0,09	33,17	0,02	0,00	0,05	0,11	0,02	0,01	52,69	m45
20,37	0,11	32,06	0,04	0,04	0,08	0,08	0,00	0,01	52,80	m46
19,80	0,09	32,38	0,02	0,02	0,07	0,12	0,05	0,12	52,67	m47
20,38	0,11	31,71	0,00	0,03	0,08	0,07	0,01	0,13	52,52	m48
19,41	0,09	32,15	0,03	0,00	0,23	0,15	0,05	0,41	52,51	m49
20,03	0,11	31,88	0,00	0,01	0,06	0,12	0,01	0,00	52,21	m50
19,16	0,08	32,59	0,00	0,03	0,04	0,19	0,04	0,08	52,20	m51
18,87	0,14	33,51	0,00	0,04	0,20	0,08	0,09	0,25	53,16	m52
19,52	0,10	32,50	0,03	0,00	0,02	0,21	0,00	0,02	52,40	m53
19,38	0,08	32,68	0,02	0,04	0,22	0,13	0,04	0,46	53,04	m54
19,32	0,09	32,75	0,04	0,02	0,16	0,16	0,06	0,32	52,92	m55
19,72	0,07	32,63	0,03	0,03	0,02	0,12	0,04	0,00	52,66	m56
20,48	0,11	31,88	0,01	0,00	0,08	0,09	0,05	0,01	52,71	m57
19,43	0,08	32,65	0,03	0,03	0,20	0,14	0,05	0,49	53,10	m58
20,13	0,19	32,00	0,01	0,05	0,07	0,10	0,02	0,01	52,58	m59
19,70	0,13	32,45	0,03	0,00	0,04	0,13	0,01	0,01	52,51	m60
0,45	0,04	54,69	0,66	0,00	0,01	0,05	0,04	0,00	55,93	Q1
0,57	0,06	54,73	0,67	0,00	0,00	0,06	0,02	0,00	56,12	Q2
0,18	0,00	54,83	0,08	0,00	0,01	0,03	0,01	0,00	55,13	Q3
0,16	0,02	55,09	0,04	0,00	0,01	0,02	0,03	0,00	55,36	Q4
0,58	0,00	54,78	0,06	0,02	0,00	0,00	0,08	0,00	55,51	Q5
0,37	0,02	55,85	0,01	0,00	0,02	0,01	0,13	0,02	56,43	Q6
0,41	0,03	55,31	0,03	0,02	0,01	0,00	0,11	0,01	55,93	Q7
0,87	0,00	55,11	0,09	0,00	0,00	0,02	0,00	0,01	56,10	Q8
0,93	0,02	54,56	0,08	0,00	0,01	0,02	0,01	0,02	55,64	Q9
1,43	0,01	54,47	0,12	0,00	0,01	0,02	0,04	0,01	56,10	Q10
0,63	0,04	55,09	0,84	0,01	0,01	0,06	0,00	0,00	56,68	Q11
0,44	0,05	55,36	0,63	0,02	0,00	0,04	0,02	0,01	56,57	Q12
0,76	0,01	54,57	0,12	0,00	0,00	0,04	0,04	0,00	55,55	Q13
1,23	0,03	54,67	0,12	0,01	0,00	0,04	0,02	0,00	56,11	Q14
1,02	0,00	54,98	0,14	0,00	0,00	0,05	0,01	0,00	56,20	Q15
1,12	0,05	55,62	0,09	0,04	0,01	0,05	0,03	0,00	57,00	Q16
0,84	0,05	55,14	0,08	0,00	0,00	0,07	0,05	0,03	56,26	Q17
1,10	0,08	54,94	0,13	0,00	0,02	0,08	0,02	0,01	56,37	Q18
0,96	0,02	55,63	0,10	0,03	0,01	0,03	0,07	0,03	56,87	Q19
0,82	0,01	55,88	0,07	0,02	0,01	0,05	0,02	0,01	56,89	Q20
0,97	0,01	55,11	0,06	0,00	0,00	0,06	0,03	0,01	56,26	Q21
0,85	0,00	55,76	0,07	0,02	0,01	0,05	0,02	0,00	56,79	Q22
0,73	0,03	56,10	0,04	0,01	0,00	0,02	0,00	0,00	56,92	Q23
0,18	0,01	56,72	0,00	0,00	0,01	0,02	0,05	0,00	56,99	Q24
0,59	0,01	55,92	0,04	0,01	0,01	0,00	0,11	0,02	56,71	Q25
0,17	0,00	56,88	0,07	0,01	0,02	0,03	0,03	0,01	57,20	Q26
0,49	0,02	55,29	0,03	0,03	0,01	0,01	0,09	0,00	55,96	Q27
0,18	0,03	55,81	0,01	0,02	0,00	0,02	0,08	0,00	56,15	Q28
1,00	0,02	54,06	0,07	0,00	0,00	0,04	0,03	0,00	55,22	Q29
0,83	0,00	54,67	0,09	0,00	0,00	0,04	0,01	0,00	55,64	Q30
0,33	0,11	54,72	0,46	0,00	0,00	0,10	0,00	0,02	55,73	Q31
0,49	0,09	54,07	0,60	0,00	0,00	0,05	0,01	0,01	55,32	Q32
0,39	0,04	55,17	0,18	0,00	0,00	0,03	0,03	0,00	55,84	Q33
0,74	0,08	54,98	0,52	0,00	0,01	0,07	0,02	0,02	56,45	Q34
0,50	0,03	55,08	0,09	0,01	0,02	0,02	0,07	0,00	55,81	Q35
0,63	0,10	54,11	0,72	0,01	0,00	0,10	0,01	0,02	55,70	Q36

0,70	0,02	53,75	0,26	0,04	0,00	0,04	0,02	0,01	54,84	Q37
0,56	0,07	54,70	0,37	0,00	0,17	0,05	0,02	0,01	55,95	Q38
0,56	0,09	54,36	0,69	0,03	0,00	0,06	0,02	0,00	55,81	Q39
0,73	0,04	54,28	0,09	0,01	0,00	0,04	0,05	0,00	55,25	Q40
0,70	0,07	53,48	0,37	0,01	0,02	0,02	0,00	0,01	54,68	Q41
0,72	0,03	54,21	0,17	0,00	0,00	0,06	0,00	0,00	55,19	Q42
0,66	0,07	54,60	0,44	0,00	0,00	0,05	0,01	0,00	55,83	Q43
0,62	0,11	54,23	0,25	0,00	0,01	0,07	0,01	0,00	55,31	Q44
1,06	0,09	54,29	0,23	0,00	0,00	0,06	0,00	0,00	55,74	Q45
0,69	0,05	54,95	0,28	0,00	0,01	0,05	0,00	0,00	56,02	Q46
0,81	0,00	54,90	0,22	0,00	0,01	0,02	0,03	0,01	55,99	Q47
0,91	0,07	54,30	0,23	0,00	0,01	0,08	0,00	0,02	55,62	Q48
0,62	0,06	54,84	0,18	0,01	0,00	0,05	0,01	0,01	55,77	Q49
0,70	0,10	54,64	0,29	0,01	0,00	0,05	0,01	0,02	55,80	Q50
0,64	0,02	54,75	0,01	0,01	0,00	0,02	0,10	0,00	55,54	Q51
0,20	0,00	56,85	0,07	0,01	0,03	0,02	0,03	0,00	57,21	Q52
0,16	0,04	55,44	0,02	0,00	0,00	0,02	0,08	0,00	55,75	Q53
0,35	0,02	55,35	0,02	0,00	0,00	0,00	0,37	0,00	56,10	Q54
0,17	0,00	56,36	0,08	0,04	0,00	0,03	0,07	0,00	56,75	Q55
0,65	0,00	54,85	0,03	0,02	0,01	0,00	0,08	0,00	55,63	Q56
0,18	0,02	56,19	0,06	0,00	0,02	0,02	0,03	0,01	56,54	Q57
0,62	0,00	55,16	0,03	0,02	0,00	0,00	0,06	0,00	55,89	Q58
0,64	0,02	56,30	0,03	0,01	0,01	0,00	0,09	0,01	57,11	Q59
0,21	0,00	55,69	0,04	0,00	0,01	0,02	0,04	0,00	56,02	Q60
18,07	0,13	31,98	0,05	0,02	0,28	0,19	0,09	0,86	51,66	I1
18,53	0,10	33,03	0,02	0,02	0,07	0,19	0,01	0,07	52,04	I2
19,15	0,09	32,83	0,03	0,02	0,17	0,12	0,03	0,27	52,71	I3
18,26	0,11	32,68	0,03	0,03	0,31	0,14	0,11	0,76	52,42	I4
19,22	0,11	32,55	0,02	0,03	0,12	0,15	0,01	0,08	52,28	I5
19,00	0,09	33,33	0,03	0,02	0,05	0,13	0,06	0,08	52,77	I6
19,11	0,10	32,61	0,04	0,02	0,26	0,13	0,03	0,57	52,88	I7
18,55	0,16	33,30	0,03	0,03	0,16	0,12	0,01	0,34	52,69	I8
18,40	0,07	32,73	0,04	0,04	0,32	0,13	0,05	0,81	52,60	I9
19,72	0,10	32,29	0,02	0,01	0,21	0,18	0,02	0,40	52,94	I10
18,91	0,10	33,24	0,01	0,03	0,13	0,11	0,04	0,34	52,90	I11
19,00	0,19	32,89	0,03	0,02	0,34	0,13	0,16	0,85	53,60	I12
21,30	0,01	30,13	0,03	0,19	0,01	0,03	0,11	0,03	51,84	I13
21,37	0,00	29,13	0,00	0,25	0,37	2,02	1,12	1,34	55,58	I14
18,98	0,12	32,35	0,01	0,03	0,19	0,13	0,06	0,69	52,56	I15
18,88	0,09	33,24	0,04	0,03	0,09	0,11	0,03	0,00	52,50	I16
19,67	0,08	32,76	0,01	0,02	0,13	0,18	0,06	0,62	53,53	I17
19,38	0,09	32,86	0,02	0,04	0,08	0,09	0,04	0,06	52,66	I18
17,55	0,10	32,51	0,06	0,03	0,34	0,16	0,08	0,93	51,74	I19
19,25	0,07	32,66	0,01	0,02	0,18	0,11	0,08	0,31	52,70	I20
18,63	0,07	32,58	0,01	0,01	0,40	0,13	0,06	0,79	52,68	I21
18,88	0,05	32,06	0,01	0,03	0,24	0,12	0,05	0,51	51,94	I22
19,60	0,08	31,80	0,01	0,02	0,62	0,18	0,13	3,22	55,64	I23
19,54	0,11	31,94	0,02	0,03	0,35	0,14	0,06	0,59	52,78	I24
18,89	0,09	33,04	0,02	0,07	0,17	0,07	0,08	0,31	52,74	I25
19,14	0,06	31,52	0,02	0,02	0,69	0,15	0,25	1,41	53,26	I26
19,33	0,06	32,33	0,02	0,04	0,31	0,16	0,04	0,66	52,96	I27
19,11	0,05	32,37	0,02	0,03	0,15	0,08	0,39	0,71	52,92	I28
19,20	0,09	33,09	0,03	0,06	0,02	0,11	0,00	0,04	52,63	I29

18,83	0,08	33,18	0,04	0,05	0,12	0,13	0,01	0,27	52,71	l30
18,65	0,11	33,11	0,00	0,04	0,47	0,07	0,09	0,69	53,22	l31
18,43	0,09	32,75	0,00	0,02	0,32	0,76	0,48	0,62	53,46	l32
19,16	0,10	32,65	0,01	0,00	0,27	0,15	0,13	0,75	53,20	l33
18,88	0,03	32,63	0,02	0,01	0,28	0,08	0,04	1,17	53,14	l34
19,22	0,13	32,21	0,01	0,03	0,27	0,08	0,09	0,17	52,21	l35
18,95	0,12	32,46	0,01	0,07	0,29	0,07	0,20	0,54	52,70	l36
19,20	0,09	32,44	0,01	0,02	0,28	0,12	0,04	0,69	52,89	l37
20,03	0,06	31,22	0,01	0,03	0,17	0,06	0,61	0,28	52,48	l38
18,97	0,13	32,04	0,02	0,04	0,33	0,10	0,07	0,66	52,34	l39
18,68	0,11	33,19	0,02	0,03	0,23	0,08	0,11	0,49	52,93	l40
18,77	0,09	32,85	0,04	0,05	0,05	0,11	0,03	0,16	52,14	l41
19,12	0,16	32,57	0,02	0,02	0,34	0,24	0,39	0,82	53,66	l42
19,55	0,13	32,43	0,03	0,02	0,22	0,17	0,10	0,70	53,34	l43
19,01	0,10	32,84	0,00	0,04	0,16	0,11	0,13	0,29	52,67	l44
19,06	0,09	32,47	0,02	0,01	0,15	0,10	0,04	0,18	52,12	l45
18,51	0,14	33,15	0,02	0,05	0,34	0,11	0,09	0,70	53,09	l46
19,16	0,12	33,24	0,03	0,04	0,12	0,13	0,00	0,08	52,91	l47
18,78	0,06	33,28	0,02	0,03	0,15	0,11	0,02	0,37	52,82	l48
17,95	0,12	32,49	0,00	0,02	0,38	0,14	0,06	0,67	51,83	l49
21,02	0,01	30,09	0,01	0,19	0,07	0,01	0,60	0,07	52,07	l50
19,46	0,10	32,44	0,08	0,06	0,25	0,15	0,04	0,37	52,95	l53
19,39	0,09	31,87	0,01	0,02	0,34	0,19	0,08	0,98	52,98	l54
19,37	0,10	32,27	0,00	0,06	0,09	0,14	0,01	0,05	52,08	l55
18,04	0,17	32,87	0,04	0,02	0,26	0,25	0,07	0,54	52,26	l56
19,44	0,14	32,65	0,03	0,03	0,14	0,10	0,11	0,03	52,65	l57
18,69	0,07	32,65	0,03	0,02	0,19	0,14	0,02	0,39	52,19	l58
19,10	0,09	32,50	0,05	0,06	0,36	0,11	0,07	0,75	53,09	l59
18,69	0,11	31,70	0,07	0,02	0,52	0,25	0,40	1,09	52,86	k1
12,31	0,04	21,45	0,00	0,00	1,74	0,15	1,02	3,79	40,49	k2
19,19	0,09	31,99	0,03	0,02	0,37	0,16	0,07	0,75	52,66	k3
18,93	0,15	32,11	0,03	0,02	0,41	0,14	0,13	0,79	52,71	k4
18,88	0,17	33,79	0,04	0,02	0,10	0,18	0,04	0,19	53,42	k5
18,64	0,12	32,26	0,03	0,02	0,32	0,14	0,11	0,84	52,49	k6
19,04	0,10	32,68	0,04	0,04	0,27	0,09	0,21	0,43	52,91	k7
18,28	0,11	28,66	0,00	0,00	0,25	0,16	0,03	0,62	48,11	k8
18,26	0,13	33,41	0,04	0,03	0,05	0,18	0,11	0,09	52,28	k9
18,44	0,16	32,99	0,01	0,02	0,05	0,13	0,11	0,19	52,09	k10
18,61	0,12	32,65	0,02	0,01	0,18	0,16	0,08	0,29	52,11	k11
18,74	0,10	31,58	0,01	0,00	0,47	0,17	0,13	1,02	52,23	k12
19,10	0,08	32,78	0,02	0,00	0,04	0,14	0,00	0,02	52,17	k13
18,74	0,14	32,22	0,04	0,03	0,45	0,11	0,23	1,00	52,97	k14
19,33	0,10	31,12	0,03	0,04	0,58	0,15	0,29	1,27	52,90	k15
19,04	0,07	32,94	0,05	0,01	0,10	0,15	0,03	0,12	52,52	k16
20,98	0,02	29,77	0,01	0,06	0,15	0,03	0,37	0,39	51,78	k17
17,65	0,18	29,56	0,03	0,00	3,11	0,11	0,18	4,38	55,19	k18
18,88	0,06	31,52	0,02	0,00	0,44	0,09	0,30	0,82	52,12	k19
18,96	0,13	32,44	0,03	0,03	0,21	0,18	0,06	0,18	52,23	k20
18,67	0,12	32,31	0,00	0,05	0,46	0,10	0,27	0,79	52,77	k21
18,49	0,08	31,83	0,02	0,04	0,45	0,12	0,24	0,93	52,18	k22
18,91	0,09	31,81	0,04	0,00	0,50	0,15	0,14	0,90	52,54	k23
18,51	0,09	31,95	0,00	0,03	0,43	0,11	0,32	1,01	52,45	k24
18,38	0,09	32,85	0,04	0,05	0,24	0,11	0,17	0,53	52,46	k25

18,91	0,10	33,37	0,05	0,03	0,39	0,12	0,14	0,55	53,66	k26
18,73	0,10	32,45	0,02	0,04	0,35	0,09	0,15	0,87	52,80	k27
18,63	0,11	32,18	0,01	0,04	0,33	0,17	0,08	0,65	52,19	k28
19,22	0,08	30,66	0,04	0,01	0,74	0,15	0,23	1,30	52,44	k29
18,87	0,06	32,58	0,00	0,03	0,15	0,14	0,06	0,54	52,43	k30
18,78	0,10	31,69	0,00	0,03	0,44	0,16	0,14	0,92	52,26	k31
19,19	0,11	32,01	0,03	0,04	0,22	0,13	0,43	0,52	52,69	k32
19,03	0,16	33,03	0,05	0,01	0,31	1,07	0,81	0,65	55,11	k33
18,83	0,06	32,61	0,06	0,03	0,22	0,10	0,06	0,24	52,21	k34
18,38	0,11	33,70	0,06	0,02	0,06	0,13	0,05	0,18	52,69	k35
19,31	0,07	32,19	0,02	0,01	0,19	0,08	0,62	0,34	52,83	k36
18,98	0,09	31,31	0,00	0,03	0,32	0,12	0,68	0,62	52,14	k37
19,03	0,04	31,46	0,05	0,04	0,23	0,07	1,06	0,52	52,50	k38
18,40	0,13	33,13	0,04	0,04	0,32	0,12	0,30	0,83	53,30	k39
18,98	0,13	32,34	0,02	0,03	0,34	0,15	0,18	0,68	52,84	k40
18,50	0,08	32,66	0,02	0,00	0,21	0,14	0,30	0,41	52,32	k41
18,44	0,12	29,36	0,03	0,05	0,16	0,10	0,05	0,39	48,71	k42
18,52	0,06	33,09	0,01	0,03	0,20	0,13	0,12	0,54	52,69	k43
19,28	0,10	32,82	0,04	0,02	0,13	0,08	0,04	0,08	52,59	k44
18,65	0,08	32,75	0,05	0,04	0,51	0,12	0,21	2,27	54,69	k45
18,87	0,07	32,22	0,04	0,03	0,36	0,12	0,06	0,86	52,63	k46
18,51	0,10	32,09	0,04	0,02	0,48	0,16	0,22	1,05	52,66	k47
18,40	0,14	31,94	0,03	0,04	0,55	0,17	0,35	1,48	53,10	k48
18,95	0,09	32,49	0,01	0,01	0,34	0,14	0,08	0,71	52,82	k49
18,71	0,07	32,02	0,03	0,02	0,47	0,14	0,12	1,04	52,61	k50
18,66	0,07	32,29	0,01	0,03	0,37	0,15	0,25	1,06	52,89	k51
18,95	0,08	32,66	0,00	0,03	0,03	0,16	0,04	0,05	51,98	k52
19,71	0,06	31,28	0,05	0,04	0,17	0,04	0,63	0,28	52,25	k53
18,87	0,07	32,70	0,00	0,00	0,13	0,20	0,06	0,43	52,47	k54
18,50	0,11	32,62	0,05	0,04	0,18	0,15	0,09	0,32	52,07	k55
18,98	0,10	32,60	0,04	0,02	0,30	0,12	0,11	0,50	52,78	k56
18,78	0,07	32,35	0,03	0,03	0,41	0,09	0,45	0,75	52,95	k57
19,11	0,06	30,81	0,01	0,02	0,70	0,17	0,16	1,33	52,37	k58
18,63	0,13	32,74	0,02	0,03	0,46	0,14	0,32	0,81	53,27	k59
19,42	0,10	33,00	0,02	0,03	0,09	0,12	0,08	0,14	53,00	k60
0,52	0,03	56,91	0,00	0,04	0,00	0,05	0,00	0,01	57,56	E1
0,60	0,03	57,10	0,01	0,07	0,00	0,00	0,01	0,00	57,81	E2
0,56	0,02	57,68	0,00	0,01	0,00	0,00	0,03	0,13	58,42	E3
0,60	0,00	57,82	0,02	0,05	0,01	0,00	0,01	0,05	58,56	E4
0,61	0,01	56,66	0,03	0,09	0,01	0,00	0,01	0,02	57,41	E5
0,62	0,02	56,76	0,00	0,04	0,02	0,01	0,01	0,03	57,52	E6
0,64	0,00	57,24	0,00	0,06	0,00	0,00	0,01	0,06	58,02	E7
0,64	0,01	57,87	0,00	0,04	0,01	0,00	0,00	0,00	58,57	E8
0,54	0,01	57,96	0,00	0,04	0,01	0,02	0,01	0,00	58,58	E9
0,60	0,02	57,66	0,00	0,05	0,02	0,09	0,00	0,00	58,43	E10
0,67	0,02	57,15	0,06	0,03	0,01	0,02	0,00	0,03	57,97	E11
0,68	0,03	56,28	0,04	0,03	0,01	0,08	0,01	0,01	57,16	E12
0,20	0,02	57,28	0,00	0,04	0,02	0,02	0,00	0,09	57,66	E13
0,65	0,00	57,41	0,00	0,03	0,00	0,02	0,01	0,01	58,12	E14
0,15	0,02	57,18	0,03	0,07	0,01	0,00	0,03	0,01	57,50	E15
0,22	0,03	58,35	0,00	0,02	0,03	0,00	0,00	0,04	58,70	E16
0,61	0,04	56,18	0,04	0,03	0,03	0,05	0,02	0,02	57,02	E17
0,33	0,02	56,92	0,00	0,02	0,02	0,02	0,00	0,00	57,34	E18

0,90	0,01	57,43	0,02	0,04	0,00	0,04	0,01	0,00	58,45	E19
0,71	0,03	56,49	0,04	0,03	0,00	0,04	0,04	0,00	57,38	E20
0,79	0,00	54,97	0,02	0,00	0,09	0,09	0,00	0,03	55,99	E21
0,74	0,06	54,54	0,03	0,00	0,13	0,13	0,00	0,08	55,71	E22
0,38	0,00	57,79	0,06	0,02	0,01	0,00	0,02	0,00	58,28	E23
0,83	0,04	56,10	0,02	0,01	0,10	0,07	0,02	0,14	57,34	E24
0,65	0,04	56,42	0,03	0,02	0,03	0,04	0,03	0,05	57,30	E25
0,55	0,03	55,36	0,03	0,01	0,04	0,06	0,00	0,05	56,13	E26
0,69	0,04	55,69	0,04	0,01	0,03	0,05	0,02	0,03	56,59	E27
0,69	0,01	55,91	0,00	0,00	0,03	0,06	0,03	0,08	56,80	E28
0,64	0,01	56,20	0,04	0,04	0,02	0,00	0,00	0,08	57,03	E29
0,90	0,03	54,45	0,00	0,07	0,17	0,05	0,00	0,17	55,84	E30
0,18	0,00	58,00	0,04	0,05	0,01	0,06	0,01	0,00	58,35	E31
0,16	0,04	56,35	0,04	0,04	0,01	0,02	0,00	0,02	56,67	E32
0,17	0,01	56,68	0,00	0,06	0,01	0,00	0,00	0,01	56,94	E33
0,58	0,01	57,09	0,01	0,09	0,03	0,05	0,00	0,00	57,86	E34
0,17	0,03	57,24	0,02	0,06	0,00	0,00	0,02	0,02	57,56	E35
0,14	0,03	57,26	0,03	0,04	0,02	0,00	0,00	0,00	57,51	E36
0,15	0,00	56,34	0,05	0,03	0,01	0,00	0,03	0,07	56,69	E37
0,17	0,02	56,97	0,02	0,05	0,00	0,01	0,01	0,00	57,25	E38
0,19	0,02	58,68	0,04	0,05	0,02	0,01	0,03	0,00	59,04	E39
0,21	0,02	58,52	0,06	0,05	0,02	0,00	0,01	0,00	58,89	E40
0,22	0,00	58,15	0,03	0,03	0,01	0,00	0,02	0,05	58,50	E41
0,59	0,00	57,10	0,02	0,05	0,01	0,00	0,00	0,04	57,80	E42
0,59	0,00	56,82	0,00	0,10	0,04	0,08	0,01	0,05	57,70	E43
0,63	0,02	57,26	0,00	0,08	0,01	0,07	0,00	0,00	58,06	E44
0,60	0,00	57,77	0,01	0,07	0,00	0,02	0,00	0,01	58,48	E45
0,77	0,06	55,71	0,04	0,01	0,01	0,06	0,01	0,00	56,65	E46
0,82	0,03	56,50	0,01	0,01	0,05	0,03	0,04	0,07	57,55	E47
0,72	0,04	55,77	0,06	0,00	0,05	0,04	0,00	0,09	56,77	E48
0,74	0,07	56,23	0,01	0,03	0,03	0,07	0,01	0,06	57,24	E49
1,05	0,02	57,32	0,01	0,00	0,02	0,02	0,01	0,00	58,44	E50
0,69	0,05	50,65	0,00	3,72	0,25	0,09	0,01	0,39	55,86	E51
0,84	0,03	54,28	0,01	0,50	0,40	0,13	0,00	0,29	56,47	E52
0,79	0,05	55,22	0,03	0,02	0,19	0,12	0,03	0,16	56,61	E53
0,64	0,04	54,96	0,04	0,09	0,11	0,09	0,00	0,19	56,14	E54
0,67	0,02	54,64	0,00	0,08	0,40	0,06	0,02	0,50	56,39	E55
0,72	0,05	52,33	0,02	0,18	0,80	0,08	0,00	1,02	55,19	E56
0,62	0,03	54,71	0,02	0,06	0,46	0,05	0,00	0,54	56,49	E57
0,60	0,04	55,35	0,02	0,11	0,36	0,05	0,01	0,43	56,98	E58
0,73	0,08	50,15	0,02	0,16	1,30	0,08	0,01	1,47	54,00	E59
0,59	0,05	52,75	0,05	0,15	0,45	0,08	0,03	0,45	54,60	E60